THE EFFECTS OF AN AC FIELD ON THE TRANSPORT OF PEPTIDES AND OTHER MOLECULES THROUGH THE α-HEMOLYSIN PORE

A Thesis Submitted to the College of Graduate Studies and Research
In Partial Fulfillment of the Requirements
for the Degree of Master of Science
In the Department of Biochemistry
University of Saskatchewan, Saskatoon

By

Elisabet Jakova

Permission to Use

In presenting this thesis in partial fulfillment of the requirements for a Postgraduate degree from the University of Saskatchewan, I agree that the Libraries of this University may make it freely available for inspection. I further agree that permission for copying of this thesis in any manner, in whole or in part, for scholarly purposes may be granted by the professors who supervised my thesis work, or in their absence, by the Head of the Department or the Dean of the College in which my thesis work was done. It is understood that any copying or publication or use of this thesis or parts thereof for financial gain shall not be allowed without my written permission. It is also understood that due to recognition shall be given to me and to the University of Saskatchewan in any scholarly use which may be made of any material in my thesis.

Request for permission to copy or make other uses of material in this thesis in whole or in part should be addressed to:

Head of the Department of Biochemistry
College of Medicine, University of Saskatchewan
Saskatoon, SK
Canada S7N 5E5

ABSTRACT

This research is based on superimposing an alternating current (AC) onto a direct current (DC) during the nanopore analysis of various peptides, single-stranded DNA, α-synuclein (AS) protein, and AS-drug complexes. Standard nanopore analysis consists of a constant DC voltage used to electrophoretically drive small molecules towards a pore. The superposition of the AC voltage at constant amplitude and different frequencies causes small molecules to oscillate as they approach the pore vestibule which will lead to alterations of the event parameters, the blockade current and blockade time. The DC voltage was set at 100 mV. It was found that a 200 mV AC voltage imposed over the DC voltage at frequencies from 10 MHz – 1 GHz was optimal to conduct the experiments. Initially, four α-helical peptides with a Fmoc-capping group on the N-terminus with the general formula Fmoc-DDA$_x$KK, were studied since their DC behaviour is well known, e.g. Fmoc-DDA$_{10}$KK (A10), Fmoc-DDA$_{14}$KK (A14), Fmoc-DDA$_{18}$KK (A18) and retro-inverse Fmoc-KKA$_{10}$DD (RI-A10). These peptides are of different length and consequently different dipole moments, which is hypothesised to alter their mobility in the AC field. It was shown that the ratio of translocations to bumping events could be manipulated by a combination of AC voltage and frequencies. In particular, A10 could be studied without interference from RI-A10. Similarly, a large intrinsically disordered protein of 140 amino acids, AS, which translocates the pore readily in a DC field could be prevented from doing so by application of an AC field of 200 mV at 100 MHz. Additionally, three fragments of AS, C-terminal, N-terminal and the ΔNAC, were studied under the same AC conditions. After an AC field was applied, the C- and N-terminal were prevented from entering the pore due to their charge. Conversely, ΔNAC behaved as expected for a peptide with a negative C-terminus and/or with a large dipole moment, and the ratio of bumping events to translocation events, increased with an increase of the AC frequency. Finally, nanopore analysis with an AC field was useful to probe the conformational states of AS which are induced by drugs. Seven drugs were chosen to be studied in an AC field since their DC blockade histograms and binding properties are known. Five neuroprotective drugs (S-1-aminoindan, 3-methoxytyramine, caffeine, (-)-nicotine, metformin) and two neurotoxic drugs (cocaine and (+)-amphetamine) were studied. Surprisingly, the neuroprotective AS-drug complexes, under the effect of the AC field, showed signs of drug stripping.

PUBLISHED WORK

Articles in refereed journals resulting in the work presented of this Thesis:

Jakova, E., and Lee, J.S. (2015). Superposition of an AC field improves the discrimination between peptides in nanopore analysis. Analyst *140*, 4813-4819.

AKNOWLEDGEMENTS

First and foremost, I would like to thank my academic mentor and supervisor Professor Jeremy S. Lee for the incredible opportunity to work as a graduate student in his lab. It has been a great three year journey full of excitement and stimulating moments. Thank you, Dr. Lee for your continuous support and precious advice, both academically and personally. Your passion for science, brilliant ideas, and imagination have inspired me to always look deeper and to pursue my goals even if initial outcomes were discouraging. Lastly, I would like to thank you for your encouragement to think creatively and to further improve myself as a scientist.

I would also like to thank all my committee members: Dr. Yu Luo, Dr. Oleg Dmitriev, and external member Dr. Peter Howard. I am grateful for their stimulating questions and academic suggestions. Overall, I am thankful for their support. I was lucky enough to take courses from both Dr. Luo and Dr. Dmitriev. I can truly say that through these courses I have learned a great deal about membrane .

Furthermore, I would like to thank my old and new lab members of Professor Lee's research team. Having you by my side has been a great pleasure and joy!

Finally, I would like to thank the Natural Science and Engineering Research Council of Canada (NSERC) and scholarships from the Department of Biochemistry's Devolved Scholarship Fund to Professor Lee for enabling me to pursue and achieve such results.

DEDICATION

I would like to dedicate this Thesis to my small Canadian family.

To my auntie, Pat Atkinson, for being a role model and showing me what a true strong, assertive, experienced and independent woman should be. In addition, for being a good friend and a good listener. Finally, I would like to thank her for teaching me that hard work always pays off and that sacrifices need to be made in order to achieve your goals.

To my uncle, Alfons Joseph-Paul Shoshi, for having tremendous patients with me and unconditional support. For teaching me the true meaning of the word perseverance and for having enormous faith in me. Lastly, for helping and being there for me every time and anytime I needed him.

TABLE OF CONTENTS

TITLE PAGES

LIST OF TABLES

TABLE PAGES

LIST OF FIGURES

FIGURE PAGES

LIST OF ABBREVIATIONS

ABBREVIATION	COMPLETE NAME
6-OHDA	6-hydroxydopamine
A10	Fmoc-$D_2A_{10}K_2$ peptide
A14	Fmoc-$D_2A_{14}K_2$ peptide
A18	Fmoc-$D_2A_{18}K_2$ peptide
A53T-YFP	A53T mutant labeled with yellow florescent protein
AC	Alternating current
AD	Alzheimer's Disease
α-HML	Alpha-Hemolysin
ALA	Alamethicin
ALS	Amyotrophic Lateral Sclerosis
AR-JP	Autosomal-Recessive Juvenile Parkinsonism
ARL	Aerolysin
AS	Alpha-Synuclein
βCB	β-Cyclodextrin
BS	Beta-Synuclein
CBD	Controlled Break-Down electrical cycles
CD	Circular Dichroism spectroscopy
CHEMFET	Chemical Field Effect Transistors
CJD	Creutzfeldt-Jacob Disease
ClyA	Cytolysin A
CNTs	Carbon Nanotubes
CSP-α	Cysteine String Protein-α
CWD	Chronic Waste Disease
DC	Direct current
DIB	Droplet Interface Bilayer
DLBs	Dementia with Lewy bodies
dsDNA	double stranded DNA

EM	Electron Microscopy
ENZYMEFET	Enzymatic Field Effect Transistors
FETs	Field Effect Transistors
FhuA	Ferric Hydroxamate Uptake component A
FIB	Focused Ion Beam
Fmoc	N-(9-fluorenyl)-methoxycarbonyl
G	Conductance
GNP	Glass Nanopore
GS	Gama-Synuclein
GWAS	Genome-wide association studies
HEPES	4-(2-hydroxyethyl)-1-piperazineethanesulfonic acid
HSP	Heat Shock Protein
I	Blockade current
IMMUNOFET	Antibody Field Effect Transistors
ISFETs	Ion Selective Field Effect Transistors
ITC	Isothermal Titration Calorimetry
l_{eff}	Effective membrane thickness
LBs	Lewy bodies
L-DOPA	L-3,4-dihydroxyphenylalanine
MAO-B	Monoamine oxidase B
MDs	Molecular Dynamics
MPD	2-methyl-2,4-pentanediol
MPPP	1-methyl-4-phenyl-4-propionoxypiperidine
MPTP	1-methyl-4-phenyl-1,2,3,6-tetrahydropyridine
MSA	Multiple-System Atrophy
MspA	Mycobacterium smegmatis porin A
NAC	Non-amyloid-β-component
NBIA	Neurodegeneration with Brain Iron Accumulations type 1
NfpA	*Nocardia farcinia* porin A
NfpB	*Nocardia farcinia* porin B
NMR	Nuclear Magnetic Resonance

pb_2Ba	positively charged presequences (pb_2) ribonuclease barnase (Ba)
PC	Personal Computer
PLK2	Polo-Like Kinase 2
PD	Parkinson's Disease
RI-A10	Retro-Inverse Fmoc-$D_2A_{10}K_2$ peptide
σ	Conductivity of the pore
S	Siemens
ssDNA	single stranded DNA
SDS	Sodium dodecyl sulfate
SN	Substantia Nigra
SNARE	Soluble N-ehtylmaleinide sensitive factor attachment receptors
T	Blockade time
TEM	Transmission Electron Microscopy
TNT	2,4,6-trinitrotoluene
Tween 20	Polysorbate 20
Wild Type	WT

1. INTRODUCTION

1.1 Introduction

The focus of this research involves superimposing an AC field onto an already existing DC field during nanopore analysis of various analytes (Stefureac et al., 2012). These include peptides, single-stranded DNA (ssDNA), α-synuclein (AS), and protein-drug complexes. It was previously shown that the addition of an AC field in a nanopore setup helped with understanding the behaviour of the pore (Ervin et al., 2008; Keyser, 2011; Lathrop et al., 2010; Sigalov et al., 2008; Sujatha et al., 2010). Recently published Molecular Dynamics (MDs) simulations have shown the strong influence that an AC field may have on the conformation of peptides and proteins (Astrakas et al., 2012; Budi et al., 2005; Toschi et al., 2009; Wang et al., 2014). The superposition of the AC voltage at a constant amplitude and different frequencies is presumed to cause the analytes to oscillate. As an analyte approaches the pore, the oscillation will lead to alterations of the event parameters, the blockade current (I) and the blockade time (T) (Lamichhane et al., 2013).

First, alpha-helical (α-helical) peptides with a fluorenylmethoxycarbonyl-capped group (Fmoc) on their N-termini, were studied because their electrophoretic DC behaviour is well documented (Chan and White, 2000; Perutz et al., 2002; Stefureac et al., 2006). Furthermore, all of these peptides have stable secondary structures, are negatively charged and are known to have diverse dipole moments that will cause them to rotate and oscillate differently in the presence of an AC field. A10 was initially studied in an AC field and was shown that the ration of bumping events increases with an increase of the AC frequency (Stefureac et al., 2012). AC studies were also conducted with AS — the protein involved in Parkinson's disease (PD) — and its three domains: N-terminus, C-terminus, and the ΔNAC. The behaviour of AS and its domains at an electrophoretic voltage of 100 mV has been previously investigated (Madampage et al., 2012; Tavassoly et al., 2014a). AS is an intrinsically disordered protein with a large negative net charge which, presumably, will lead to fast oscillation in an AC field (Goedert, 2001; Recchia et al., 2004; Ulmer et al., 2005). As well, studies were performed to observe conformational changes in AS-drug complexes in response to an AC field. Several drug analytes known to bind AS have been previously tested with nanopore analysis and isothermal titration calorimetry (ITC), and this information was useful in choosing the analytes for the

present study (Kakish et al., 2015a; Larkin et al., 2013; Tavassoly et al., 2014a; Tavassoly and Lee, 2012).

To summarize, this thesis will focus on combining a constant AC amplitude with different AC frequencies (in the MHz range) to elucidate the performance of different analytes and the strength of the binding of various drugs. This may help to develop a system that could explain the behaviour of analytes and complexes as they interact with the pore.

1.2 Single molecule biosensors

Nanopores are just one example of a biosensor. In 1956, Leland C. Clark described the concept of a biosensor (Clark, 1956). He discussed the development of an oxygen electrode (what is now called the Clark electrode) that would be inserted in the blood and tissue during cardiac surgery to observe and control the level of oxygenation. Six years later he improved the biosensor concept by expanding the range of analytes that could be tested, but most importantly he demonstrated how to make these biosensors more specific. The first biosensors were obtained by trapping glucose oxidase in a dialysis membrane on an oxygen electrode (Clark and Lyons, 1962). Throughout the '70s, different authors worked on improving and increasing the diversity of biosensors by manufacturing electrochemical, pH, potentiometric or conductometric sensors (Palchetti and Mascini, 2010).

Biosensors were manufactured and used in the '80s to observe the transport of different molecules through lipid membranes (Hall, 1986). Generally, a biosensor is a biological tool used for the detection of an analyte in a biochemical or biophysical experiment, which consists of a receptor, a transducer and the reader (Hall, 1988; Turner et al., 1987). The receptor is a biological component such as an antibody-antigen or enzyme-substrate incorporated and closely restrained in the transducer (Yamamoto et al., 1978). The transducer itself is a sensing device capable of converting the biological event into a processable output that is shown in the reader (Cooper and Hall, 1988). Biosensors have been designed and developed to work *in vivo* and *in vitro* and thus are ubiquitously used in cellular biochemistry and have revolutionized analytical technology (Koschwanez and Reichert, 2007; Notingher, 2007).

Biosensors are used in many disciplines. In medicine, they monitor the levels of drugs, hormones, sugars, antibodies and proteins in the body fluids of patients (Lowe et al., 1981; Sibbald et al., 1984). In industry, biosensors measure the levels of gas pollution, toxins, ions

and carbohydrates (Dorward and Barisas, 1984; Terry et al., 2005). In agriculture, they control the levels of nutrients in plants grown hydroponically (Albery et al., 1985). Biosensors have also been used for the detection of pesticides, herbicides and military poisons (Sassolas et al., 2012). Biosensors can be classified as molecular-, cellular- or tissue-based (Pancrazio et al., 1999). As shown in Figure 1, molecular biosensors make use of ion-selective channels, nucleic acids, antibodies and enzymes (Cheng et al., 1998; Cornell et al., 1997; Edman et al., 1997; Minami et al., 1991; Potyrailo et al., 1998).

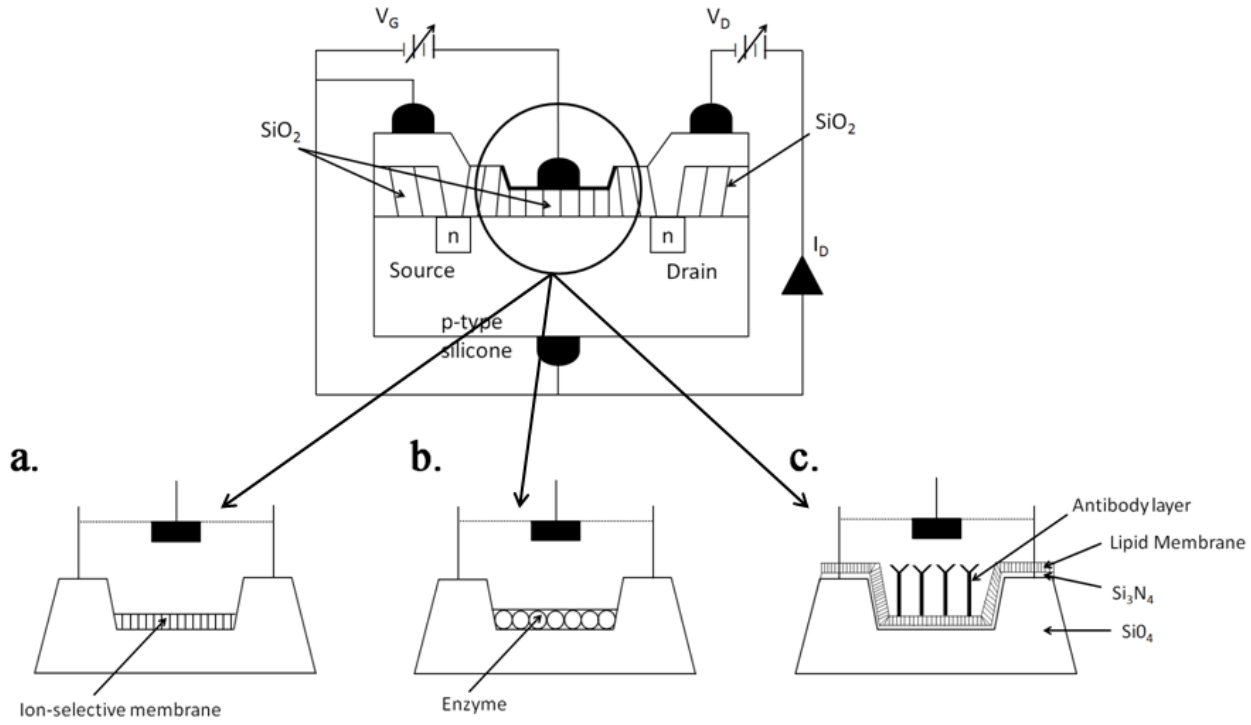

Figure 1.1 Types of cell-based potentiometric biosensors developed by incorporating different biological sensors at the gate of the Field Effect Transistor (FET). **a.** Ion-selective FET (ISFET); **b.** Enzyme sensor (ENZYMEFET) and **c.** Antibody-antigen binding sensor (IMMUNOFET). Reprinted and adopted with the permission from (Cooper and Hall, 1988).

Field Effect Transistors (FETs) are potentiometric sensors that convert biological reactions into electrical signals. Some Ion Selective ISFETs, such as quadruple-gate chemical FET (CHEMFET), are used during surgery (Sibbald et al., 1984). During a surgical procedure, biosensors measure the blood concentrations of Na^+, K^+, Ca^{2+} and H^+ in real time. Today, CHEMFETs have reached the same status as ion-selective electrodes that can simultaneously

detect many cations and anions. Some ISFETs are linked to an enzyme, but instead of measuring an enzymatic reaction, they measure cation levels. For example, when cross-linking penicillinase to a pH-FET, the production of penicillin is able to be measured by calculating the levels of H^+ (Caras and Janata, 1980). In contrast, a pH-FET can also be linked to an enzyme, which is known as an ENZYMEFET, to measure the rate of an enzymatic reaction. For example, incorporating the acetylcholinesterase enzyme into a pH-FET can enable the measuring of the direct levels of acetylcholine (Van der Schoot and Bergveld, 1988). As shown in Figure 1.1, the principle of IMMUNOFETs is to attach an antibody to the surface of the sensor to cause changes in the ionic current intensity. Two examples of IMMUNOFETs include a gate restrained anti-syphilis antibody and a gate restrained anti-albumin antibody on a FET sensor (Collins and Janata, 1982).

Cell biosensors, on the other hand, are used mostly for environmental and pollutant screening with different whole-cell receptors being used for different analytes (Horn and Marty, 1988). Cell-based biosensors utilize microorganisms, especially *Escherichia coli*, to detect compounds such as formaldehydes and chenodeoxycholic acid (Belkin et al., 1997). Cell fluorescence assays are used for high-throughput screening, especially in chemistry, biology and physics for qualitative distributions of subcellular proteins, nucleic acids and lipids (Dunn et al., 1994); cell metabolism biosensors, such as eukaryotic cells and neurons, are used in measuring the extracellular pH (Owicki and Wallace Parce, 1992). Intracellular and extracellular potential biosensors are used for monitoring cardiac impulses in different embryonic myocytes and estimating the levels of analytes, such as serotonin from the neurons of the visceral ganglion, in the common pond snail (Connolly et al., 1990; Skeen et al., 1990). Electrode impedance assays were used to monitor macrophages, endothelial cells, and fibroblasts (Kowolenko et al., 1990). Finally, multichannel recordings are used for fast and nonspecific measurements of different dications, like Ca^{2+} and Mg^{2+}, with multi-electrode arrays (Canepari et al., 1997). While the whole-cell receptor brought new advantages, other problems appeared. One problem with the multiple enzyme sensors was their lack of selectivity and specificity towards analytes (Pancrazio et al., 1999; Ziegler, 2000). For example, the use of multiple enzyme layers on carbon nanotubes (CNTs) has been used to detect different proteins or DNA strands. Recently, it was shown that such sensors attached on CNTs are able to detect

as few as 80 copies of DNA, but even though they are able to detect a small amount of DNA strands, they lack selectivity (Munge et al., 2005).

Tissue-based biosensors are used for detecting and measuring hazardous organisms in the environment and hormones in the human body for medical research. (Acha et al., 2010). As the name indicates they are based on a tissue that contains a protein that interacts with the analyte to be detected. There are two types of tissue biosensors: the biosensor in which the protein sensor is incorporated directly into the tissue, and the biosensor in which the protein is expressed by means of initially inserting a gene into this tissue. (Pancrazio, 2001; Reininger-Mack et al., 2002).

While biosensors have a large number of advantages, their main one is in their inexpensive preparation (Nankai et al., 1992). Additionally, some biosensors preserve their biological activity and can withstand buffer aggregation making them exceedingly reliable (Emregül, 2005). They also give out real-time results without needing to be cleaned through an analytical procedure (Xu et al., 2009). Furthermore, biosensors can be extremely selective and specific over a broad range of concentrations, and are able to resist decomposition, even after hours of experimentation (Haes and Van Duyne, 2002). Finally, the detection schemes often do not require fluorescence or additional labelling (Huang et al., 2008; Lee et al., 2012).

Biosensors also have considerable disadvantages when it comes to the use of FETs and ISFETs. Such disadvantages include electrical noise, external contamination, solution leaking across the gates of the sensor, destabilization of biomolecules after many hours of running, as well as possible aggregation of the biosensor in aqueous solutions. Nevertheless, this technology is constantly improving as the collaboration of physical, biological and computer sciences continues to evolve. However, there are still major biological issues with this technology that need to be resolved, such as the stability and reproducibility of the ISFETs *in vitro* (Meusel and Vering, 1998).

1.2.1 Cell membrane transporters

The nanopores used in this thesis are examples of transporters that facilitate transport of analytes across the membrane (see Figure 1.2 a. facilitated diffusion). Membrane transporters are based on two types of diffusion, down or against an electrochemical gradient. A summary of the major types of transporters is shown in Figure 1.2.

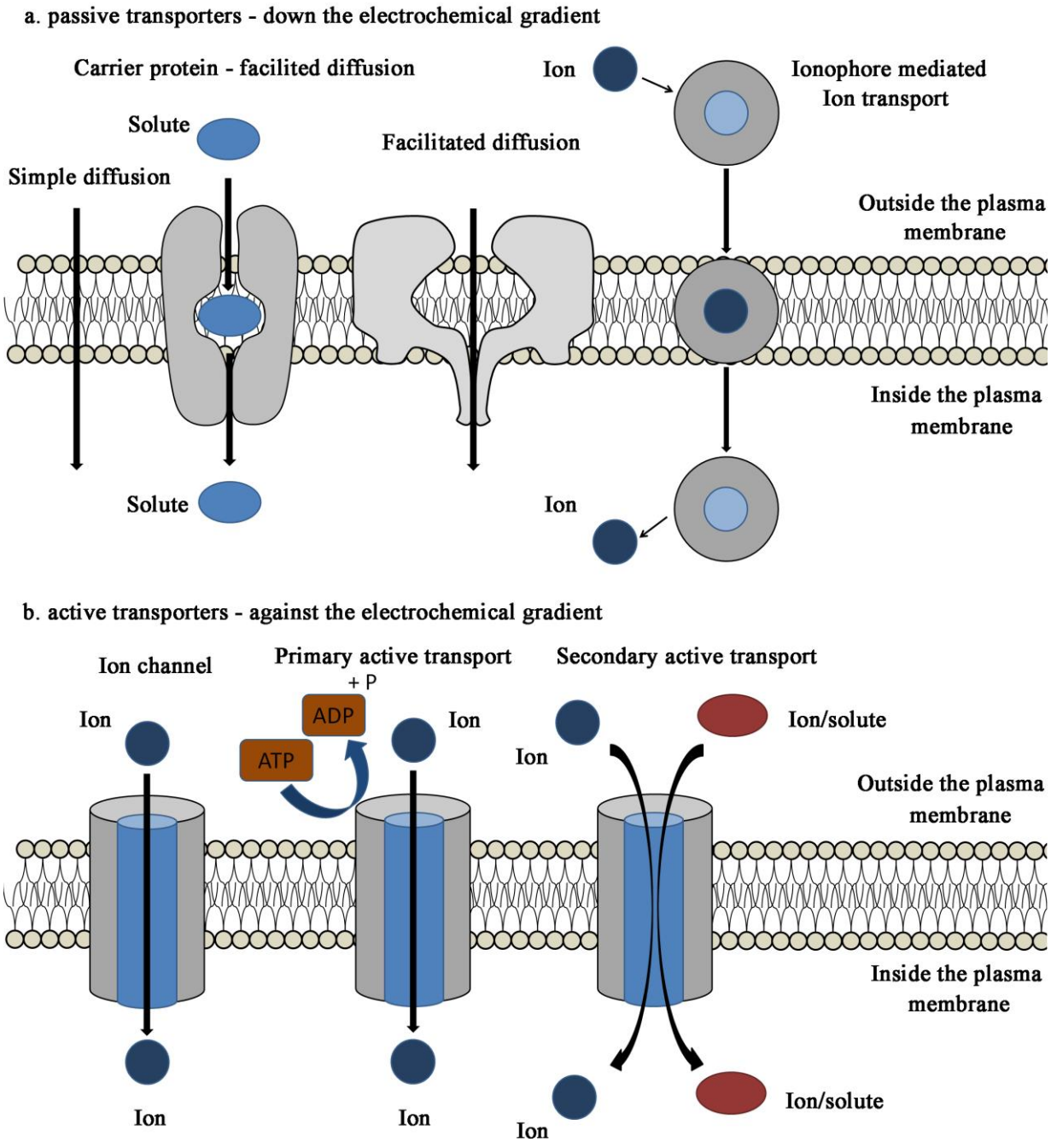

Figure 1.2 Summary of the different cell membrane transporters.

A small number of molecules, mostly non-polar molecules, can move across the cell membrane without a membrane-bound facilitator or transporter. Generally, transporters such as membrane proteins and/or ion channels facilitate the diffusion of larger, polar or charged molecules down their electrochemical gradients (Mulder, 1996). Glucose, sodium and

potassium ions are examples of molecules whose transport is facilitated across the cell membrane. Transporters that move ions and molecules against their concentration and/or electrochemical gradients require energy. That is why this form of transportation is called "active" (Lennernäs et al., 1996). Primary active transporters usually obtain their required energy for the movement of solutes from ATP hydrolysis, as in the case of the Na^+/K^+ and the proton-ATPase pumps, such as multiple drug resistance transporters. Secondary active transporters obtain their required energy by transporting one analyte down its electrochemical gradient; the energy released by the transportation of this analyte is used to power another analyte to move against its electrochemical gradient. These are classified as cotransporters which are divided into two groups: (a) symporter such as the Na^+/glucose (both analytes are transported in the same direction) and (b) antiporter such as the Na^+/Ca^{2+} (the analytes are counter-transported) (Gouaux and MacKinnon, 2005; Morth et al., 2011; Nelson et al., 2008).

As mentioned, simple diffusion requires an ion-channel (Janshoff and Steinem, 2006; Kasianowicz et al., 1996). Ion channels are transmembrane proteins with apertures that can be adjusted by a chemical, biochemical or electrical stimulus (Hille, 2001). They were initially found in neurons. These channels differ from ion pumps in three ways: (a) the ionic flux of these channels is greater than the flux of the pumps; (b) the ion channels cannot be saturated; and (c) these channels can be gated by aptamers, such as single-stranded RNA (ssRNA) and ssDNA molecules, or other ligands (Nelson et al., 2008). Recently, simple channels have been co-opted to develop single molecule biosensors (Baaken et al., 2011; Jetha et al., 2009). These single molecule biosensors are water-soluble polypeptides that self-assemble into a pore that has an internal diameter from 1 to 2 nm. Combining protein engineering, chemical modification and the ability to control the open pore via a voltage stimulus, these pores can be called target-responsive biosensors (Bayley and Cremer, 2001). Due to their small scale that is measured in nanometers, these pores are called nanopores (Murray, 2008). There are many advantages to these analytic pores, including their ability to analyse small molecules.

Overall, the focus of this thesis will be on biological pores used for analysis. These pores are usually simple channels that allow facilitated diffusion of ions and other small molecules, such as nucleic acids, DNA fragments, peptide, small protein and protein/drug complexes down an electrochemical gradient.

1.3 Nanopore Technology

Many methods are being developed for single molecule detection. A major part of this technological growth is due to the ability to stabilize nanopores with new capabilities, functions, and properties involved in the detection and imaging of single-molecule sensing (Huang et al., 2007). Nanopores are single-molecule Coulter counters a method invented by Coulter in the early 1950s, which consist of a nanometre aperture through an insulating membrane (Coulter, 1956). Applying a voltage across this membrane results in an electrochemical gradient that drives ions through the nanopore (Bayley and Martin, 2000; Howorka and Siwy, 2009). The use of these nanopores dates back nearly twenty years (Kasianowicz et al., 1996). A variety of self-assembling bacterial pores and solid-state pores have been investigated, but perhaps the most popular of these is the α-hemolysin (α-HML) toxin derived from *Staphylococcus aureus* (Jetha et al., 2009). This gave birth to a new method for detecting single molecules in a real-time screening technique known as nanopore analysis (Gu and Shim, 2010).

1.3.1 Fundamentals of Nanopore analysis

Nanopore analysis is a method that is influenced by environmental factors such as temperature and pressure, but it yields rapid, sensitive and reliable results (Cooper and Hall, 1988). The rapid results are due to the use of an immobilized device which is fitting for real-time monitoring and analysis of different conformations (Branton et al., 2008). In contrast, techniques like Nuclear Magnetic Resonance (NMR) may not be suitable for studying multiple analyte conformations. Similarly, X-ray crystallography cannot be used to study intrinsically disordered proteins. Therefore, understanding the dynamics and folding of these analytes at a molecular level may only be possible using nanopore technology. The most important advantage of nanopore sensing is that molecules can be detected without labelling. Uniquely, this technique requires less than an hour to non-destructively analyze thousands of single molecules (Wanunu et al., 2009).

A lipid bilayer is stretched across a small opening that separates two chambers. A pore is then inserted into the membrane and, upon application of a voltage, an ionic current (measured in picoampere (pA)) will be recorded. Any large molecule, such as a peptide or a protein that interacts with the pore, will cause a drop in the current for a time, which is measured with a

patch clamp apparatus (Lamichhane et al., 2013). In most cases, three types of events can be observed. The ideal case will have only translocations, but bumping and intercalation events are frequently encountered. These events are shown in Figure 1.3: (a) Translocation events, where the analytes go through the pore, causing a large current blockade; (b) Intercalation events, where the analytes are trapped in the entrance of the pore, and will diffuse back after a period of time, causing an intermediate current blockade; and (c) Bumping events, where the molecules approach the pore, but then diffuse away without entering, causing a small current blockade (Christensen et al., 2011; Meng et al., 2010).

Initially, this technology was applied to nucleic acids and has advanced to the level that rapid DNA sequencing with nanopores is now available (Schneider and Dekker, 2012). More recently, peptides and proteins have been studied (Mohammad and Movileanu, 2008; Stefureac et al., 2006). The application of nanopore analysis for sequencing proteins may be decades away, but this technology has proved to be useful for studying protein folding. For example, (a) Initial analysis of A-β peptides, which are deposited as amyloid plaques in Alzheimer disease (Zengin et al., 2013); (b) AS, which is implicated in Parkinson disease (Tavassoly et al., 2014a); and (c) Prion proteins, which misfold in transmissible spongiform encephalopathy (Chiti and Dobson, 2006; Madampage et al., 2012).

One disadvantage of alpha-hemolysin (α-HML) pores is that they have a small transmembrane opening of 1.5 nm and, thus, even small proteins will not translocate and often only give rise to bumping events. Unfortunately, bumping events are very rapid with small blockade currents and result in very little discrimination between proteins (Simon and Blobel, 1992). In 2004, the Lee group published the first paper for nanopore-based peptide analysis (Sutherland et al., 2004). It was shown that the peptide's structure was able to be studied with the help of α-HML. Several peptides with a collagen-like sequence $(G\text{-}P\text{-}G)_n$ (n= 1 P1, n=2 P2, and n=3 P3) that were end labelled with ferrocene were analysed in the standard set up at 100 mV DC. The peptides with more collagen repeats were shown to give larger blockade currents and blockade times. From the analysis of the blockade histograms and scatter plots, it was shown that nanopore analysis had the ability to differentiate these peptides based on their conformations (single, double and triple helix). Since then, other pores have been investigated.

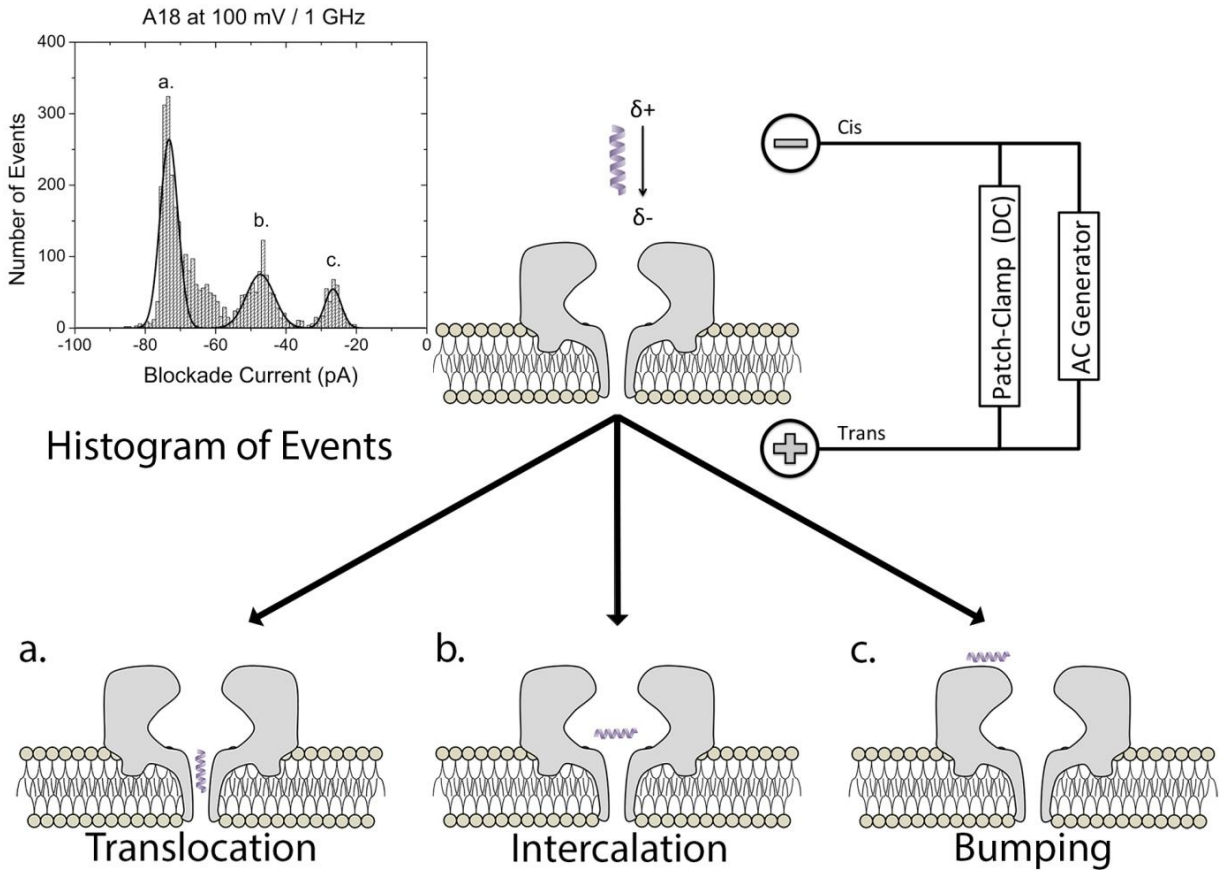

Figure 1.3 There are three possible types of events when a peptide interacts with α-HML pores. The AC voltage causes peptides to oscillate at the entrance of the pore.

1.4 Structure of Alpha-Hemolysin and other protein pores

Nanopores can be biological or synthetic. Most of the pores used for biosensing are protein ion channels. With a rigid conformation, these pores give reliable and repeatable results. Several protein nanopores can be used in nanopore analysis, such as aerolysin (ARL) derived from *Aeromonas hydrophila*, ferric hydroxamate uptake component A (FhuA), Cytolysin A from *Salmonella typhi* (ClyA) or hetero-oligomeric pore from *Nocardia farcinica* porin A (NfpA) and porin B (NfpB). Nevertheless, most of this work has been done using an α-HML pore (Mohammad et al., 2012; Singh et al., 2012; Soskine et al., 2013). For example, analytes such as collagen-like peptide, AS and mutants, β-Amyloids and barnase were analyzed with α-HML (Madampage et al., 2012; Mohammad et al., 2008; Sutherland et al., 2004; Wang et al., 2011). However, cationic peptides were analyzed with the NfpA and NfpB (Singh et al., 2012). Lysozyme, human thrombin, and bovine thrombin were analyzed with ClyA (Soskine et

al., 2012). Lastly different lipids (e.g. 1-lauroyl-2-hydroxy-sn-glycero-3-phosphocholine) were analyzed with FhuA (Mohammad et al., 2012).

Some of these protein pores have been modified via protein engineering for various uses in biochemistry and biotechnology (Bayley, 1997, 1999). These modified pores could help detect molecules that cannot be analyzed with a standard nanopore and, thus, improve the detection levels of cytotoxic agents (Gu et al., 2001; Panchal et al., 1996). In some cases, a receptor is attached in the lumen of the ion-channel via protein engineering or chemical adjustment. For example, β-Cyclodextrin (βCB), a noncovalent molecular adapter, can be inserted into either the wild-type (WT) or mutant α-HML pore lumen (Bayley and Jayasinghe, 2004; Gu and Bayley, 2000).

α-HML is a self-assembling bio-pore that inserts into a lipid bilayer, giving a structure with reproducible dimensions and surface properties (Jetha et al., 2009). α-HML derived from *Staphylococcus aureus* is a monomeric protein with a molecular mass of approximately 33 kDa and a length of 293 amino acids (Bayley, 1995). It is soluble in water and also very toxic to mammalian erythrocytes, lymphocytes and endothelial cells (Bhakdi and Tranum-Jensen, 1991). The crystal structure of α-HML solved in the late 90's was revealed to be a heptameric transmembrane protein that resembles a mushroom (Gouaux, 1998; Song et al., 1996). A more recent crystal structure was published January 2011 (Tanaka et al., 2011). These two studies, revealed that each pore-forming monomer comes together seven times in a noncrystallographic axes (Galdiero and Gouaux, 2004). Initially, the monomer is bound to the bilayer where a heptameric pre-pore is eventually formed. Afterwards, a stem grows and penetrates the membrane bilayer, resulting in a membrane-bound heptameric pore (Aksimentiev and Schulten, 2005; Montoya and Gouaux, 2003; Walker et al., 1992).

The crystal structure, as shown in Figure 1.4, revealed that α-HML is composed of three domains: the cap (10 nm in outer diameter and *cis*-opening 2.6 nm), the rim (7 nm long and 3.7 nm wide from the stem) and the stem (5.2 nm in height and diameter 2.6 nm with a *trans*-opening around 2 nm) (Song et al., 1996). The cap domain is surrounded by seven β-sandwiches. The rim domain, located below the cap, has four β-strands. Lastly, the stem is constructed by fourteen antiparallel β-strands, which form a β-barrel (Tanaka et al., 2011). The interior architecture is very interesting. The channel through which the analytes pass varies in width. It starts at 2.6 nm in the *cis* side opening, which is followed by a large 4.6 nm gap in the

vestibule and then by a narrow 1.5 nm region just after the vestibule. The width of the stem is mostly constant at ~2 nm, but slightly larger at the end of the *trans* side, where it is 2.6 nm, similar to the *cis* side (DeGuzman et al., 2006; Wu et al., 2014).

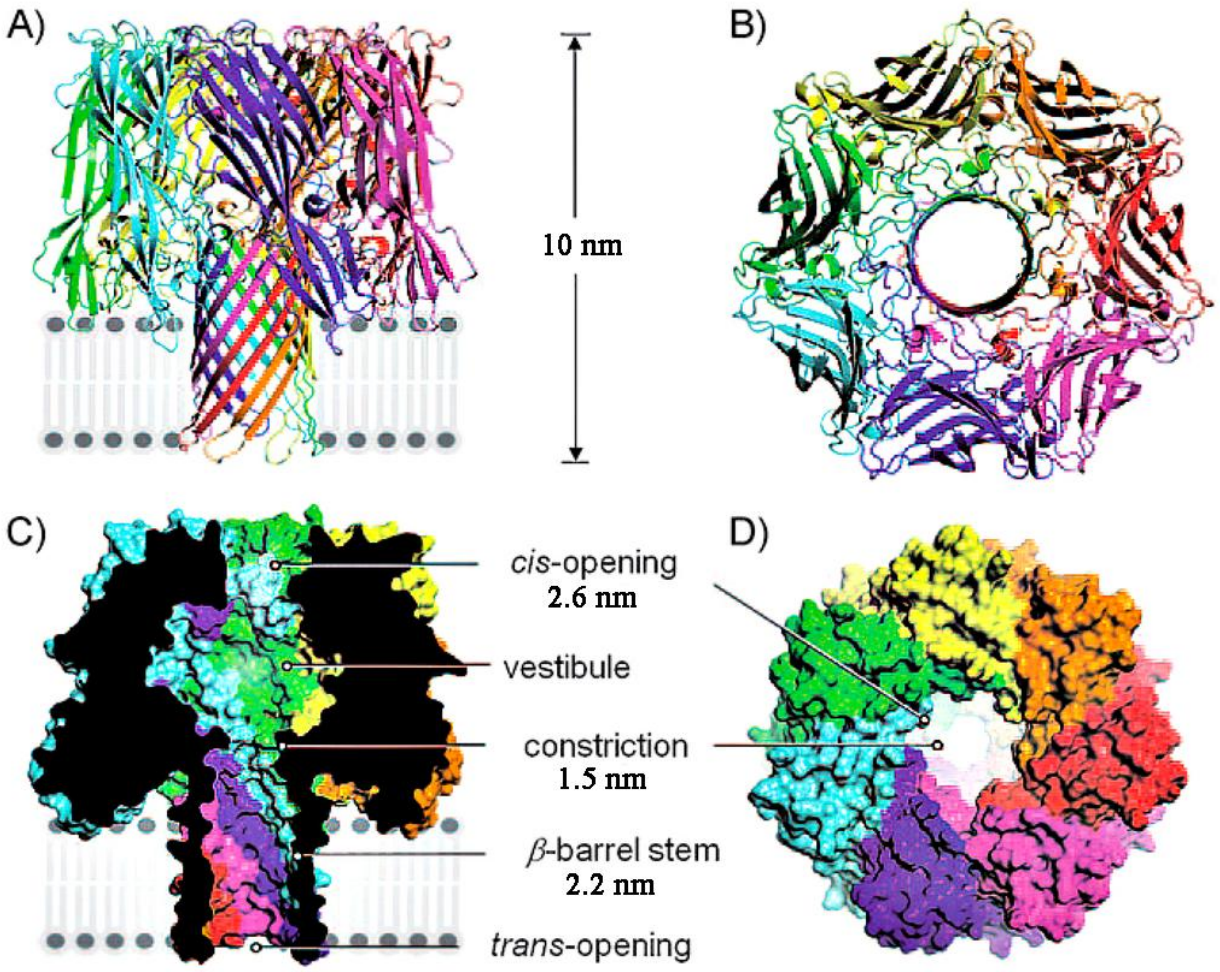

Figure 1.4 A. Side and **B.** Top view of α-HML in the lipid bilayer. **C.** and **D.** Cross section of the pore with the corresponding parameters of the vestibule, the rim and the stem. Reprinted and adapted with the permission from (Ma and Cockroft, 2010) Copyright © 2010 WILEY-VCH Verlang GmbH & Co. KGaA, Weinheim. All rights reserved.

α-HML, being a pore with reproducible dimensions and surface properties, is often used in nanopore analysis. Under an applied DC voltage of 100 mV, each inserted channel has a current of 100 pA. Once a pore is inserted, it can remain intact for hours in 1 M KCl. The pore can operate within a wide pH-range (2 to 12), but optimal conductance levels, with negligible background noise, are obtained at pH values between 7.5 to 8 (Kasianowicz and Bezrukov,

1995). The ionic current passing through the pore channel is detected with patch-clamp instruments. The large vestibule helps analytes to orientate before they enter the pore. The amino acids in the interior of the lumen (e.g. valine, isoleucine, leucine, phenylalanine, tyrosine and threonine) create a very hydrophobic environment, which facilitates the passage of anions and biological molecules (Song et al., 1996; Venkatesan and Bashir, 2011).

An example of another self-assembling pore is ARL (Degiacomi et al., 2013; Howard and Buckley, 1986; Wilmsen et al., 1990). Even though there is not yet a full crystal structure for the ARL pore, high-resolution Electron Microscopy (EM) has shown that the diameter of this pore is smaller than the α-HML pore as shown in Figure 1.5 and 1.6 (Parker et al., 1994).

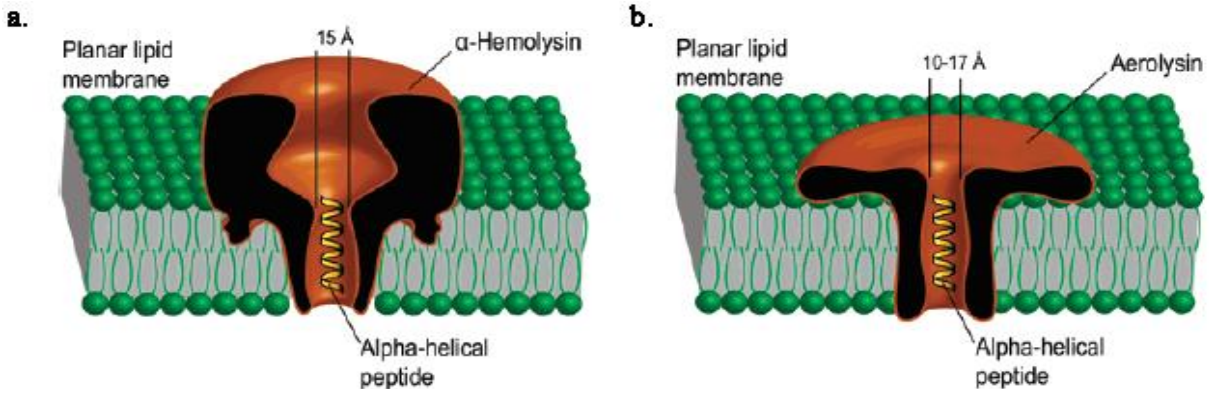

Figure 1.5 Graphic representation of the two bacterial pores inserted in a lipid bilayer while an α-helical peptide is passing through the stem of the pore. **a.** α-HML and **b.** ARL. Reprinted with the permission from (Stefureac et al., 2006). Copyright © 2006 American Chemical Society. All rights reserved.

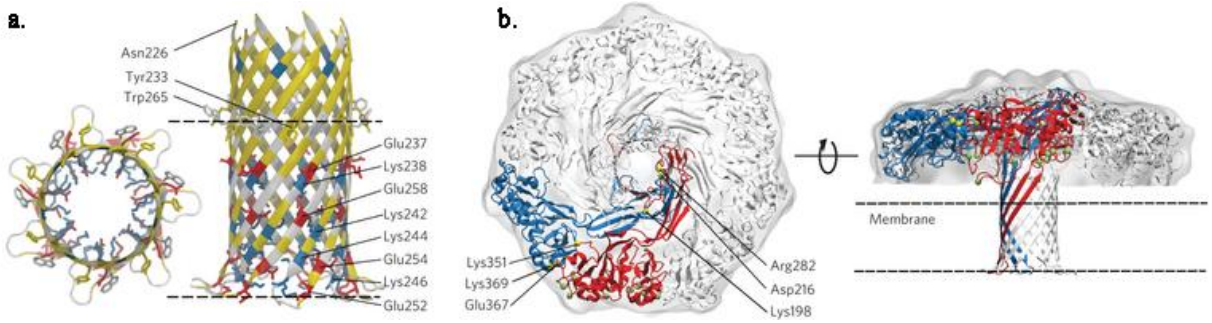

Figure 1.6 a. Schematic structure of the aerolysin stem. **b.** Top and side view from cryo-EM map of the 3D model of the heptameric pore. Reprinted with the permission from (Degiacomi et al., 2013) Copyright © 2013, Nature Publishing Group. All rights reserved.

The ARL pore lacks a vestibule, which in other pores may be helpful for aligning molecules towards the pore entrance. Additionally, this pore has a smaller constriction and longer stem (see Figure 1.6), which makes this pore a poor choice for analyzing long and/or bulky analytes as a greater number of bumping events will be observed (Degiacomi et al., 2013; Moniatte et al., 1996). Therefore the smaller open pore current of 50 pA for ARL is consistent with its smaller size compared to α-HML (Stefureac et al., 2006).

Currently, there is another biological nanopore being investigated especially for DNA sequencing: Mycobacterium smegmatis porin A (MspA) (Faller et al., 2004). As seen in Figure 1.7, MspA is a 9.6 nm long pore that has an external diameter of 8.8 nm and a *cis* diameter of 4.8 nm. The pore may be more useful than α-HML because it has a much smaller vestibule, a thick rim and a 1.2 nm opening on the *trans* side of the pore. With such a larger diameter, MspA has a higher conductance than α-HML, ~4.9 nS for MspA and ~1 nS for α-HML in a 1 M KCl solution, because the conductance is proportional to the square of the diameter.

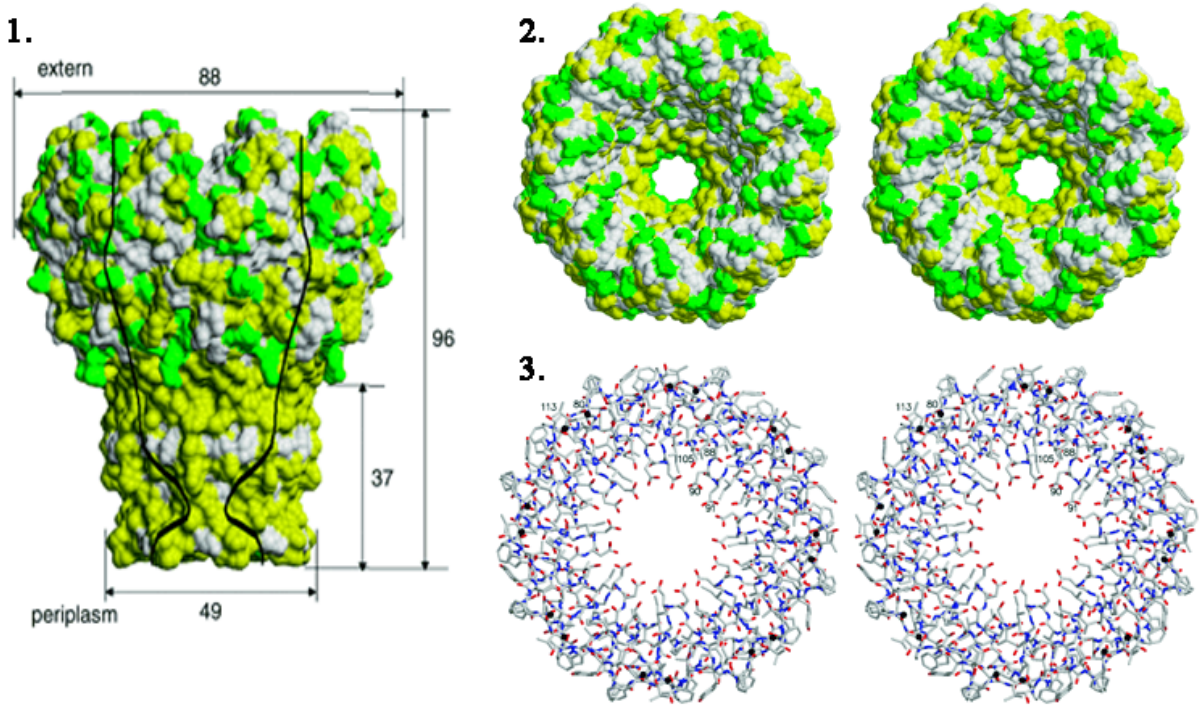

Figure 1.7 3D details of the outer surface (yellow = nonpolar region and green = polar region) of the MspA (**panel 1**) and its vestibule (**panel 2**) as well as a 1.9 times magnified version in atomic details of the pore vestibule. Reprinted and adopted with the permission from (Faller et al., 2004) Copyright © 2004 American Association for the Advancement of Science. All rights reserved.

In addition, even though the natural MspA looks very promising for DNA sequencing because of its shape and *cis* diameter, the negative charges at the constriction will prevent ssDNA from translocating (Manrao et al., 2011). For this reason, MspA was modified into M1-MspA, via protein engineering, to improve translocation. Three negatively charged aspartic acids residues were replaced with neutral asparagines residues, to allow the translocation of ssDNA (Butler et al., 2008).

Two other examples of nanopores include the glass membrane nanopore (GNP) (Figure 1.8 a) and droplet interface bilayers (DIB) (Figure 1.8 b). The GNP is supported over a lipid bilayer in an aqueous solution, whereas the DIB is formed in an oil solution (Bayley et al., 2008). Before the optimal GNP was produced there were a lot of problems with leakage from the glass surface (Fertig et al., 2002; White et al., 2007). GNPs are fabricated by adhering a platinum wire in a glass capillary, which serves as the electrode, and smoothing the capillary until the platinum disk is in the nanometer range (Zhang et al., 2007). The GNP was surrounded by 3-cyanopropyldimethylchlorosilane to create a hydrophobic surface; and afterwards, a second layer of lipids was painted on both the interior and exterior glass surfaces, forming an extraordinarily stable bilayer. The bilayer is known to last up two weeks at room temperature and resists voltages up to 800 mV. Furthermore, ion channels such as α-HML can uniquely be removed by applying a small pressure to the bilayer which will disrupt the stability of the membrane.

In contrast, the DIB is a complex of two water droplets in a lipid suspension as shown in Figure 1.8 b (Funakoshi et al., 2006; Gu and Shim, 2010; Tsofina et al., 1966). It is manufactured by inserting a droplet of aqueous solution in the lipid phase, thus forming a layer of droplet-lipid interfaces. Secondly, the two droplets are manufactured to communicate with each other and their lipids layers fuse into a bilayer on the interface, thus giving them the name droplet interface bilayers. Lastly, different proteins channel are added to monitor analytes in the aqueous solution (Holden et al., 2007).

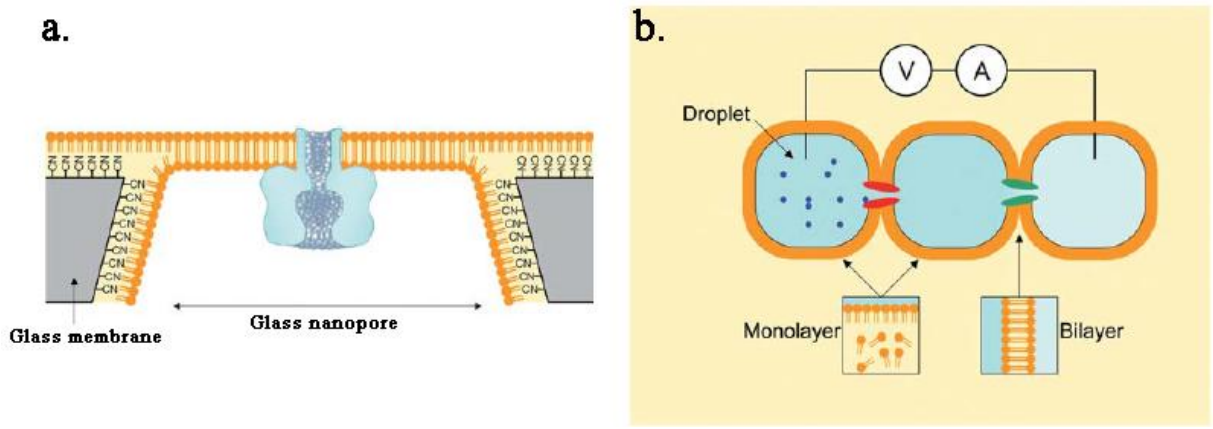

Figure 1.8 Other forms of nanopores. **a.** Inclusion of a biological pore in a lipid bilayer that is hanging over a glass nanopore. **b.** Droplet interface bilayer and its network. Reprinted and adapted with the permission from (Gu and Shim, 2010) Copyright © 2010 The Royal Society of Chemistry. All rights reserved.

1.4.1 Other mutants of Alpha-Hemolysin

The use of α-HML in nanopore analysis for certain analytes is limited due to the small cis opening, as well as the highly hydrophobic interior that acts as a barrier to bulky and/or polar molecules. To improve translocation, one possible solution would be to mutate α-HML. To date, many successful mutants of α-HML have been made. A different bioengineered version of α-HML was obtained by altering seven residues of methionine at the 113 position of the pore lumen to phenylalanine, M113F (Guan et al., 2005). The new pore has aromatic side chains that interact with organic and aromatic molecules. Additionally, this pore enhances the denaturation of short DNA duplexes (Gu and Bayley, 2000; Gu et al., 2001). The military might find this altered version of the pore very useful in distinguishing 2,4,6-trinitrotoluene (TNT) from other nitroaromatic molecules on the basis of the event parameters. This new way of stochastically detecting TNT, may also be useful for distinguishing hidden explosives and other terrorist agents (Guan et al., 2011; Guan et al., 2005). Biochemists have found this mutated pore helpful to elucidate noncovalent interactions between aromatic molecules and to detect metal ions (Braha et al., 1997). Additionally, an engineered version of α-HML called H5 — named because its five amino acids between the 130-134 position were replaced with histedines — was used to transport trehalose inside the membrane of mammalian cells (Eroglu et al., 2000; Walker et al., 1994). Intracellular trehalose, in very low concentration, has been shown to increase the survival of these cells during cryopreservation.

In 2008, the Movileanu laboratory engineered three successful versions of α-HML. The first was made by changing seven amino acids of the trans opening to aspartic acid residues ($K131D_7$), the second by making the same mutation at the constriction site of the pore ($K147D_7$) and the last one by combining the two mutations together ($K131D_7/K147D_7$) (Mohammad et al., 2008). The lab was able to determine that pb_2Ba (a designed protein with a positively charged sequence, pb_2, and a ribonuclease barnase, Ba) interacts with the new α-HMLs, giving different blockade currents related to the presence of electrostatic blockades. An additional alteration involves the building of an aptamer by binding the Cys^{17} amino acid of the pore lumen to an oligonucleotide via disulfide bonds (Rotem et al., 2012). βCD is another aptamer that is inserted into the α-HML WT or one of its mutants. It is widely used in detecting organic analytes, proteins, DNA and therapeutic agents (Howorka et al., 2001; Movileanu et al., 2000; Nimjee et al., 2005). Many pharmaceuticals are not only distinguished but can be quantified when bound to βCB, even though stochastic detection of these drugs could also be possible using direct mutagenesis of the pore without the help of an aptamer (Gu et al., 1999). For example, an antidepressant, such as imipramine, can be distinguished from a first-generation antihistamine, such as promethazine, by comparing the blockade time histograms (Asandei et al., 2011).

1.4.2 Solid state pores

Alternatively, synthetic nanopores can be made using nanotechnology (Li et al., 2001; Storm et al., 2003). Control over the nanopore size is crucial for the analysis of various analytes. As pointed out from the description of the α-HML structure (see Figure 1.8), the 1.5 nm constriction acts as a boundary for the translocation of globular proteins and double-stranded DNA (dsDNA) (Tanaka et al., 2011). Furthermore, α-HML, as well as all the other biological pores, are very sensitive to changes in pH, temperature, buffer and salt concentrations as well as background noise. In the late 90's, constructed metal nanotube membranes were capable of transporting selective ions (Nishizawa et al., 1995). This technique didn't meet expectations because of the continuous clogging observed once an analyte was inserted.

In the early 2000s, many groups started fabricating different sized nanopores in silicon and silicon nitride membranes (Kim et al., 2006; Li et al., 2001; Storm et al., 2003). Solid-state

pores are manufactured by focussing electron or ion beams onto synthetic membranes using techniques like (a) Transmission Electron Microscopy (TEM) or (b) Focused Ion Beams (FIBs) (Ayub et al., 2010). By altering the intensity of the two beams, it is possible to control the size of the pore in real time. These solid-state pores were shown to allow more control over both the diameter and the channel length depending on the synthetic membrane chosen. An additional advantage was that solid-state pores are more stable and have the option of incorporation into robots and arrays (Dekker, 2007).

Conversely, these solid-state pores have several disadvantages. For example, with solid-state pores crafted in silicon nitride membranes, it is difficult to create a precise pore size (Janshoff and Steinem, 2006; Oukhaled et al., 2011). Additionally, even though it is a precise technique, it is very difficult to attain small pores unless the membrane is really thin, in the 50 nm range (Patterson et al., 2008). The background noise would also interfere with recording the ionic current when the experiment is running, which will lead to uncertainty and difficulties in processing and analyzing the data.

Recently, a new technology was developed that has shown promising results in decreasing the electrical noise, as well as enabling more precise control of the pore diameter (Eric et al., 2012). The technique uses controlled break-down electrical cycles (CBD). Applying repeated high electric fields to silicon nitride membranes in an aqueous solution creates the pore. The apparatus is an electrically engineered modification of EM. Other than that, it uses the same low-pass filter as would be used in a standard protein nanopore experiment. The formula below describes how to calculate the diameter of the pore when the other parameters from previous calculations are already known or are discovered during the running of the experiment (Eric et al., 2012; Stefan et al., 2011).

$$G = \sigma \left\lfloor \frac{4l_{eff}}{\pi d^2} + \frac{1}{d} \right\rfloor^{-1} \rightarrow d = \frac{G}{2\sigma} * \left(1 + \sqrt{1 + \frac{16\sigma l_{eff}}{\pi G}} \right)$$

The thickness of the membrane (l_{eff}) and the conductivity of the cylindrical pore in a buffer solution (σ) are constant values, which are based on the previous literature and the purchased membrane (Stefan et al., 2011). The conductance (G), measured in Siemens (S), is calculated by knowing the voltage applied (V) and the ionic current (I). This is made possible by optimizing the voltage and the intensity of the current. Finally, these pores not only will have different sizes for analyzing many molecules but also are very functional due to their low

level of noise. The CBD technique was successfully replicated in December 2013 in Saskatoon with two solid pores at 1.14 nm and 2.70 nm. No further work has been undertaken on this project since that time.

A new technique for sequencing ssDNA makes use of graphene nanogaps (Schneider et al., 2010). This new solid-state nanopore will lead to the faster detection of the chemical nature of the nucleotides (Akca et al., 2011; Postma, 2010). This technique is still being developed, but, it has been shown to be a very promising sequencing tool.

1.4.3 Superimposing an AC field on a standard Nanopore analysis

In 2012, Radu Stefureac, working in the Lee Lab, discovered that the application of an AC voltage on top of the electrophoretic DC voltage improved the discrimination between peptides (Stefureac et al., 2012). It was observed that in a DC field, peptides with small dipole moments produce more bumping than peptides with large dipole moments since the former don't orient as quickly. It was shown that it is difficult for the smaller peptides to orient in the lumen and translocate through the pore (Stefureac et al., 2006). It was hypothesized that the AC voltage would interact with peptide's dipole moment at the pore vestibule, which would prevent molecules with large dipoles from translocating. In other words, nanopore analysis could now be used to discriminate molecules based on their dipole moments (Stefureac et al., 2012). An AC voltage with different MHz frequencies was applied using an HP 8662A signal generator. The time scale for events is in the ms range that coincides with KHz frequencies. Thus, only frequencies above 10 MHz were attempted. As well 500 MHz was the upper limit of the generator. Many different combinations of AC frequencies and amplitude were tested. It was found that an amplitude of 200 mV AC voltage imposed over a constant DC voltage caused molecules with small dipole moments to enter the pore more easily compared to molecules with large dipole moments for frequencies from 10-500 MHz (Stefureac et al., 2012). A complete view is shown in Figure 1.9.

The AC voltage in this thesis was conducted with an HP E4420B (ESG-A Series Analog RF Signal Generator) where the upper limit of the generator was 2 GHz. Higher AC frequencies of 1.5 GHz and 2 GHz showed no significant changes in the blockade current histograms of the α-helical peptides and so 1 GHz was chosen as the highest frequency.

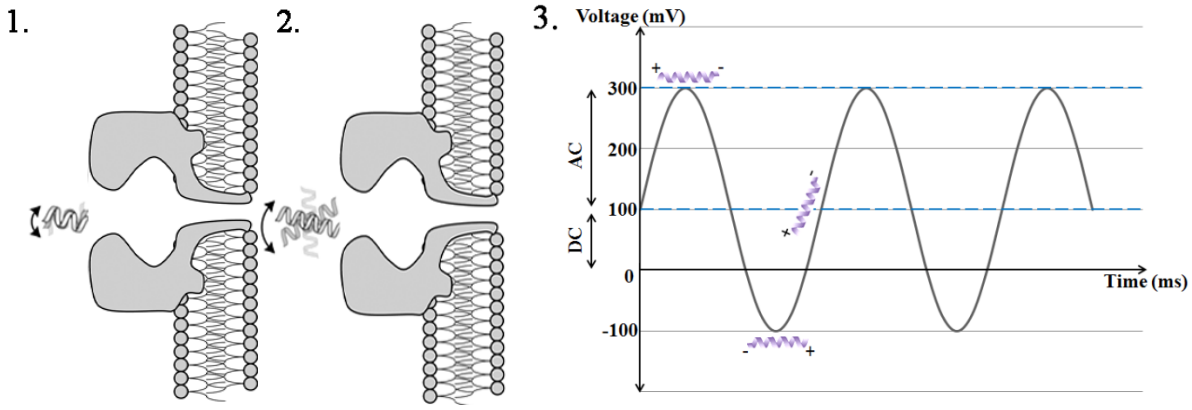

Figure 1.9 Cartoon showing that short peptides with smaller dipole moments rotate slower in an AC field (**panel 1**) and can enter the pore more easily than long peptides with larger dipole moments which rotate faster (**panel 2**). Changes in peptide orientation according to the AC frequency (**panel 3**). Adopted with permission from (Stefureac et al., 2012) Copyright © 2012 The Royal Society of Chemistry. All rights reserved.

1.5 Peptides and small molecules

Nanopore analysis has been used for analytical studies for over two decades with multiple small molecules such as RNA (Venkatesan and Bashir, 2011), DNA (Schneider and Dekker, 2012), peptides (Christensen et al., 2011; Stefureac et al., 2006), small proteins (Stefureac et al., 2008), protein-drug complexes (Tavassoly et al., 2014a); and antibodies (Larkin et al., 2013). The use of nanopores for DNA sequencing was first theorized in 1995, and first published in 1998 (Church et al., 1998). The hypothesis at that time was that by inserting a ssDNA molecule into a bacterial pore, such as α-HML or MspA, the drops in the ionic current would depend on the nucleotide passing through. Thus, detailed features of the current trace would reveal the sequence of the ssDNA.

The first successful experiment in detecting ssDNA in the α-HML pore was achieved in 1996 (Kasianowicz et al., 1996). It proved that sequencing of nucleic acids is possible in a nanopore. Peptides and proteins have been studied in nanopore analysis as well. Many sequences have been studied showing that peptide properties like size, net charge, structure, hydrophobicity, and topology are crucial to understanding the behaviour of peptides in the nanopore setup. The observation of patterns in the current traces and processed results, of the different peptides, has led to a better understanding and interpretation of what might happen when a peptide interacts with the pore (Christensen et al., 2011; Krasniqi et al., 2012). Examples of such peptides include Fmoc-capped α-helical and collagen-like peptides (Stefureac

et al., 2006; Sutherland et al., 2004); β-harpin peptides (Goodrich et al., 2007) and Zn-finger peptides (Stefureac and Lee, 2008).

Additionally, many proteins have been tested in nanopore analysis: histidine-containing proteins (Mereuta et al., 2012), myelin basic protein (Baran et al., 2010), maltose-binding protein and prion proteins (Krasniqi and Lee, 2012; Madampage et al., 2010). Nevertheless, there are still several other proteins with either no charges in their termini or with a positive net charge that cannot be steered electrophoretically into a biological nanopore and are therefore difficult to study (Madampage et al., 2010; Stefureac et al., 2008; Stefureac et al., 2010; Zhao et al., 2009). It is still difficult to predict how a small molecule will behave in a nanopore. It might be a simple electrophoretic motion, electroosmotic flow or controlled diffusion. Correlating the effect of the voltage on the translocation values, T and I, remains complicated.

1.5.1 Structure and properties of peptides

The work conducted with the Fmoc-capped α-helical peptides, with general formula Fmoc-$D_xA_yK_z$, and a maximum length of 44.5 Å, dates back almost a decade (Stefureac et al., 2006).

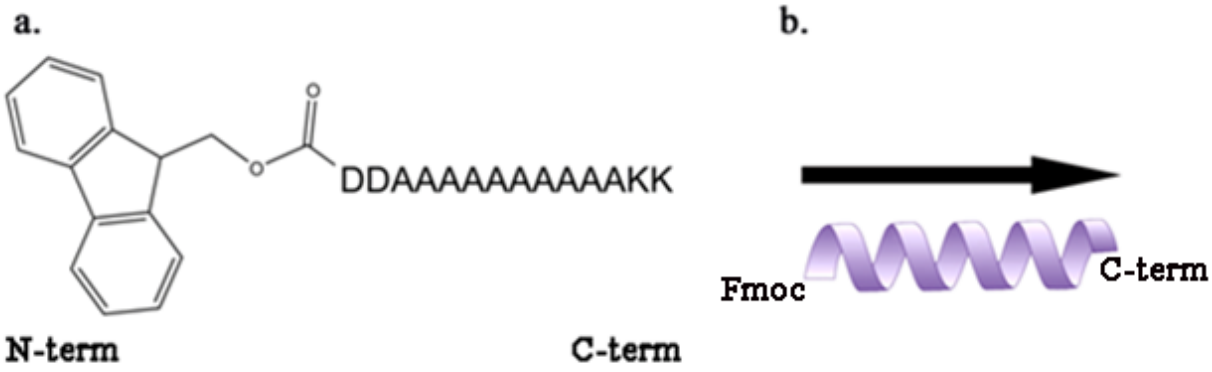

Figure 1.10 a. Structure and sequence of the Fmoc-$D_2A_{10}K_2$ peptide. **b.** The dipole moment of the α-helical A10.

These peptides have been shown to have very stable secondary structures based on Circular Dichroism spectroscopy (CD) (Perutz et al., 2002). The two negative aspartates (D) residues and the two positive lysines (K) residues give these peptides a substantial dipole moment that is useful in their analysis within an AC field. These peptides were originally

capped on the N-terminus with Fmoc group, giving them a negative net charge, electrophoresing them into the pore vestibule and, thus, increasing the translocation events relative to peptides that were not Fmoc-protected (Stefureac et al., 2006). These properties permitted the peptides to orient into the lumen and pass easily through the pore. Peptides with different lengths yield different histograms of blockade current intensities, as well as duration times. Thus, these peptides were useful models to study the effect of an AC field.

1.6 Alpha-Synuclein

AS is a much longer peptide with a large dipole moment. There was little known about AS before 1997, but during that year, two major discoveries brought a lot of attention to the scientific and medical community. First, a point mutation of Alanine to Threonine at the 53rd position, A53T, was found to be related to a familial form of Parkinson's disease (Polymeropoulos et al., 1997). Second, Lewy bodies (LBs), that are fibrils composed of aggregates of protein located in PD patients in the Substantia Nigra (SN) of the brain, were found to have a strong reaction to antibodies to AS (Spillantini et al., 1997). These two discoveries led to numerous studies, the main focus of which was to understand what effect the mutation had and how the accumulation of AS leads to PD. This led to the finding of the SNCA gene, which encodes AS (Singleton et al., 2003). In addition, a great deal of focus was placed on identifying the steps in the molecular pathways leading to the accumulation of AS in the brain, as well as possible therapeutic treatments (Breydo et al., 2012).

1.6.1 Structure of Alpha-Synuclein and domains

AS is an intrinsically disordered peptide of 140 amino acids in length with seven partial repeats of 11 amino acids (Goedert, 2001). The structure and the dynamics of the micelle-bound human AS protein were obtained in 2005 (Ulmer et al., 2005). The protein is natively unfolded in aqueous solution, but it forms an α-helical structure when bound to a lipid bilayer containing phospholipids and finally it forms a β-sheet when aggregation occurs (Stefanis, 2012). The protein's name is an arrangement of "Syn" and "nuclein" since the protein is located in the presynaptic nerve terminals in the nucleus (Goedert, 2001). AS is composed of three domains: The N-terminus (N-term), the non-amyloid-β-component (NAC) and the C-terminus (C-term). The N-term domain is the membrane-bound domain of the protein, which consists of

residues 1-60. It is an α-helical structure that contains binding domains for apolipoprotein complexes. Additionally, this domain has seven repetitions of the sequence, KTKEGV (Clayton and George, 1998; Maroteaux et al., 1988). The non-amyloidal-β component (NAC) consists of residues from 61-95 and is very hydrophobic, playing a major role in the misfolding of the protein which later will lead to the formation of fibrils in the brain (Lücking and Brice, 2000). The C-term domain, consisting of residues from 96-140, is a very acidic region that is very proline-rich, but has no distinct structure (Uéda et al., 1993). The C-terminus has a net charge of -12 whereas the N-term has a net charge of +4 (see Figure 1.11). Therefore, the protein enters the pore through its C-terminus and AS is expected to have a very large dipole moment.

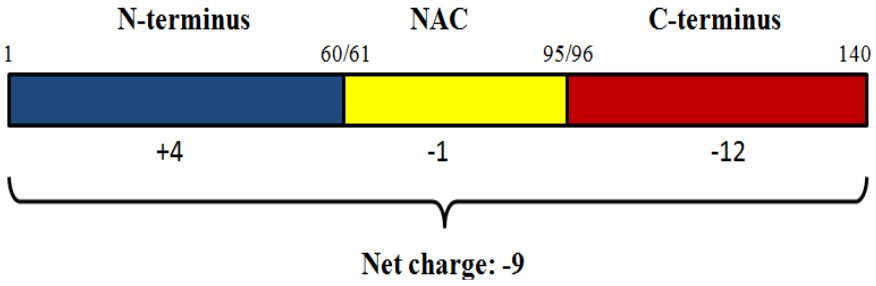

Figure 1.11 The domains of α-synuclein, including separate and total net charges. Reprinted and adapted with permission from (Tavassoly et al., 2014b) Copyright © 2014 FEBS Journal. All rights reserved.

AS belongs to the neuronal synuclein family that includes β-synuclein (BS) and γ-synuclein (GS), but AS is different from the other two due to its NAC region (George, 2002). Both BS and GS have been linked to PD, even though there are no traces of these two proteins in LBs (Galvin et al., 1999). BS and GS may be involved in degradation of the hippocampus receptors in PD and other neurodegenerative diseases, with symptoms that include loss of short-term memory, olfaction trouble, and loss of spatial memory and navigation. Surprisingly, the WT version of BS was shown to be neuroprotective, preventing AS aggregation which leads to neuronal death. On the other hand, point mutations in BS such as V70M or P123H were shown to be related to Dementia with Lewy Bodies (DLBs). The mutations of BS in the 70th and 123rd position are dominant traits. Using techniques such as histopathology and immunohistochemistry, it was shown that BS is in brain sections of the DLBs patients (Ohtake et al., 2004; Park and Lansbury, 2003). Overexpression of Synoretin, a member of the GS

subfamily, was found in the retina of Alzheimer's disease (AD) patients (Surguchov et al., 2001). AS is found largely in the brain, but also in small amounts in such organs as the heart, the kidney, the lungs, muscle tissue, as well as others (Baltic et al., 2004). Interest is focussed on the presence of AS in the brain as related to its main function and relationship with PD. AS is initially observed during neuronal development in the fetus. Subsequently, AS is implicated in the neuron structure, especially in the synapse region, and was shown to be involved in neuronal transmission (Murphy et al., 2000). Proof of its involvement in synaptic transmission was revealed in 2005 when it was shown that AS regulates cysteine string protein-α (CSP-α), a presynaptic protein linked to loss of neuronal function (Chandra et al., 2005). For the above-mentioned reasons, one of the functions of AS seems to be related to controlling assembly of the soluble N-ethylmaleimide-sensitive factor attachment receptors (SNARE) complex (Chandra et al., 2005). This research was based on a mouse model. The Chandra group noticed that knocking out the protein CSP-α in mice caused neurodegeneration. Mice born with a CSP-α-deficiency showed failings in synaptic transmission within 2 to 3 weeks of age, and after they were 1 to 4 months the CSP-α-deficiency proved lethal. Additionally, the deletion of CSP-α was shown to cause loss of the proper assembly of the SNARE complex. For example, levels of plasma membrane SNARE proteins like SNAP-25, SNAP-32, synaptobrevin were decreased in the CSP-α knockout mice (20-40%). All these proteins are involved in the release and regulation of neurotransmitters. These CSP-α knockout mice were then treated with transgenic WT AS where, surprisingly, it was shown that the SNARE complex assembly was corrected. Independent assays on sodium dodecyl sulfate (SDS) gels showed that the SNARE complex assembly was indeed abnormal in the mice with CSP-α knockout and regular after the expression of WT AS.

Thus, it appears that the function of AS is related to synaptic transmission and modulator of neurotransmitter release. Nevertheless, the physiological role of α-synuclein still remains unknown.

1.6.2 Clinical significance of alpha-synuclein in Parkinson's disease

Diseases due to protein misfolding have become a widespread focus for many groups. The term "Protein misfolding diseases" refers to the neuropathology of the abnormal deposit of proteins not only in PD patients, but in patients with other neurodegenerative diseases such as

Multiple-System Atrophy (MSA), AD, Amyotrophic Lateral Sclerosis (ALS), DLBs and Neurodegeneration with Brain Iron Accumulations type 1 (NBIA) (Kahle, 2008; Stefanis, 2012; Zilkova et al., 2006). The usage of this new terminology started back in 1997 when it was discovered that the SNCA gene plays a big part in sporadic familial PD (Baba et al., 1998). The discovery of point mutations in the SNCA gene has led to the detection of other familial forms of PD. Additionally, both duplication and triplication of the locus containing the SNCA gene or mutations of the 4q21-23 human chromosome, have been related to rare familial PD (Forman et al., 2005; Savitt et al., 2006). PD is clinically diagnosed by L-dopa-responsive motor impairments including slowness of movement, muscular rigidity and tremors (Forman et al., 2005; Giasson et al., 2004; Jankovic, 2008; Stefanis, 2012). PD is the second most common neurodegenerative disease after AD. There are multiple isolated genetic factors that cause degeneration of the nervous system and lead to PD (Farrer, 2006; Feany, 2004; Giasson et al., 2004). However, these point mutations are extremely uncommon forms of familial PD. More than 90% of sporadic PD is characterized by the accumulation of AS in LBs (Forman et al., 2005; Stefanis, 2012). Accumulation of AS occurs when the natively unfolded protein begins to aggregate into β-sheet like structures that may form inclusion bodies called LBs.

The genetic factors of PD were the first to be discovered. In 1990, it was observed that many members of a family in Contursi Terme, a village in Southern Italy, had PD. Responsible for the increased number of cases of this disease was a defect in the 4q21-23 chromosome, which is the chromosome to which AS maps. The first mutation observed of the SNCA gene was the replacement of guanine with adenine at 209 position, leading to an A53T point mutation (Polymeropoulos et al., 1997). As expected, this new revelation led to a more profound study of the SNCA gene. Thus, it was possible to detect more point mutations of familial PD: (a) A30P, where guanine at position 88 is substituted with cytosine in the SNCA gene, leading to a replacement of alanine at the 30th site of AS with proline (Krüger et al., 1998); (b) E46K, the other mutation of AS where a negatively charged glutamate is mutated to a positively charged lysine. This AS mutant is known to cause a much higher level of misfolding leading to a higher amount of aggregation than the other two mutations, A53T and A30P (Zarranz et al., 2004); (c) H50Q, a mutation within exon 4 of SNCA, which leads to a replacement of histidine with glutamine (Appel-Cresswell et al., 2013); and (d) G51D, leading to the discovery of a new parkinsonian-pyramidal syndrome, from a French family. This new

PD phenotype was shown to have a generally faster progression of the disease with the death of the patient within a few years (Lesage et al., 2013). Additionally, the SNCA gene is also related to autosomal-dominant familial PD through duplication and triplication (Singleton et al., 2003). For example, carriers of the triplication of the gene are predicted to have three fully functional copies of SNCA. It is possible that the increased dosage of this gene is the cause of PD in this case, although, it is very important to mention that the SNCA gene is also linked to sporadic cases of PD through genome-wide association studies (GWAS) (Klein and Ziegler, 2011; Nalls M. A. et al., 2011).

Figure 1.12 summarizes the causes that enhance the aggregation of AS, which later leads to neuronal death in PD.

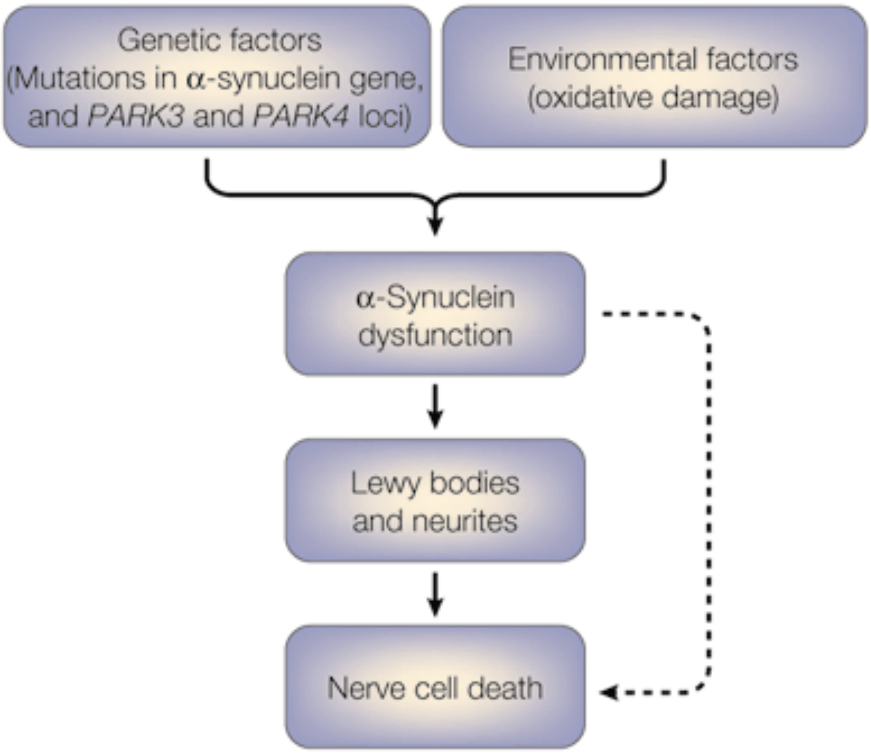

Figure 1.12 Nerve cell death model of PD. Reprinted with the permission from (Goedert, 2001) Copyright © 2001 Macmillian Magazines Ltd . All rights reserved.

In 2015, the Prusiner lab identified a strain of AS that causes MSA that could possibly be a prion (Prusiner et al., 2015). Prions are proteins that are capable of misfolding in different ways and are known to cause Transmissible Spongiform Encephalopathy (TSE), a condition in

where cerebral cortex deterioration leads to holes that make that part of the brain look like a sponge (Kupfer et al., 2009; Prusiner, 1998). It is possible to compare them to viruses because, at least, one of these misfolded conformations is transmissible to other animals, similar to a viral infection. The Prusiner lab studied brains of MSA and PD deceased patients. The group homogenized these brains to test for transmission in genetically engineered cells expressing AS and the A53T AS mutation and in transgenic mice expressing A53T. The MSA samples were transmitted to the cells and transgenic mice, while there was no transmission for the PD samples. This led to the assumption that the AS strain that causes MSA could be a prion because it was transmissible and caused severe neurodegeneration (Prusiner et al., 2015).

1.6.2.1 Misfolding that leads to aggregation

As mentioned, PD pathology is triggered by the aggregation of AS. AS is a stable intrinsically disordered protein; nevertheless, under certain conditions, it can aggregate and form inclusion bodies. Classical LBs, are eosinophilic inclusions that are approximately 10 nm wide found in dopaminergic neurons (McKeith et al., 1996). The deposition of AS into LBs is a progressive result of aggregation that takes place within neurons of the SN of the brain.

The aggregation of AS is shown to the right of Figure 1.13. The aggregation starts when the native unfolded AS misfolds into spherical- ring- or string-like structures. These structures represent an intermediate stage where the protein is partially folded. This type of misfolding is generated by point mutations of AS as well as environmental factors. These partially folded structures start the oligomerization of the protein due to their hydrophobic surfaces. These new-formed oligomers are β-sheets-like structures and can be observed *in vitro* via EM, but very difficult to detect *in vivo*. It is possible to trap a few of the oligomeric forms on native gels or study by size-exclusion chromatography (Emmanouilidou et al., 2010). Further enhancement of this oligomerization will lead to fibrillization and eventually will form fibrils that will accumulate to LBs. As shown in the left side of Figure 1.13 there are several factors that might enhance the aggregation of AS into protofibrils, such as the familial mutations A53T, A30P, and E47K. Surprisingly, only A30P and A53T form more protofibrils than the WT version of AS, whereas the E47K mutation forms fewer protofibrils than the WT. Furthermore, A53T forms more fibrils than the WT version, as well as all the other mutations (Conway et al., 2000). There are further examples on the left side of Figure 1.13 of different modifiers.

Stimulation of the polo-like kinase 2 (PLK2) by electrical changes in the neurons enhances aggregation. PLK2 is responsible for the phosphorylation of AS at Ser129, thus forming more oligomers and fibrils. Additionally, calpain protease truncations and nitration, through nitric oxide (NO) all modify AS and increase its aggregation potential (Cookson, 2009).

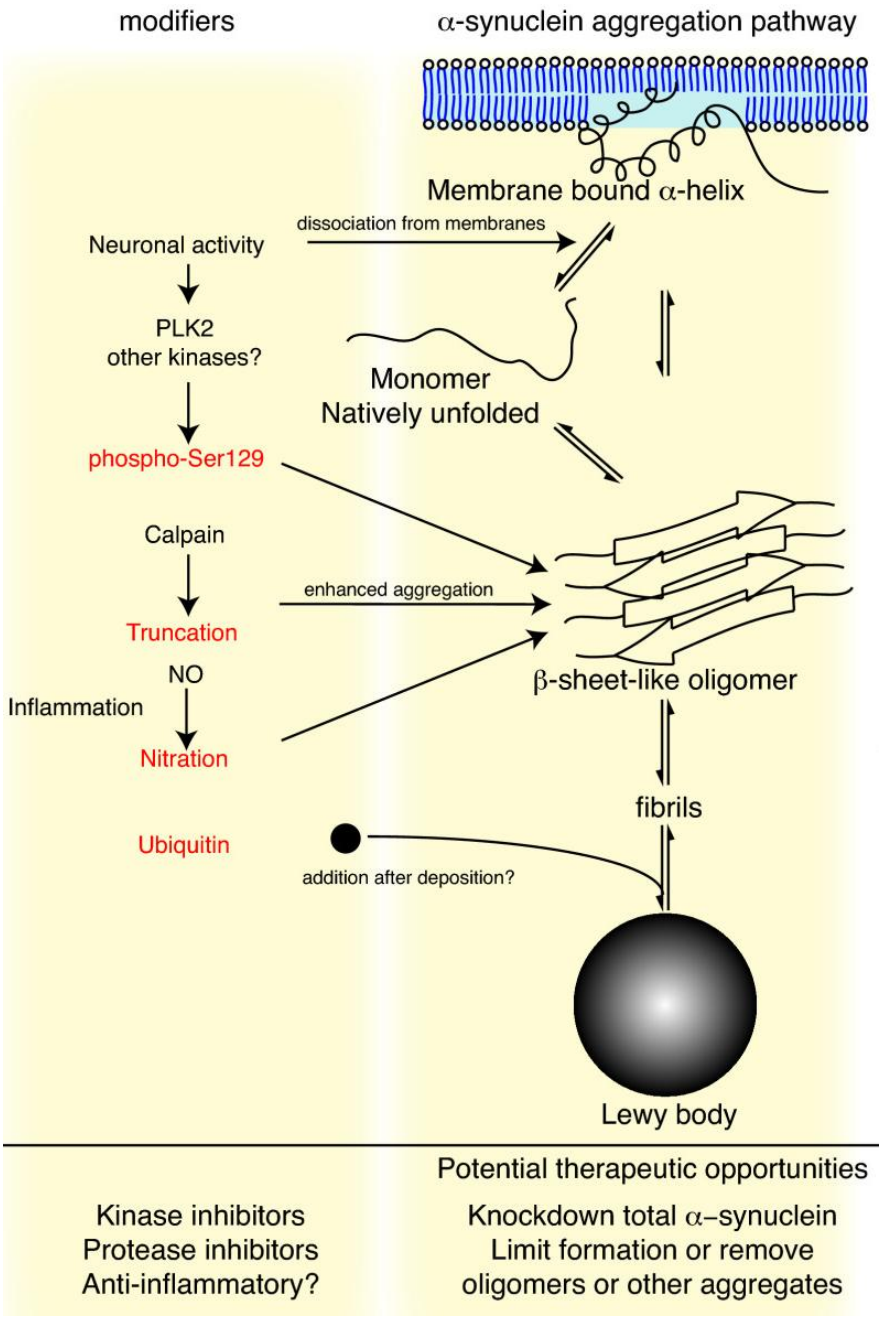

Figure 1.13 The chain reaction of the AS aggregation and its toxicity. Reprinted and adapted with the permission from (Cookson, 2009) Copyright © 2009 Cookson; licensee BioMed Central Ltd. All rights reserved.

1.6.2.2 Role of other factors in Parkinson's disease

The PARK family, including PARK 1, 3, 4, 6 and 11, represent a series of genes that, if mutated, are responsible for the pathogenesis of familial PD (Bekris et al., 2010; Farrer et al., 1999; Gasser et al., 1998; Valente et al., 2001). An additional protein related to PD is parkin, which is encoded by the *PARK2* gene. Mutations of the *PARK2* gene are known to cause a familial form of PD, which is known as autosomal-recessive juvenile parkinsonism (AR-JP) (Kitada et al., 1998). The physiological function of this protein is unknown, much like the function of AS, but it is hypothesized that parkin helps in degrading other proteins that are toxic to the neurons responsible for dopamine production and transportation. However, it is still not clear how the loss of parkin function leads to death of these neurons. It has been shown that a protein called synphilin-1 links parkin and LBs in PD (Engelender et al., 1999). It was shown that the protein-protein complex between AS and synphilin-1 is overexpressed and is the cause for the rapid formation of these inclusion bodies (Moore et al., 2005). In addition to *PARK2*, 10 more genes were found to be related to forms of PD. These genes are divided into two groups: (a) autosomal dominant (AD) and (b) autosomal recessive (AR). As for the *parkin* mutations such as PARK2 or PARK6, which are known to cause PD, they have no relation to fibril pathology (Kitada et al., 1998; Valente et al., 2001).

Environmental factors have also been studied as external causes of PD (Di Monte et al., 2002). Many reports of PD cases from factors such as heavy metals have been published. For instance, iron and manganese accumulation in the SN part of the brain could possibly induce dopamine to auto-oxidize and produce free radicals, which play a significant role in PD pathogenesis (Montgomery, 1995). Another factor is 1-methyl-4-phenyl-1,2,3,6-tetrahydropyridine (MPTP), a secondary compound created unintentionally during the production of 1-methyl-4-phenyl-4-propionoxypiperidine (MPPP), which is an opioid analgesic drug (Exner et al., 2012). MPTP as itself is not toxic, but once it crosses the blood-brain barrier it metabolizes into 1-methyl-4-phenylpyridinium (MPP^+). It is the MPP^+ cation that induces death of the dopaminergic neurons of the pars compacta in the SN region. Pesticides, such as rotenone and paraquat, are also factors and induce oxidative stress and degeneration of dopaminergic neurons (Berry et al., 2010; Franco et al., 2010). Additionally, synthetic organic compounds like 6-hydroxydopamine (6-OHDA) which is known as oxidopamine, is used to

selectively destroy dopaminergic neurons (Breese et al., 2005). Finally, head-related injuries may also trigger PD (Liu et al., 2003).

1.7 Protein-Drug complexes

The use of nanopore technology to discover drugs that bind to AS, is being researched as a possible way to treat Parkinson's disease (Kakish et al., 2015b; Tavassoly et al., 2014a).

1.7.1 Drugs that interact with Alpha-Synuclein

Drugs that are known to bind to AS and change the conformation, would be optimal candidates for studies in an AC field. Several drugs that are known to have neuroprotective or neurotoxic effects were tested using both nanopore analysis and ITC (Kakish et al., 2015a; Kakish et al., 2015b; Tavassoly et al., 2014a). These studies were conducted to obtain a better understanding of the drug-AS conformational changes and possible binding sites. Several drugs have shown to help relieve the symptoms of PD, including rasagiline, which is an inhibitor of MAO-B and is widely used by PD patients (Gallagher and Schrag, 2008; Kakish et al., 2015b). It prevents the breakdown of dopamine in neuronal mitochondria, which increases its chance for re-absorption and later use by the synapse. In contrast, numerous recreational drugs such as heroin and methamphetamine have been shown to induce PD symptoms by interfering with dopamine metabolism in neurons. Initially, caffeine and nicotine were taken into consideration after epidemiological studies showed that the intake of coffee and the smoking of tobacco in high doses had a direct association with PD (Quik, 2004; Ross et al., 2000). These drugs have been shown to help prevent PD; suggesting a neuroprotective role (Ascherio et al., 2001; Kelton et al., 2000; Villafane et al., 2007). It is assumed that these drugs bind to AS, forming a loop conformation, as shown in Figure 1.14 b; therefore, they prevent the NAC region of these proteins from aggregating (Tavassoly et al., 2014a). Later, other drugs, such as S-1-aminoindan, 3-methoxytyramine, and metformin, have been shown to have neuroprotective abilities as well (El-Mir et al., 2008; Huang et al., 1999; Patil et al., 2014; Scatton et al., 1983). Alternatively, drugs like amphetamine and cocaine were shown to increase the risk of PD (Graybiel et al., 1990; Myers and Earnest, 1984). They are assumed to form a compact complex with AS leaving the NAC region free, thus promoting aggregation (Kakish et al., 2015a).

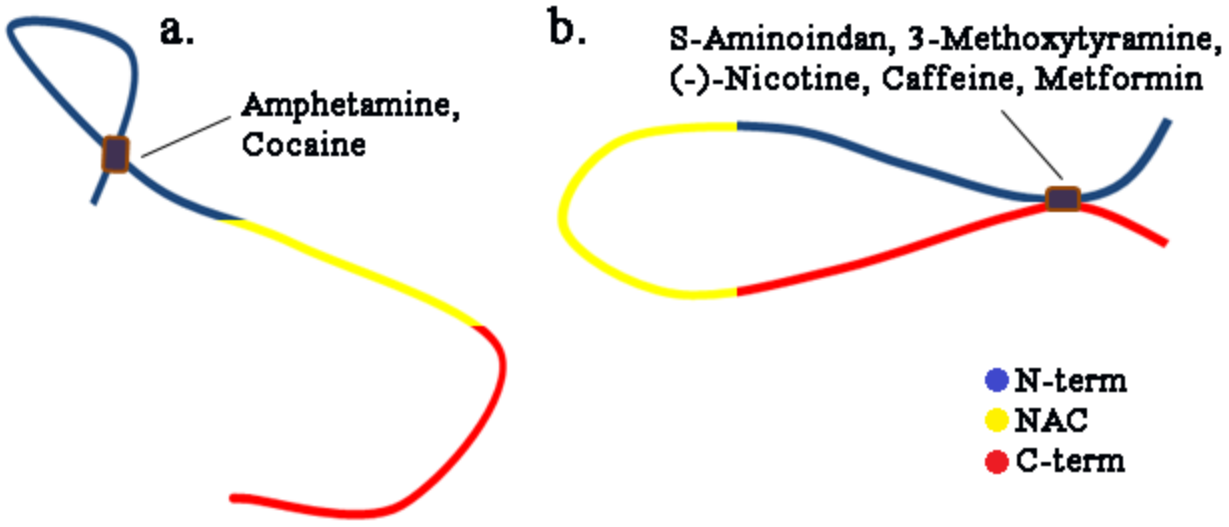

Figure 1. 14 Two possible conformation of the drug-AS complexes. **a.** The drug binding site is in the N-terminus which makes the protein to intake a half a bow configuration and **b.** The drug binding cite is in both the N- and C-terminus forming a loop conformation.

As previously observed, the blockade current histogram of AS alone is mostly composed of translocation events with intensity at -86 pA (Madampage et al., 2012). Each drug that binds to the protein causes a current shift with respect to the translocation events and/or an increase in the bumping event proportions. For nicotine, only the (-)-nicotine isomer has been shown to bind to both the N-and C- termini forming a loop conformation (Figure 1.14 b), whereas the (+)-nicotine isomer binds to the N-terminus forming a half bow conformation (Figure 1.14 a) (Tavassoly et al., 2014a). Published results have shown that (-)-nicotine causes a major shift in the translocation events from -86 pA to -65 pA (Tavassoly et al., 2014a). Based on the conformations the drug-protein complex adopts once the drug binds to AS it was assumed that (-)-nicotine has a neuroprotective effect (Kakish et al., 2015a). Additionally, 3-methoxytyramine is a metabolite of the previously studied 3-methoxydopamine, which is derived from dopamine, but is more stable and less susceptible to oxidation (Karoum et al., 1994; Wood and Altar, 1988). Dopamine binds to AS and forms a loop conformation because it binds to the N-terminus as well as the C-terminus (Tavassoly et al., 2014b). Dopamine-like drugs were proven to behave like dopamine and, as such, can stimulate the nerve cells. For example, L-3,4-dihydroxyphenylalanine (L-DOPA), which is metabolized to dopamine, has been shown to be a good therapy for PD patients as their motor symptoms were significantly ameliorated, although, it also causes various side effects (Cools, 2006; Cotzias et al., 1969).

The blockade histogram of 3-methoxytyramine is the same as 3-methoxydopamine and has a single peak that is shifted to -40 pA. This suggests the same change in structure of AS that is been observed previously in the case of 3-methoxydopamine (Tavassoly et al., 2014a). Thus, it is assumed that this drug could be neuroprotective as well.

Metformin is another drug tested with nanopores that is given to patients with diabetes, especially type 2 diabetes (Dunn and Peters, 1995; Group, 2002). Metformin has a unique structure compared to the other six drugs since it has no aromatic ring and is a small dication. It was publicized in 2014 that metformin helped PD-induced mice, with chronic MPTP administrations, by acting as a neuroprotective drug (Patil et al., 2014). Its blockade histogram revealed a major peak that is shifted to -65 pA. Therefore, this drug is presumed to be neuroprotective as well. Finally, S-1-Aminoindan may also be neuroprotective. It has a major translocation peak at -73 pA, which reveals that the drug binds tightly to the protein and helps AS from misfolding (Kakish et al., 2015b).

The second group of drugs studied in this thesis includes those that interfere with the transport of dopamine in neuron synapses, such as amphetamine. Amphetamine binds to AS causing a large bumping peak and a smaller translocation peak at the same position as AS (-86 pA). Abusers of amphetamine have been shown to have an increased risk of having PD later in their lives, an observation similarly seen in methamphetamine abusers (Curtin et al., 2015). Lastly, cocaine is also known to be a drug that interferes with dopamine transportation or its metabolism in neurons (Gawin and Ellinwood, 1988). Some cases of long-term cocaine abuse have been shown to increase the risk of PD and some other Parkinson-like symptoms (Lloyd et al., 2006). There is an ongoing debate on the relationship between cocaine and PD (Dhopesh et al., 1997).

1.8 Hypothesis

The main hypothesis of this thesis is that superimposing an AC voltage in nanopore analysis is useful for various applications. Application of an AC voltage can be used to discriminate between α-helical peptides based on differences in their dipole moments. Additionally, the application of an AC field can be employed to investigate the conformational changes of AS-drug complexes.

1.9 Objectives

a. To study the discriminatory effects of different combinations of AC frequencies and DC amplitudes for α-helical peptides and ssDNA fragments.

Initially, a simple series of peptides will be analysed consisting of the previously studied α-helical peptides of different lengths. These include Fmoc-$D_2A_{10}K_2$, Fmoc-$D_2A_{14}K_2$ and Fmoc-$D_2A_{18}K_2$ (Stefureac et al., 2006). Also a retro-inverse sequence of Fmoc-$D_2A_{10}K_2$ will be analyzed (Fmoc-$K_2A_{10}D_2$). Our goal is to show that the translocation of these peptides can be altered, or even prevented, by applying the right combination of AC frequency and DC voltage. Lastly, two ssDNA will be analyzed, oligo-dT20 and d18, to show how ssDNA would interact in an AC field. In all studies, the DC voltage will be fixed at levels of 60 mV, 100 mV and 140 mV. Superimposed on this will be a 200 mV AC voltage with frequencies between 10 MHz and 1 GHz.

b. To investigate the effect of an AC fields on the behaviour of AS and its fragments.

These studies will be extended to larger proteins such as AS (Tavassoly and Lee, 2012). Different AS conformations may be readily distinguished in an AC field because of differences in their dipole moments. Peptide fragments of AS, such as N-terminus, C-terminus and ΔNAC will also be studied. Our goal is to show that longer proteins with a large dipole moment can be prevented from translocating through the α-HML pore in the presence of an AC field.

c. To observe and elucidate the effect of the AC field on AS-drug complexes.

Our goal is to show that with the help of an AC field we are able to distinguish the different AS conformations induced by seven drugs (S-1-aminoindane, 3-methoxytyramine, metformin, caffeine, (-)-nicotine, cocaine and (+)-amphetamine), as they bind to different sites of the protein (Kakish et al., 2015b; Tavassoly and Lee, 2012).

2. MATERIALS AND METHODS

2.1 Reagents, Equipment and Software

Table 2.1 and 2.2 describes the chemical and biological reagents, equipment and software that were used in this thesis, including the information of their suppliers.

Table 2.1 a. List of chemical and biological compounds with their respective suppliers.

Reagents and Equipment	Supplier
a. Chemical and Biological Compounds:	
1,2-diphytanoyl-sn-glycero-3-phosphocholine in chloroform	Avanti Polar Lipids
3-Methoxytyramine hydrochloride	Sigma-Aldrich
4-(2-Hydroxyethyl)piperazine-1-ethanesulfonic acid (HEPES)	BDH
(-)-1-Aminoindan	Sigma-Aldrich
(+)-Amphetamine	Sigma-Aldrich
Alpha-Hemolysin	Sigma-Aldrich
Alpha-Synuclein	rPeptide
Alpha-Synuclein, N-term (1-60)	rPeptide
Alpha-Synuclein, C-term (96-140)	rPeptide
Alpha-Synuclein ΔNAC	rPeptide
Caffeine	Sigma-Aldrich
Cocaine hydrochloride (solution)	Sigma-Aldrich
Decane (anhydrous)	Sigma-Aldrich
Disodium Ethylenediaminetetraacetic dehydrate (EDTA-NA_2)	Sigma-Aldrich
DNA strands	Regional DNA synthesis lab
Fmoc-$D_2A_{10}K_2$ (A10)	CHI Scientific
Fmoc-$D_2A_{14}K_2$ (A14)	CHI Scientific
Fmoc-$D_2A_{18}K_2$ (A18)	CHI Scientific
Metformin (hydrochloride)	Sigma-Aldrich
Methanol (%)	Thermo Fisher Scientific
(-)-Nicotine, analytical standard	Sigma-Aldrich
Nitrogen (compressed gas)	Praxair
Nuclease-free water	Life Technologies
Potassium chloride (KCl)	EMD
Potassium phosphate dibasic (K_2HPO_4)	Thermo Fisher Scientific
Potassium phosphate monobasic (KH_2PO_4)	Thermo Fisher Scientific
RI-Fomc-$K_2A_{10}D_2$	CHI Scientific
Sodium hydroxide, pellets (NaOH)	EMD

Table 2.1 b. List of supplies, equipment and software with their respective suppliers.

Reagents and Equipment	Supplier
b. Equipment, software and supplies:	
BC-535 amplifier	Warner Instruments
Borosilicate glass capillaries (round)	Produstrial
Digitizer, DigiData 1440A	Axon Instruments
Falcon tubes	VWR
Faraday Cage	Warner Instruments
Filters (0.2 μm)	Sarstedt
Glass beakers, vials and caps	Kimble Chase & VWR
Headstage model BC-535	Warner Instruments
HP E4420B Signal generator	TRS RenTelco/Agilent
LPF-8 eight-pole low pass Bessel filter	Warner Instruments
Microcentrifuge, Hettich Mikro 20	Hettich Zentrifugen
Microliter syringes	Hamilton
Microcentrifuge tubes, non-stick	Thermo Fisher Scientific
NanoAnalyze (software)	TA Instruments
Nitrile gloves	Kimberly-Clark
ONEAC PC750A power supply	ONEAC
Origin 7 (graphing software)	OriginLab
Paintbrush size 000	Island Blue
Parafilm	VWR
pClamp 10.4 (analyzing software)	Axon Instruments
Perfusion bilayer chamber and cup	Warner Instruments
pH meter	Thermo Fisher Scientific
Pipettes	Eppendorf
Pipette tips (10, 200, 1000 and 5000 μl)	Thermo Fisher Scientific
Silver paste	Alfa Aesar
Silver wire	Alfa Aesar
Syringe needles	Becton Dickinson
Syringes (μl)	Hamilton
Syringes (ml)	Becton Dickinson
Tektronix TDS220 digital oscilloscope	Tektronix

Table 2.2 List of companies and their addresses.

Supplier	Address
Alfa Aesar	Alfa Aesar, Ward Hill, MA, USA
Avanti Polar Lipids	Avanti Polar Lipids, Alabaster, AL, USA
Axon Instruments	Molecular Devices, Sunnyvale, CA, USA
BDH	VWR International, Edmonton, AB, Canada
Becton Dickinson	Becton Dickinson Canada, Mississauga, ON, Canada
CHI Scientific	CHI Scientific, Maynard, MA, USA
EMD	EMD Millipore, Gibbstown, NJ, USA
Eppendorf	Eppendorf Canada, Mississauga, Ontario, Canada
Hamilton	Hamilton Company, Reno, NV, USA
Hettich Zentrifugen	Andreas Hettich GmbH & Co.KG, Tuttlingen, Germany
Island Blue	Island Blue Print, Victoria, BC, Canada
Kimberly-Clark	Kimberly-Clark Inc., Mississauga, Ontario, Canada
Kimble Chase	Kimble Chase, Vineland, NJ, USA
Life Technologies	Life Technologies, Burlington, ON, Canada
ONEAC	ONEAC, Libertyville, IL, USA.
OriginLab	OriginLab, Northampton, MA, USA
Praxair	Praxair, Saskatoon, SK, Canada
Produstrial	Produstrial, LLC; Larkspur Lane, Fredon, NJ, USA
Regional DNA synthesis lab	University of Calgary, Calgary, AB, Canada
rPeptide	rPeptide, Bogart, GA, USA
Sarstedt	Sarstedt, Montreal, QC, Canada
Sigma-Aldrich	Sigma-Aldrich Canada Ltd., Oakville, ON, Canada
TA Instruments	New Castle, PA, USA
Tektronix	Tektronix, Beaverton, OR, USA
Thermo Fisher Scientific	Fisher Scientific Company, Ottawa, ON, Canada
TRS RenTelco	TRS-RenTelco, Dollard-des-Ormeaux, QC, Canada
VWR	VWR International, Edmonton, AB, Canada
Warner Instruments	Warner Instruments, Hamden, CT, USA

2.2 Nanopore Technology

2.2.1 Nanopore analysis apparatus

All the nanopore experiments conducted in this thesis used a patch-clamp setup. As seen in Figure 2.1, the system is composed of several components: (a) the perfusion cups, (b) the silver/silver chloride electrodes, (c) the head-stage. The components were located inside (d) a Faraday cage. The head-stage was connected simultaneously to (e) the patch-clamp amplifier and (f) the signal generator, the latter is connected beforehand to (g) an oscilloscope to adjust the AC voltage. The ionic signal makes its way to (h) the digitizer and finally can be monitored (i) as a screen shot on a computer via the Clampex© software.

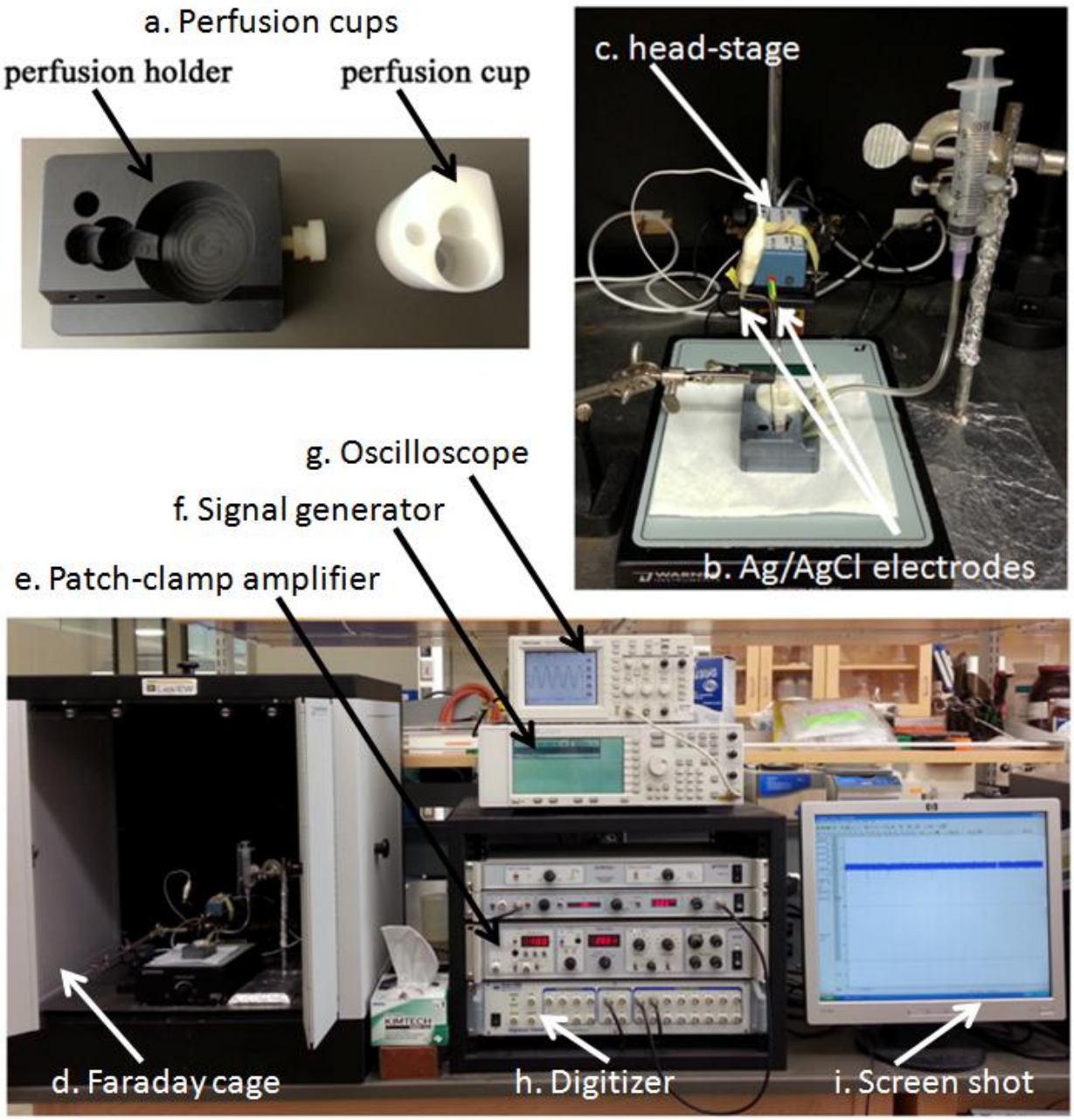

Figure 2.1 Images of the patch-clamp setup: **a.** perfusion cups composed by the perfusion cup and the holder, **b.** Ag/AgCl electrodes, **c.** head-stage, which are located in **d.** the Faraday cage. The head-stage is connected to: **e.** patch-clamp amplifier, **f.** signal generator, **g.** oscilloscope, **h.** digitizer and lastly **i.** screen shot.

The perfusion unit is composed of two cups (Figure 2.1 a): (a) the Teflon perfusion cup (white) has a small aperture of 150 μm, where the bilayer membrane will be painted and (b) the Delrin cup holder (black), which has a nylon screw to tighten the perfusion cup to prevent

leakage between the two chambers. Both compartments have the same volume capacity of 1 ml. The two compartments, *cis* (black) and *trans* (white) are separated by the perfusion bilayer. These cups are easily maintained and have a long life. The perfusion unit was then placed on a nitrogen floating table (Kinetic Systems), which will reduce any external vibrations or signals, in the bounds of a Faraday cage (Warner Instruments) to protect the nanopore experiment from external electrical and static noises. An Ag/AgCl electrode was then placed in each compartment; the cathode placed in the *cis* side and the anode placed in the *trans* side. Before the start of an experiment, the electrodes were cleaned off prior oxidation layers with sand paper and placed in bleach for 2 to 3 hours. The two electrodes are directly connected to the head-stage (BC 535, Warner Instruments). The signal is later transmitted to the 10 kHz low-pass filtered with an eight-pole Bessel filter patch-clamp (Warner Instruments), where DC voltages of 60, 100 and 140 mV were applied. Simultaneously the signal is transmitted to the HP E4420B signal generator (ESG-A Series Analog RF Signal Generator, 2 GHz, Hewlett Packard), where an AC voltage of 200 mV with frequencies between 10 MHz-1 GHz was applied. The AC amplitude and frequencies were initially regulated by Tektronix TDS 220 (2 Channel, digital real time Oscilloscope 100 MHz, 1 GHz/s) then added to the head-stage. The patch-clamp and signal generator voltage is combined by a joined cable and is applied directly to the head-stage. Lastly, the signals were digitized at 100 kHz by Digidata 1440 (Axon Instrument) and then recorded by a Personal Computer (PC) running PClamp 10.1 (Axon Instrument). All the equipment involved the nanopore analysis apparatus was powered by a power bar (ONEAC) to reduce noise coming from the main supply.

2.2.2 Formation of the lipid bilayer and insertion of the pore

Prior to each bilayer painting, the $CHCl_3$-lipid solution was dried under a vacuum for 3 to 4 hours and then re-dissolved in 25 µl of decane to a 30 mg/ml final concentration (Stefureac et al., 2006). Initially, this lipid bilayer was made by twice painting 1,2-diphytanoyl-sn-glycero-3-phosphocholine from Avanti Polar Lipids (Alabaster, Alabama) with a size 000 brush onto the 150 µm aperture of the Teflon wall in the perfusion cup (white). The lipid bilayer was then dried under a 10 pound per square inch (10 psi) flow of compressed nitrogen gas. The perfusion cup was then inserted in the holder (black) and tightened. After the cups are secured in the Faraday cage, they are filled with 1 ml electrolyte solution. The electrolyte solution used for

the Fmoc peptides and the DNA strands was 1 M KCl with 10 mM potassium phosphate (9.87 ml of 100 mM of dipotassium phosphate + 0.13 ml of 100 mM monopotassium phosphate) buffer pH 7.8 (Christensen et al., 2011). While, the buffer used for the AS, its domains, and AS-drug complexes studies contained 1 M KCl in 10 mM HEPES at a pH 7.8, with the addition of 1 μM of EDTA only on the *cis* side to chelate dicovalent metal such as Cu^{2+}, Zn^{2+} or Mg^{2+} that might be present in the solution (Krasniqi and Lee, 2012).

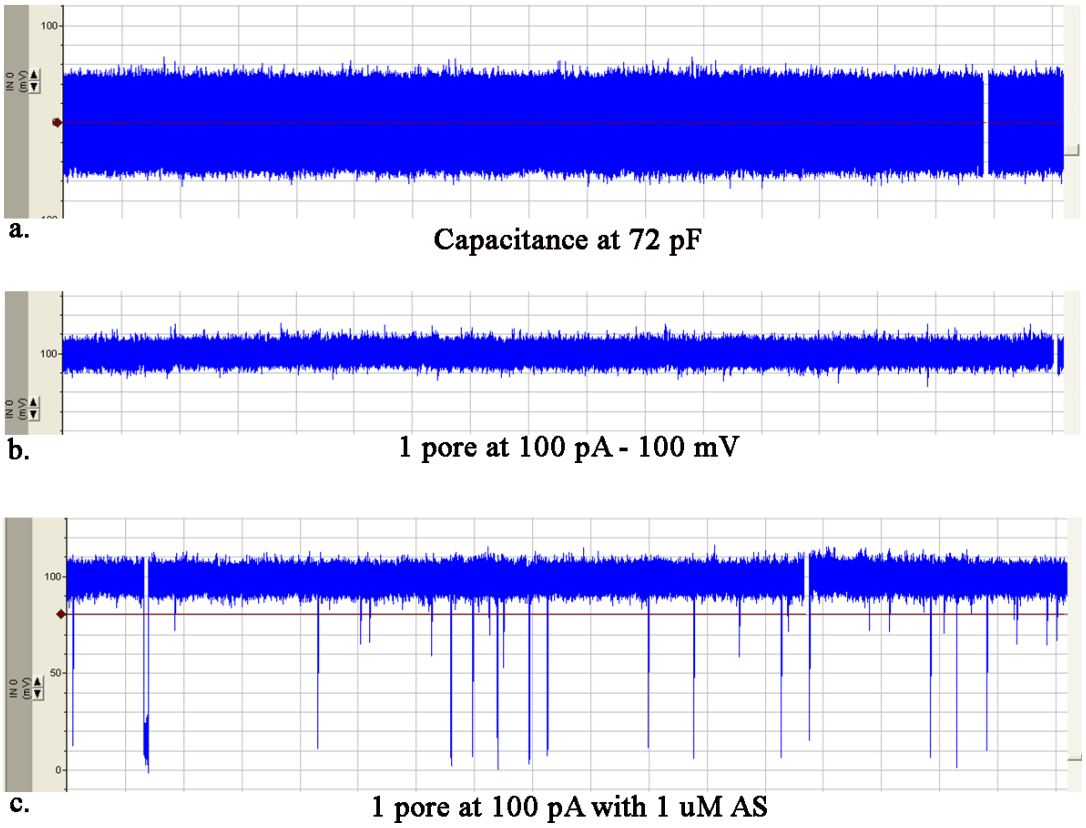

Figure 2.2 a. Capacitance at 72 pF. **b.** An optimal inserted pore (100 pA) at a DC potential of 100 mV. **c.** Bumping, intercalation and translocation events observed after 1μM AS was inserted.

A voltage of 100 mV was applied from the patch-clamp to make sure a stable bilayer membrane was formed. Afterward, the brush was used to thin the multilayer coating in the *cis* side until a stable membrane was formed. Additionally, to help control the stability of the membrane, a 5 ml syringe was inserted in the *cis* compartment through a hole located on the right side of the cup holder. After a stable membrane was formed and the capacitance is in the range of 70 pF range, the pore solution was added (Figure 2.2 a). The stock solution of α-

HML, from Sigma Aldrich Canada, Ltd. (Oakville, Ontario), at 0.5 mg per vial, was diluted with 2 ml of 1 M KCl in 10 mM potassium phosphate buffer, to achieve a concentration of 0.25 mg/ml. The amount inserted in the *cis* compartment is between 5 to 15 µl, bringing the final concentration between 1.25 µg/ml to 3.75 µg/ml. For an optimal inserted pore at a DC potential of 100 mV, the open pore current should be 100 pA or a multiple (Figure 2.2 b). Once a stable pore is obtained, the analyte can be added and tested (Figure 2.2 c).

The first analytes to be tested were the α-helical peptides. These peptides were custom designed by CHI Scientific (Maynard, MA, USA) and a Fmoc- group capped to the N-terminus (98% pure). The peptides were dissolved in 1 M KCl with 10 mM potassium phosphate at 2 mg/ml concentration and once a stable pore is inserted, 10 µl of the stock solution was added to the *cis* compartment bringing the final concentration to 0.002 mg/ml. Spartan software calculated the length of these peptides whereas the molecular weight was calculated by GenScript online software. Both the length and the molecular weight were later confirmed by CHI Scientific (Maynard), the company that manufactured these peptides. The dipole moment was calculated manually (Creighton, 1993). ssDNA was tested, at a final confirmation of 1 µM. The ssDNA were synthesized by the regional DNA synthesis lab (University of Calgary). Additionally, AS and its three domains, N-terminus, C-terminus and the ΔNAC were purchased from rPeptide (Bogart, GA, USA) all having protein purity >95%. The peptides were dissolved in 1 ml of nuclease-free water to a final concentration of 1 mg/ml for α-synuclein and 0.5 mg/ml for its three domains. For each peptide the final concentration in the *cis* compartment was 1 µM. Finally, the seven drugs were acquired from Sigma-Aldrich (Oakville, Ontario, Canada) with purity >98%. The drugs were dissolved in methanol at a concentration of 2 mM. 5 µl of the stock solution was added to the *cis* chamber to give a final drug concentration of 10 µM.

2.2.3 Data collecting, processing and graphing

Any large molecule such as a peptide, ssDNA, protein or protein-drug, which interacts with the pore, will cause a drop in the blockade current (I) for a blockade time (T), which is measured with the patch clamp apparatus (Figure 2.3) (Lamichhane et al., 2013). An AC amplitude of 200 mV and five frequencies: 10, 50, 100, 500 MHz and 1 GHz were investigated with an HP E4420B signal generator (ESG-A Series Analog RF Signal Generator, 2 GHz,

Hewlett Packard). The signal produced during the interaction of an analyte with the pore was received by the patch-clamp and filtered by the LPF-8 eight-pole Bessel filter (Warner Instruments). Lastly, the signal was forwarded to the digitizer (Axon Instrument) where the analog signal is converted to digital. The signal is then recorded in real time via the Clampex software, PClamp 10.1 (Axon Instrument) which is visually displayed to a PC. The PClamp 10.1 used a fixed-length mode to recorded the events as seen from the screen shot in Figure 2.2 c. The files recorded have no more than 500-600 events. These files were later processed using the Clampfit software where the background noise was removed and events were divided into three groups: translocation, intercalation, and bumping. Finally, the events were graphed using the Origin software (OriginLab) where the blockade current population of each event was fitted using a Gaussian function. From these graphs it was possible to obtain the blockade current and the proportion of events at each current. Additionally, with the help of the same Origin software, it was possible to calculate the characteristic blockade time of each population using an exponential function (ExpDecay1).

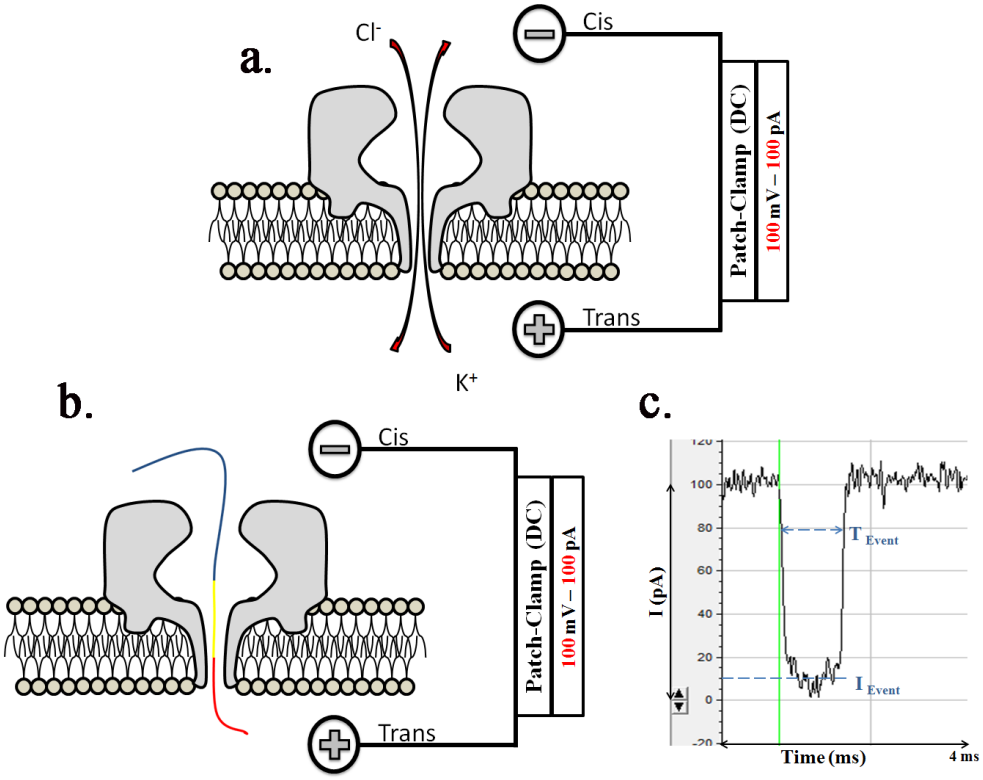

Figure 2.3 a. The patch-clamp setup at a 100 mV DC allows the ions to flow in the pore and create an ionic current, **b.** The interruption of the current when an analyte interacts with the pore and **c.** the disruption of the blockade current and time caused by the analyte.

3. RESULTS

3.1 Nanopore analysis of four alpha-helical Peptides

Earlier nanopore work at a 100 mV DC voltage, was conducted with α-helical peptides of the general formula fluorenylmethoxycarbonyl (Fmoc)-$D_xA_yK_z$ (Amblard et al., 2006; Stefureac et al., 2006). These are listed in Table 3.1 along with several common properties. As seen in Table 3.1, these sequences have the same net charge, but different lengths and dipole moments. RI-A10 is composed of D-amino acids and has a larger negatively charged C-terminus, giving a larger dipole moment than A10.

Table 3.1 The sequence of the peptides, their molecular weights, their net charges, their lengths and their dipole moments (calculated from modeling simulations using Spartan software).

Peptide	Molecular weight (g/ml)	Net charge (at pH 7)	Length (Å)	Dipole Moment (Debye)
Fmoc-$D_2A_{10}K_2$ Abbrev: A10	1436.59	-1	28.2	260
Fmoc-$D_2A_{14}K_2$ Abbrev:A14	1720.9	-1	33.7	329
Fmoc-$D_2A_{18}K_2$ Abbrev:A18	2005.22	-1	39.1	400
RI-Fmoc-$K_2A_{10}D_2$ Abbrev: RI-A10	1436.59	-1	28.3	373

3.1.1 Behaviour of A10, A14 and A18 in an AC field

Previously, it was shown that the ratio of translocation to bumping events of α-helical peptides could be manipulated by a combination of AC frequencies with a 60 mV DC voltage (Stefureac et al., 2012). In this thesis, this observation was extended further to possibly find a correlation between the dipole moment and the AC voltage. Three peptides, A10, A14 and A18, were tested with the help of nanopore analysis with and without the application of an AC field. The dipole moment of each peptide was calculated using the Creighton formula (Creighton, 1993).

$$D = (Q * R) + d$$

The dipole (D) of these peptides was calculated based on the shortest length (R) between the two elementary charges (Q) from the molecular modeling using the Spartan software and the dipole of an α-helix based on the number of alanines per peptide (d) (Stefureac et al., 2006). A10, A14, and A18 are composed by L-amino acids, and each of these peptides has two elementary charges. Additionally, the charge dipole is in the same orientation as the helical dipole. As seen in Table 3.1, from A10 to A18, the dipole moment increases with the increase of the length. It is assumed that each peptides will behave differently in an AC filed based on its dipole moment and length.

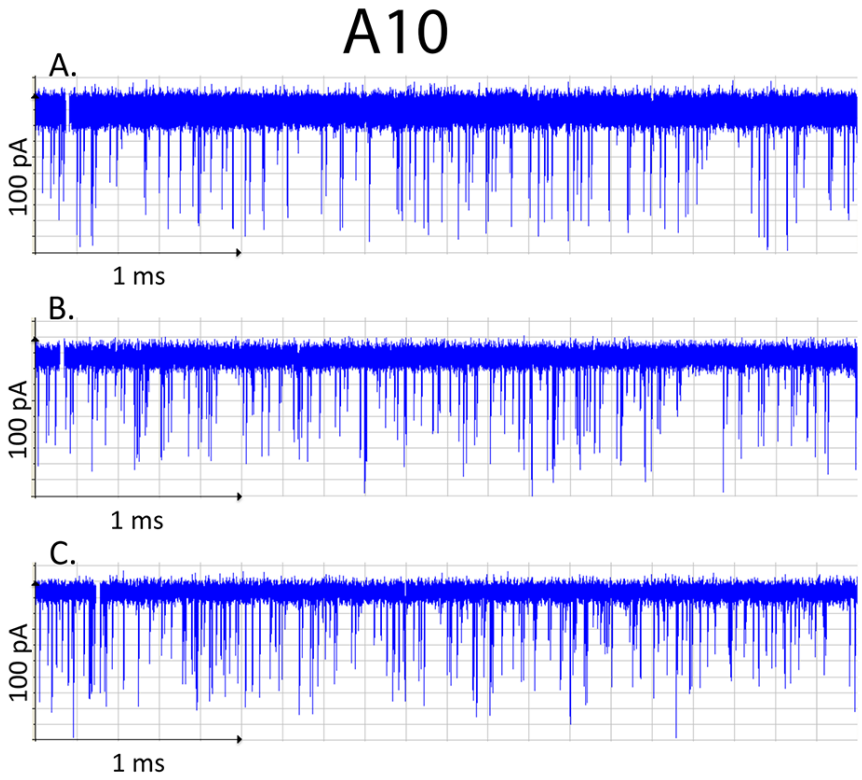

Figure 3.1 Screen shots of traces for A10. **a.** DC voltage at 100 mV, no AC voltage, **b.** AC voltage of 200 mV with a 10 MHz frequency, **c.** AC voltage of 200 mV with a 100 MHz frequency.

For A10, the current traces are shown in Figure 3.1, covering 4 s with and without an applied AC voltage. In the first panel (Figure 3.1 a) the long spikes for A10, around -65 pA, are a result of the peptide going through the pore (translocation events), while the short ones, around -20 pA, are a result of the peptide hitting the pore but not passing through (bumping

events). An initial frequency of 10 MHz caused an increase in the ratio of bumping events to translocation events for A10, which further increased when 100 MHz was applied, as shown in Figure 3.1 b and c.

These events were analyzed and are shown as blockade current histograms in Figure 3.2.

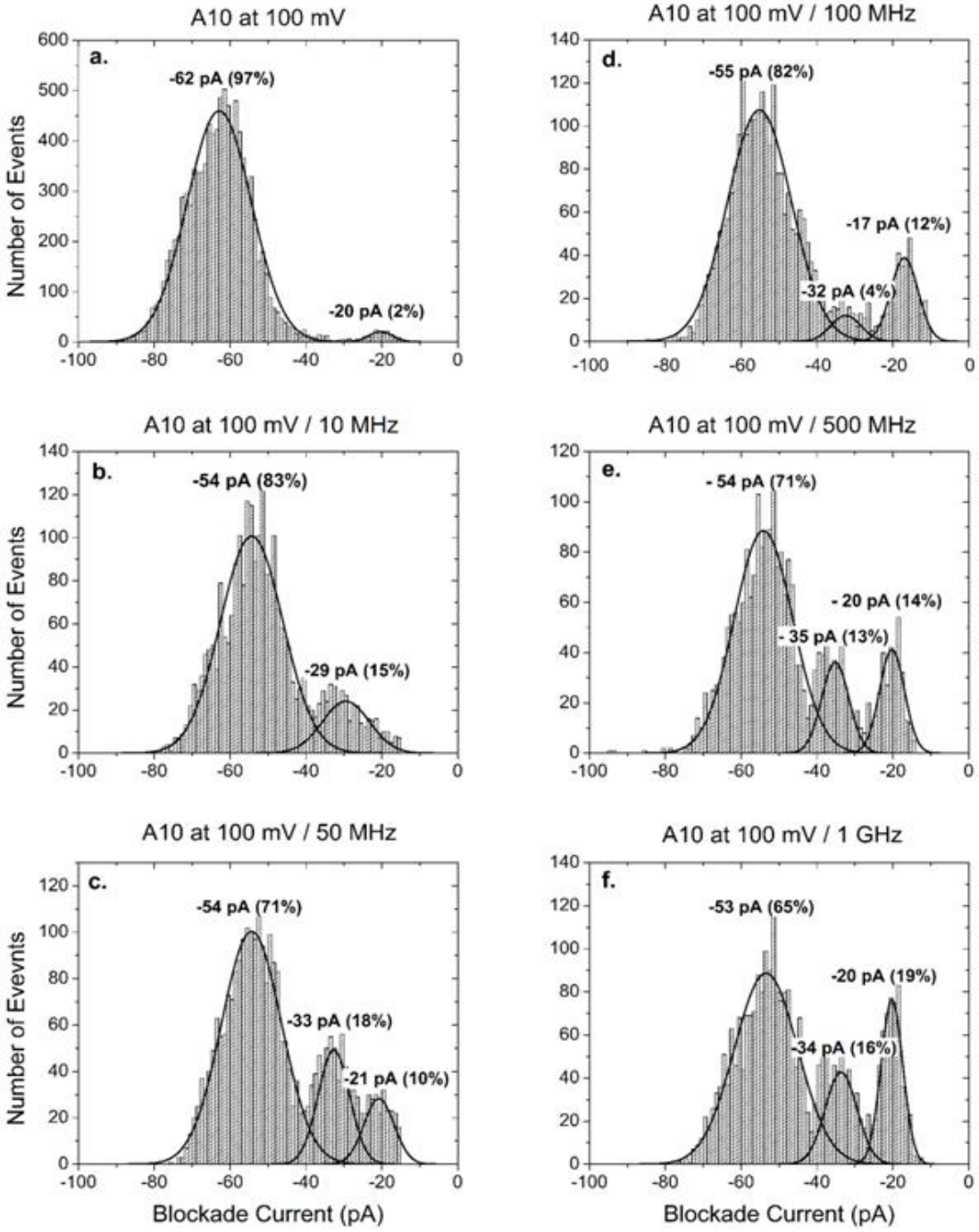

Figure 3.2 Blockade current histograms for A10 at 100 mV DC. **a.** No AC, **b.** 10 MHz, **c.** 50 MHz, **d.** 100 MHz, **e.** 500 MHz and **f.** 1 GHz.

For A10, three observations can be made after the application of the AC field. First, the translocation peak shifts, from -62 pA to -54 pA, which was not a result of a conformational change in the pore since the open pore current remained constant. Second, when the AC frequency was increased from 10 MHz to 1 GHz, the percentage of translocation events decreased from 83% to 65%, respectively. This phenomenon was also observed previously at 60 mV when the percentage of translocations dropped from 62% at 10 MHz to 40 % at 500 MHz (Stefureac et al., 2012). And third, when frequencies of 50 MHz or higher were applied, an intermediate peak appeared at -33 pA which was attributed to intercalation events. It is suggested that when the peptide enters the pore, the AC field causes it to oscillate perpendicular to the pore vestibule prevented it from crossing the pore.

The blockade histograms for A14 at 100 mV DC as shown in Figure 3.3, are similar to A10 at the same voltage, as shown in Figure 3.2. The nanopore study of A14 at 100 mV DC and with a 200 mV AC field with frequencies in the range 10 MHz - 1 GHz is shown in Figure. 3.3. A14 has a single peak at -64 pA (Stefureac et al., 2006). Similarly to A10, with the application of an AC frequency, a major shift of the translocation peak to -52 pA was seen while a second peak at -34 pA also appeared (see Figure 3.3 b). A third small peak is present at -19 pA after a 50 MHz frequency was applied (see Figure 3.3 c). Therefore, the peak at -34 pA should be labeled as intercalation events and the peak at -19 pA as bumping events. Similarly to A10, with the increase of the frequency a significant increase of the bumping population from 4% at 50 MHz to 32 % at 1 GHz was observed. Furthermore, the population of translocation events decreased with the increase of the frequency, from 84% at 10 MHz to 56% at 1 GHz (Figure 3.3 b-f). The higher proportion of bumping events of A14 compare to A10 is thought to be due to A14 having a higher dipole moment which will cause a faster oscillation in an AC field and thus more bumping into the pore.

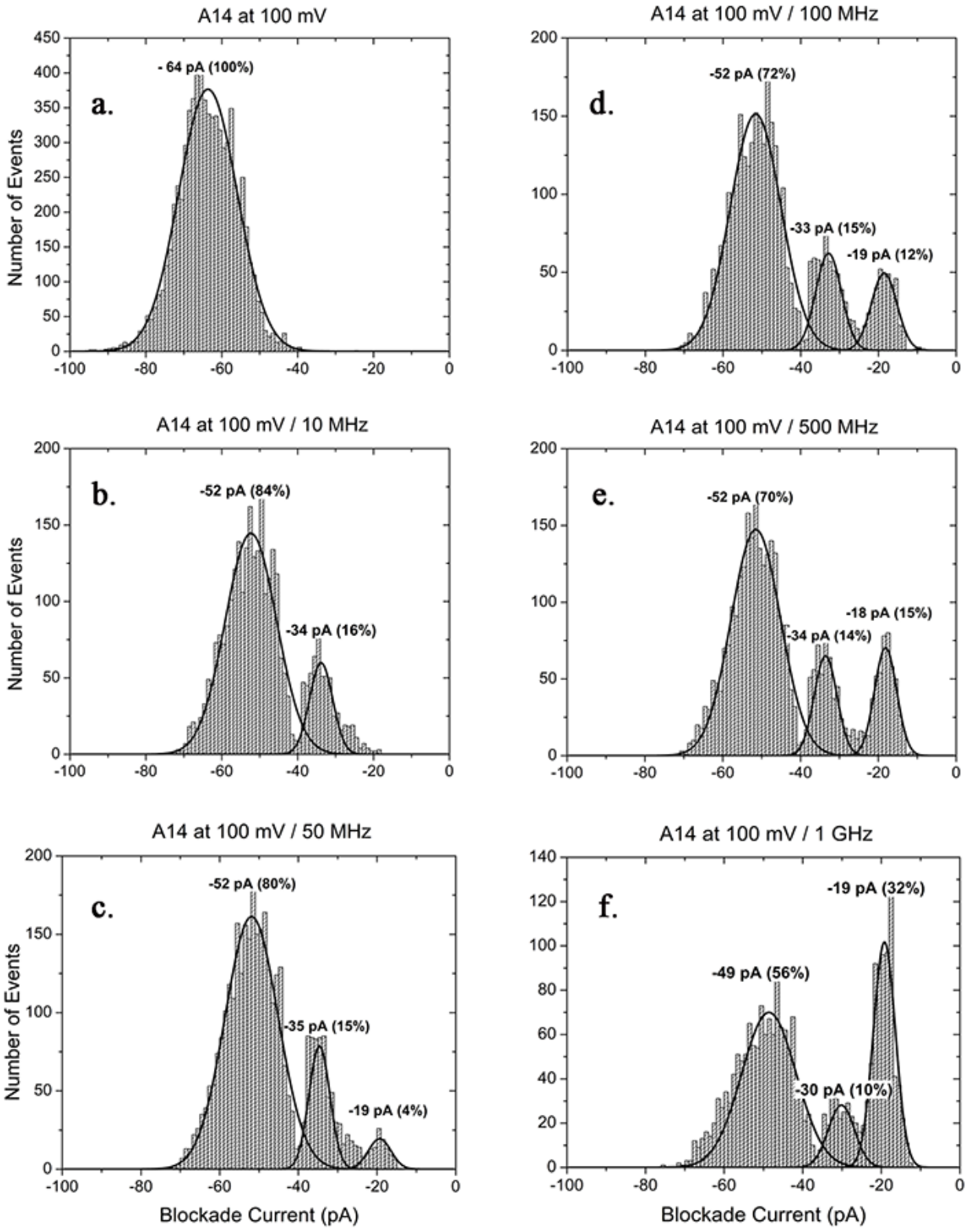

Figure. 3.3 Blockade current histograms for A14 at 100 mV DC with: **a.** No AC, **b.** 10 MHz, **c.** 50 MHz, **d.** 100 MHz, **e.** 500 MHz and **f.** 1 GHz.

Figure 3.4 shows current blockade histograms for A14 results at 140 mV DC with and without the applied AC field. With no applied AC voltage a broad translocation peak of 72% is present at -82 pA with a smaller intercalation peak at -52 pA (Figure 3.4 a). When an AC voltage of 10 MHz was applied, the translocation peak disappeared whereas the intercalation peak shifted to -58 pA (Figure 3.4 b). Additionally, a bumping peak appeared at -35 pA. The profile of the events doesn't change with increasing AC frequencies, as seen from the percentages of intercalation and bumping events in Table 3.2. A similar behaviour was observed for A10 at a 140 mV DC voltage. We assume that a combination of a high DC voltage (140 mV) with an AC field has no significant effects on the oscillation of the peptide regardless of the AC frequency.

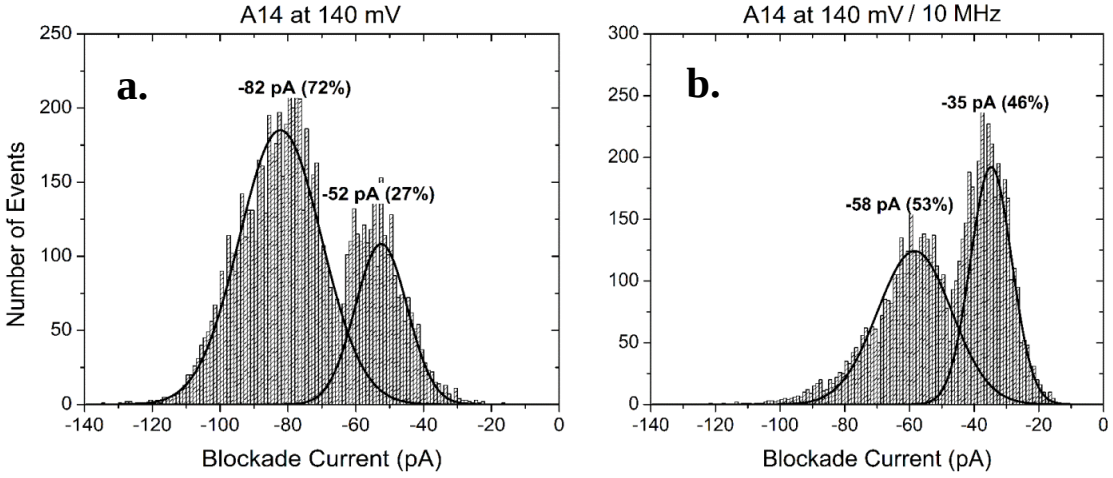

Figure 3.4 Blockade Current histograms for A14 at 140 mV DC with: **a.** No AC and **b.** 10 MHz.

The largest α-helical peptide analyzed in an AC field was A18. First, with no AC voltage applied there are only translocation events centered at -66 pA, but with the application of an AC field with a frequency of 10 MHz a second peak emerges at -45 pA (see Figure 3.5 b). The blockade current of this peak is not large enough to be qualified as translocation events or small enough to indicate bumping. Thus, the peak at -45 pA is probably due to intercalation. With the increase of the frequency to 50 MHz a third peak appeared at -27 pA due to bumping events, in addition to a shoulder on the translocation peak at -73 pA. A possible reason for the shoulder at -65 pA (Figure 3.5 c) is due to translocation of A18 as would be observed in the absence of an AC field. Consistent with this hypothesis is the 0.29 ms duration of these events,

as shown in Figure 3.6 which is similar to the duration in the absence of an AC field (Stefureac et al., 2006). In contrast, the very sharp peak at -73 pA is probably due to a bent structural conformation, a model for which will be presented in the Discussion. Despite an increase in frequency, there were no further notable changes in the event profiles (Figure 3.5 c-f).

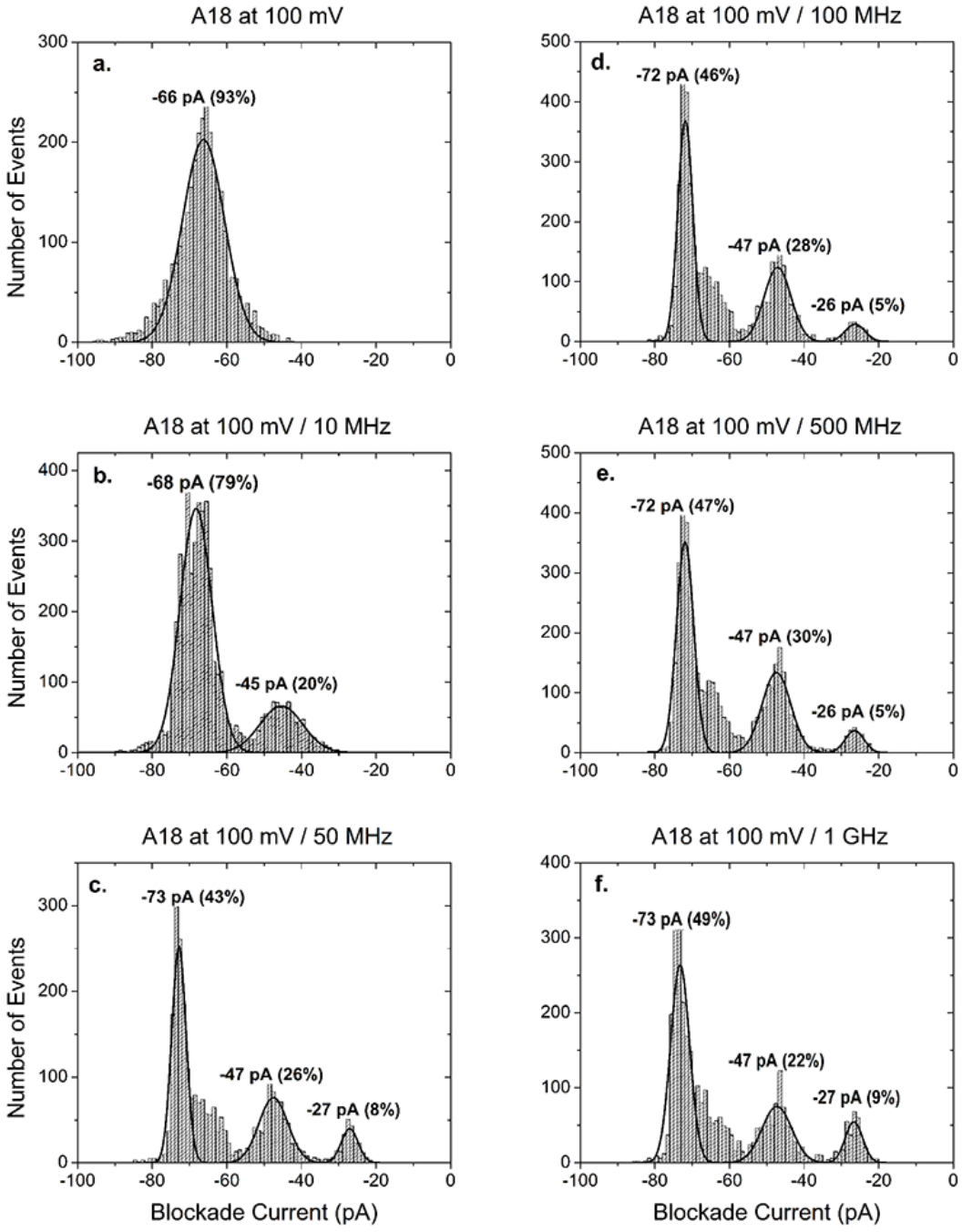

Figure 3.5 Blockade current histograms for A18 at 100 mV DC. **a.** No AC, **b.** 10 MHz, **c.** 50 MHz, **d.** 100 MHz, **e.** 500 MHz and **f.** 1 GHz.

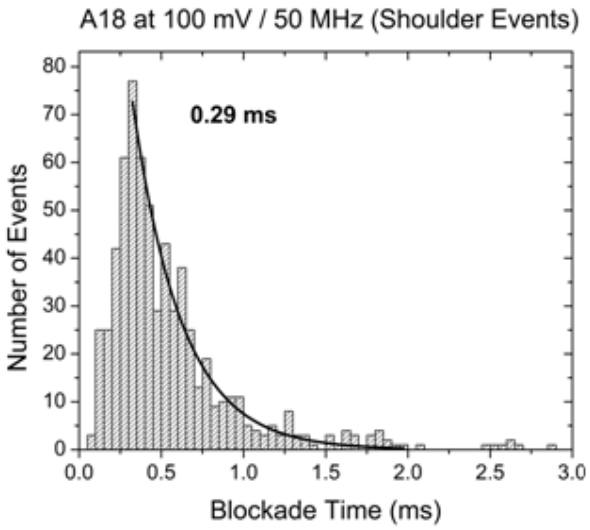

Figure 3.6 Time histogram of the shoulder events for A18 at 100 mV DC with 50 MHz AC.

To elucidate the changes in the blockade currents for A18 starting at 50 MHz, the blockade times for the translocation events of A18 at 60 mV, 100 mV, and 140 mV were measured as shown in Figure 3.7. The fit to a single exponential is reasonable at 60 and 140 mV, but it is clear that the time at 100 mV is significantly longer (see Figure 3.7 b). The results are summarized in Figure 3.8, where the increase of the translocation time for A18 at 100 mV is clearly observed at 50 MHz and 500 MHz.

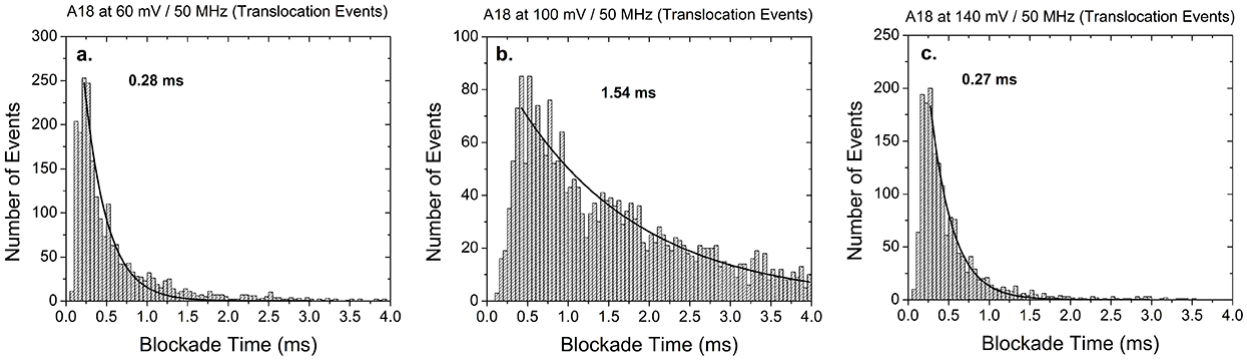

Figure 3.7 Time histograms of translocation events for A18 at 50 MHz AC and DC voltages of 60, 100 and 140 mV.

It is reasonable to assume that peptides with larger dipole moments are effected more by the AC field. It appears that as the AC frequency increases so does the proportion of bumping events. This observation is consistent with the results in Table 3.2.

Table 3.2 Summary of the percentages of translocation, intercalation and bumping events for A10, A14 and A18 with 60, 100 and 140 mV DC and 10 MHz to 1 GHz AC. (The error estimated for the percentage of events is ±10 %)

AC Freq. (MHz)	Peptide	60 mV			100 mV			140 mV		
		Trans Event (%)	Inter Event (%)	Bump Event (%)	Trans Event (%)	Inter Event (%)	Bum Event (%)	Trans Event (%)	Inter Event (%)	Bum Event (%)
No AC	A10	100	-	-	97	-	2	80	19	-
	A14	100	-	-	100	-	-	72	27	-
	A18	100	-	-	93	-	-	92	-	7
10	A10	88	-	11	83	15	-	-	55	45
	A14	70	-	29	84	16	-	-	53	46
	A18	55	39	4	79	20	-	75	11	13
50	A10	45	-	54	71	18	10	-	54	45
	A14	70	-	29	80	15	4	-	48	51
	A18	50	49	-	43	26	8	69	9	21
100	A10	58	-	41	82	4	12	-	53	47
	A14	54	-	45	72	15	12	-	40	59
	A18	61	38	-	46	28	5	65	10	24
500	A10	30	-	69	71	13	14	-	60	39
	A14	47	-	52	70	14	15	-	44	55
	A18	57	42	-	47	30	5	57	9	33
1000	A10	60	-	39	65	16	19	-	58	41
	A14	65	-	34	56	10	32	-	39	60
	A18	60	39	-	49	22	9	55	12	32

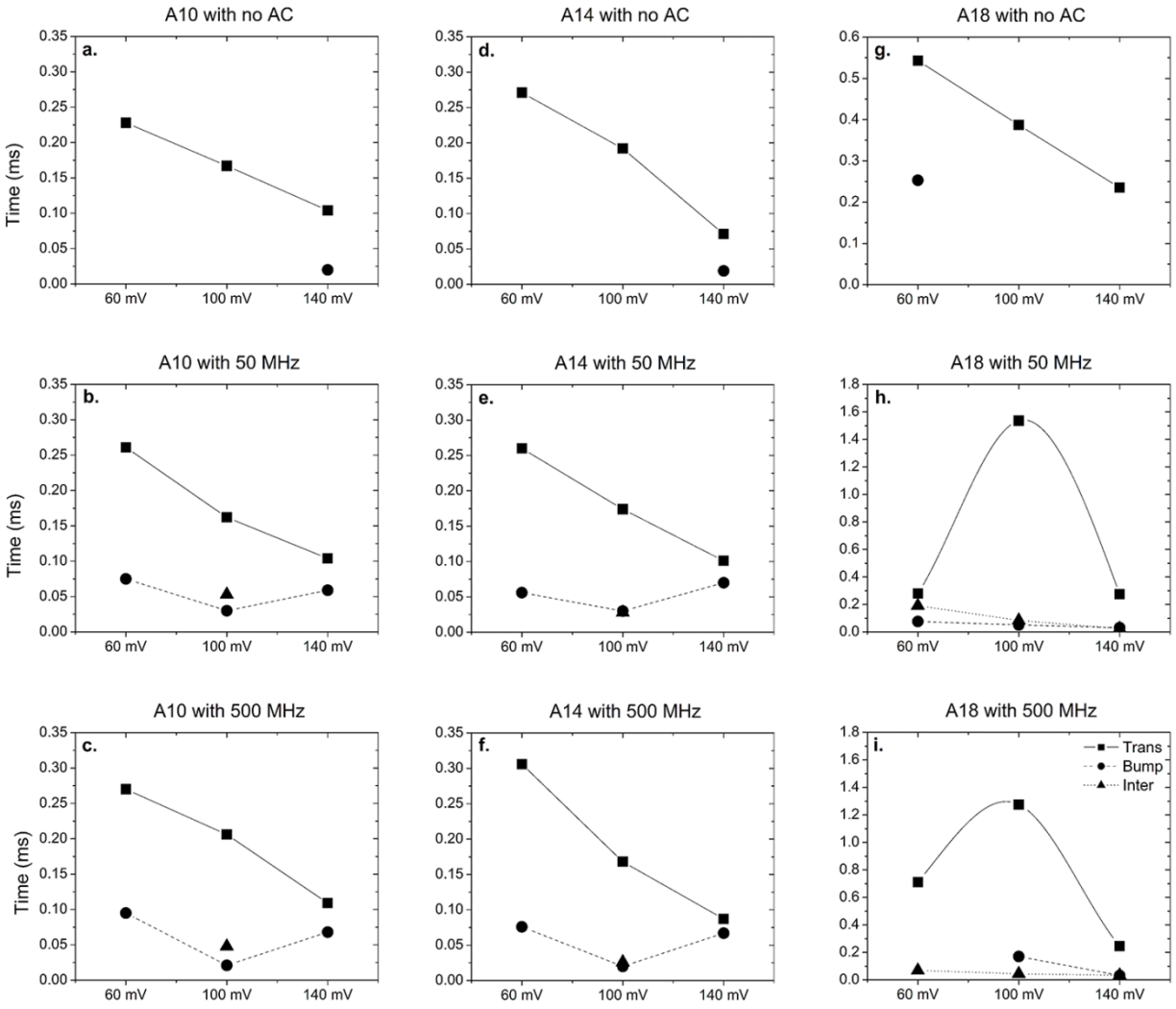

Figure 3.8 Event times as a function of the DC voltage for **a.** A10, **d.** A14 and **g.** A18 with no AC frequency applied; **b.** A10, **e.** A14 and **h.** A18 with 50 MHz AC; and **c.** A10, **f.** A14 and **i.** A18 with 500 MHz AC.

A10, A14 and A18 were studied at DC voltage offsets at 60, 100 and 140 mV (see Table 3.2). The blockade times are summarized in Figure 3.8. Without an applied AC field, the time for translocation decreased with voltage and increased with the length of the peptide, as expected. In all cases, the bumping or intercalation events were much faster. The addition of an AC field did little to change this pattern for A10 and A14, but for A18, at both 50 and 500 MHz, the time of the events reached a maximum at 100 mV. In the absence of an AC field, the value of T at 100 mV was about 0.40 ms but at 50 and 500 MHZ, it was 1.55 ms and 1.25 ms, respectively. At 60 mV and in the absence of an AC field, T is 0.55 ms, but at a frequency of

50 MHz, it decreased to 0.28 ms. Therefore, an AC field of 50 MHz can dramatically decrease or increase the event time depending on the DC voltage.

3.1.2 Behaviour of RI-A10 in an AC field

A retro-inverse peptide of A10 was studied as well. RI-A10 is an α-helix as well but is composed of D-amino acids and it has a larger dipole moment than A10 due to having three negative charges in the C-terminus (see Table 3.1). The dipole of the helix remains in the same direction as the direction of the charge dipole. Current traces are shown in Figure 3.9, covering 16 s for RI-A10 with and without an applied AC voltage.

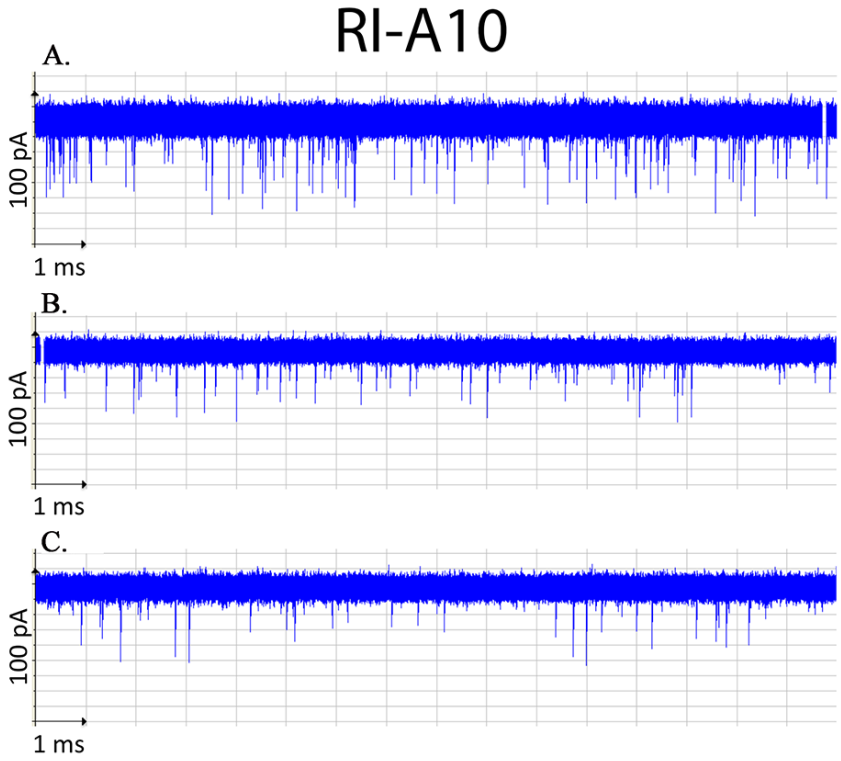

Figure 3.9 Screen shots of traces for RI-A10. **a.** DC voltage at 100 mV, no AC voltage, **b.** AC voltage of 200 mV with a 10 MHz frequency, **c.** AC voltage of 200 mV with a 100 MHz frequency.

For the RI peptide (Figure 3.9 a), in comparison to A10, the current trace was different. The translocation events for RI-A10 were around -60 pA and the bumping events around -25 pA. Even in the absence of an AC voltage, the frequency of events for RI-A10 was lower than for A10. In the other two panels in Figure 3.9, an AC field was applied with a constant amplitude of 200 mV and two different frequencies. When an AC voltage was applied at a 10

MHz frequency, the RI-A10 was prevented from translocating. Short bumping events are evident around -30 pA. Even at 100 MHz, bumping events constitute most of the current trace for RI-A10. These events were analyzed and are shown as blockade current histograms in Figure 3.10. In contrast to A10, the blockade current histograms for RI-A10 are simple and showed that the proportion of translocation was reduced to less than 5% at all frequencies.

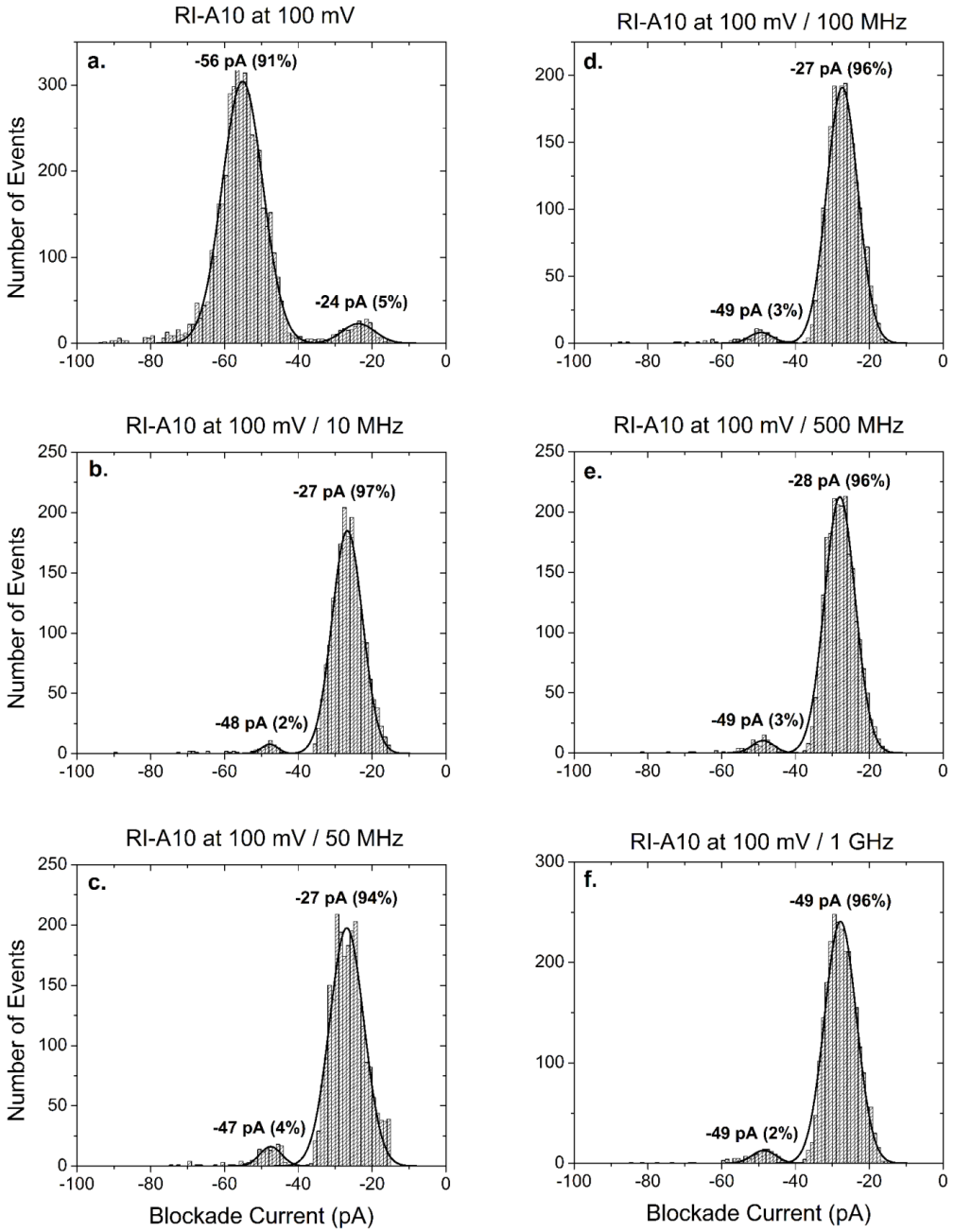

Figure 3.10 Blockade current histograms for RI-A10 at 100 mV DC. **a.** No AC, **b.** 10 MHz, **c.** 50 MHz, **d.** 100 MHz, **e.** 500 MHz and **f.** 1 GHz.

This behaviour is presumed to be due to the larger dipole moment, which will cause the RI-A10 to oscillate faster. Additionally, the highly charged C-terminus, which enters the pore first, will be greatly affected by the AC field and it is assumed to make it more difficult for RI-A10 to orient itself into the pore vestibule and translocate. We assume that this could be a possible explanation for the drastic increase of the bumping events with the application of an AC field compared to A10.

3.1.2.1 Equimolar mixture of A10 and RI-A10

Superposing an AC field onto a standard nanopore DC current may be of practical use in discriminating a molecular mixture. A10 and RI-A10 have similar molecular properties but they produce very different blockade current profiles when AC frequencies are applied (see Figure 3.2 and 3.10). An equimolar mixture of the two peptides, as seen from the current traces in Figure 3.11, was initially analyzed without an AC frequency, which gave a broad translocation peak at -59 pA and a minor bumping peak at -28 pA (see Figure 3.12 a).

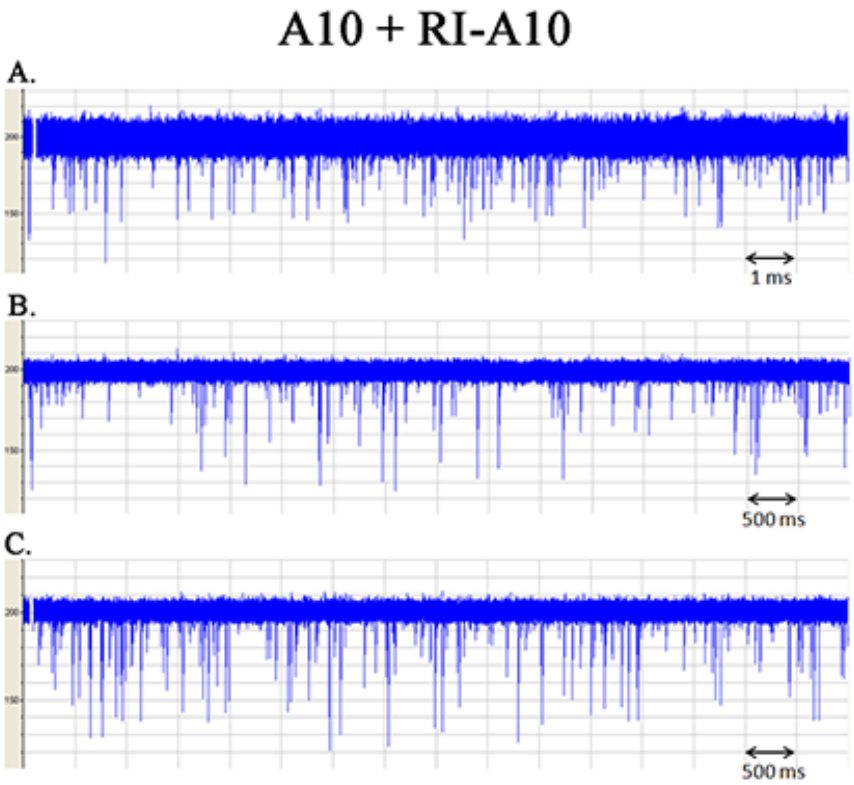

Figure 3.11 Screen shots of traces for the equimolar mixture of A10 and RI-A10; **a.** DC voltage at 100 mV with no AC voltage, **b.** AC voltage of 200 mV with a 10 MHz frequency, and **c.** AC voltage of 200 mV with a 100 MHz frequency.

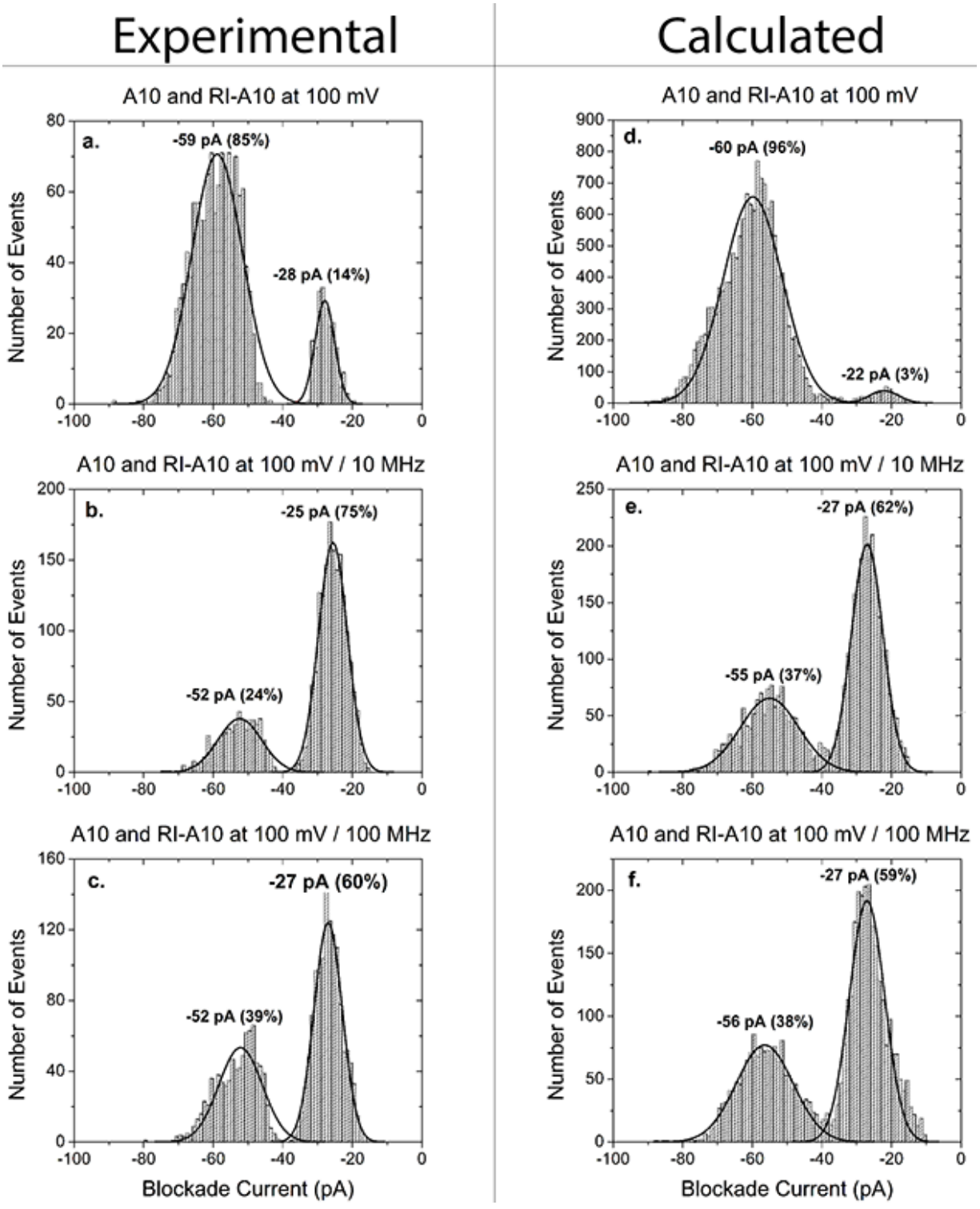

Figure 3.12 Blockade Current histograms for a mixture of A10 and RI-A10 at 100 mV DC for no AC, 10 MHz and 100 MHz applied. **a.**, **b.** and **c.** are values from the experiment; **d.**, **e.** and **f.** were calculated by adding the individual histograms.

The calculated blockade current histogram also give a broad translocation peak at -60 pA but the bumping peak is significantly smaller at about 3% (see Figure 3.5 d). There may be a small degree of interference between the two peptides, which causes a higher percentage of bumping events (Figure 3.11 a). The addition of an AC field at 10 and 100 MHZ, respectively, increased the proportion of bumping events because as expected, the RI-A10 is prevented from translocating (see Figure 3.10 and Figure 3.12 b and c). There is a good fit of the two blockade current histograms, the calculated and the experimental, especially at 100 MHz (see Figure 3.12 c and f).

3.2 Nanopore analysis of two ssDNA, d18 and oligo-dT20

Nanopores were initially used to detect single-stranded DNA so the effect of an AC field was considered interesting. The experiment was conducted on two separate strands, d18 and dT20 at 1 μM concentration, in 1 M KCl + 10 mM KPi buffer at pH 7.8.

d18: ATT ACC ACT TCT AGG ATA

poly-dT20: TTT TTT TTT TTT TTT TTT TT

Surprisingly, as shown in the current traces covering 16 s for each strand, the event frequency is very different for the two strands: d18 has 0.68 events sec^{-1} whereas dT20 is much faster with 6.75 events sec^{-1}. As seen in Figure 3.13 a, the long spikes for d18, around -85 pA, are due to the DNA strand translocating while the short ones, around -40 pA, are due to the strand bumping into the pore. For the dT20 strand, the translocation events are around -80 pA and the bumping events around -34 pA.

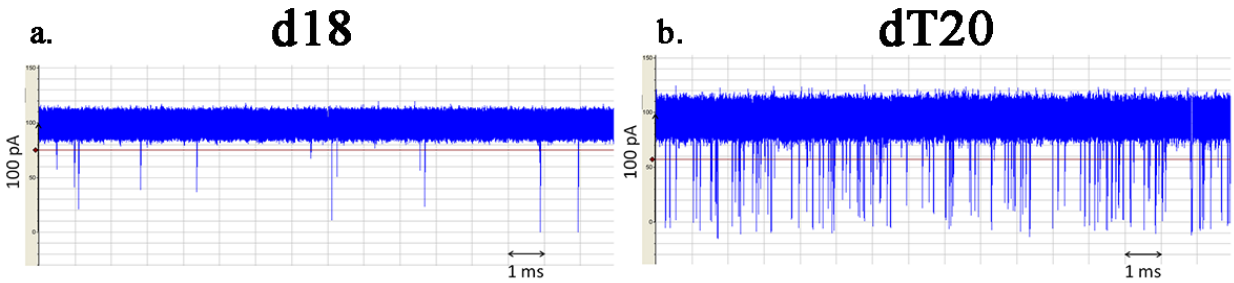

Figure 3.13 Current traces for single stranded DNA fragments **a.** d18 and **b.** dT20 at a DC field of 100 mV.

These events were analyzed and converted to blockade current histograms in Figure 3.14 for d18 and Figure 3.15 for dT20.

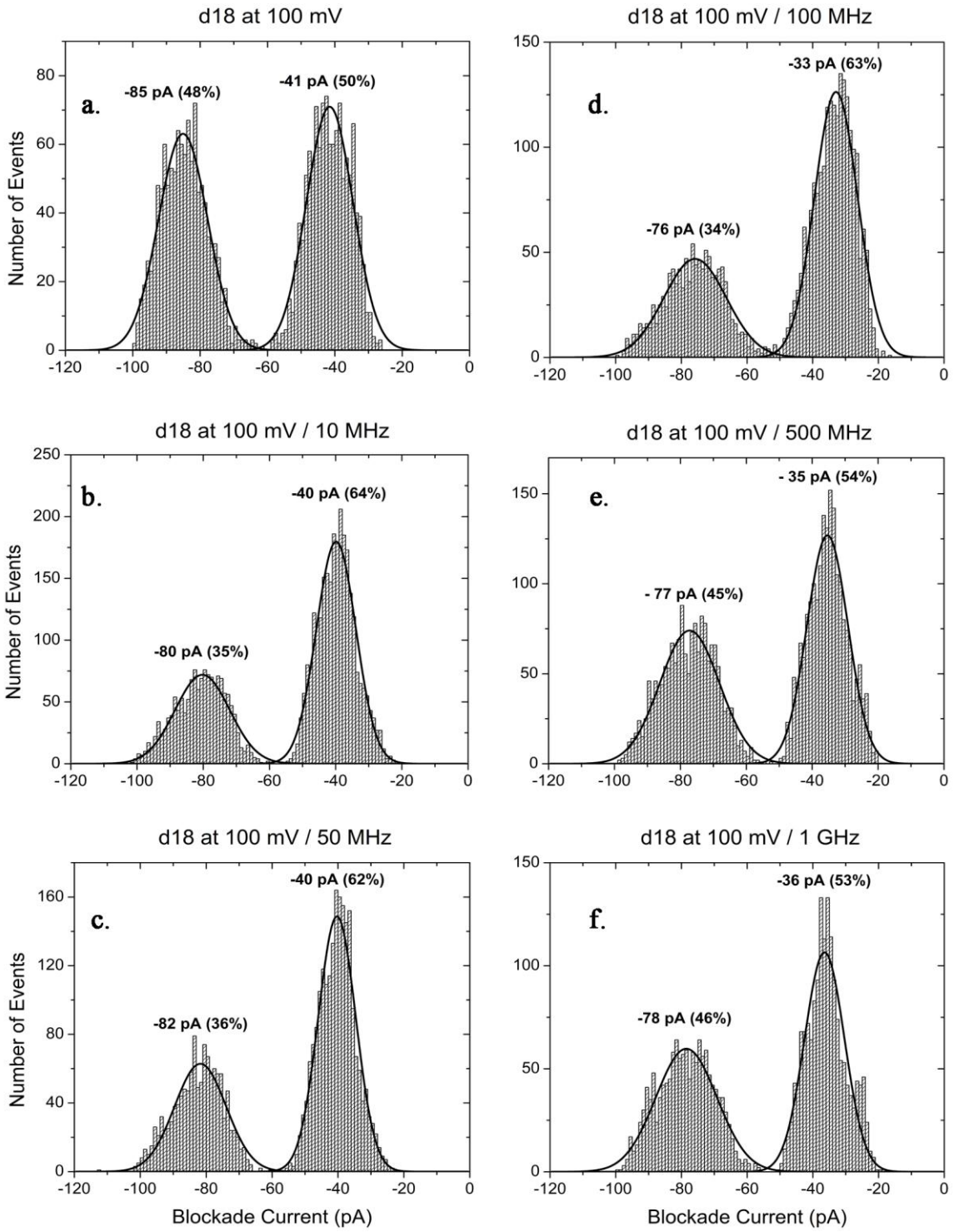

Figure 3.14 Blockade current histograms for single stranded DNA d18 at 100 mV DC. **a.** No AC, **b.** 10 MHz, **c.** 50 MHz, **d.** 100 MHz, **e.** 500 MHz and **f.** 1 GHz.

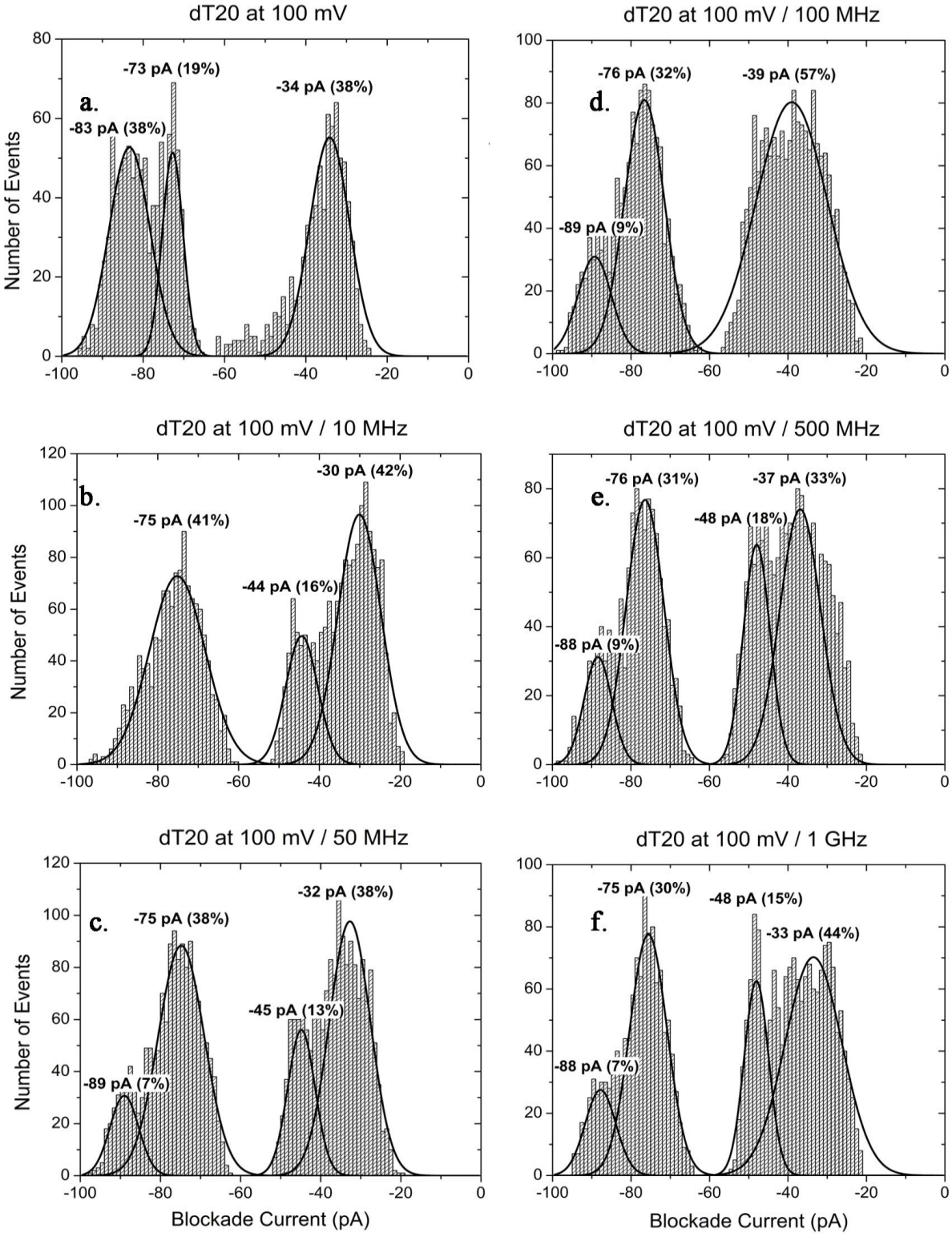

Figure 3.15 Blockade current histograms for single stranded DNA oligo-dT20 at 100 mV DC. **a**. No AC, **b**. 10 MHz, **c**. 50 MHz, **d**. 100 MHz, **e**. 500 MHz and **f**. 1 GHz.

For d18, with no AC field, there was a translocation peak at -85 pA and a bumping peak at -40 pA with similar event frequencies. At 10 MHz AC, the translocation peak shifted to -80 pA and also decreases in proportion from 49 % to 25%. Only small changes to the histograms were observed as the frequency increased (see Figure 3.14 c-f).

For dT20, the blockade current histograms are complicated; even without the application of an AC field, the translocation peak is divided into two peaks at -83 pA and -73 pA (Figure 3.15 a). At all AC frequencies, the ratio of translocation is reduced while the ratio of the bumping peak increased. As shown in Figure 3.15 b, there is a major translocation peak at -75 pA and a bumping peak at -30 pA, with a small shoulder at -44 pA. Starting at 50 MHz, the translocation events have a small shoulder at -89 pA, which doesn't change even at 1 GHz. The bumping peak is either split into two peaks upon application of an AC field or it becomes very broad (e.g. at 100 MHz in Figure 3.15 d). It is assumed that oligo-dT20 enters the pore from both ends, 5' end and the 3' end, as seen previously in the literature (Chen and Li, 2007). This might be a possible explanation why there are two bumping and translocation peaks for oligo-dT20. A detailed illustration of these observations will be presented in the Discussion.

The blockade time of the translocation events was calculated for both strands at a 100 mV DC in the absence of an AC field, as shown in Figure 3.16. It is necessary to indicate that the events of dT20 at the -73 pA peak were not included in the calculation of the final translocation time, as shown in Figure 3.16 b. Even though the translocation events have different blockade current profiles, they appear to have similar blockade times.

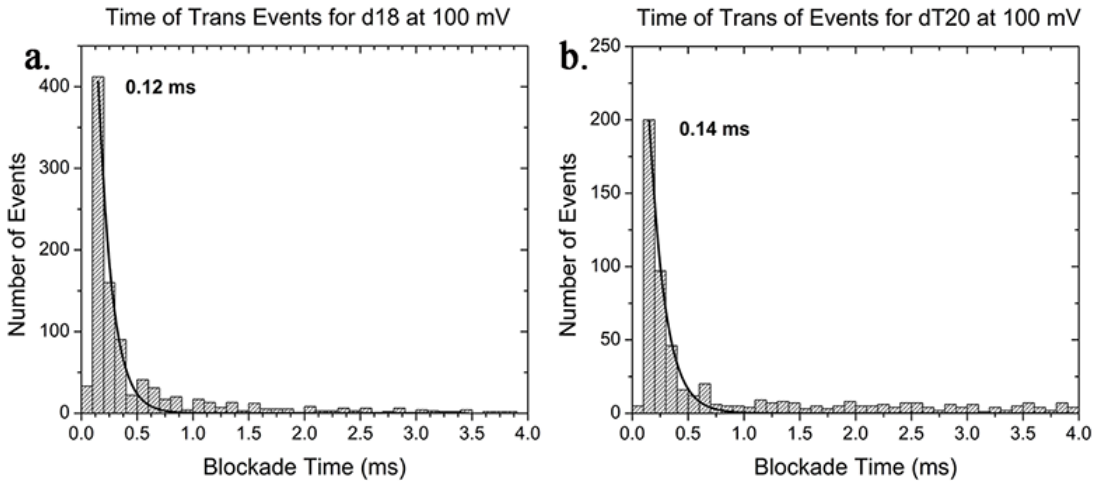

Figure 3.16 Time histograms of translocation events for single stranded DNA **a.** d18 and **b.** dT20 at 100 mV DC.

3.3 Alpha-Synuclein

AS is a peptide of 140 amino acids, which is intrinsically disordered under most conditions. The C-terminus has a net charge of −12 while the N-terminus has a net charge of +4 and the entire peptide has a final net charge of -9. It is electrophoretically driven through the pore from the C-terminus under standard conditions (Tavassoly et al., 2014b). Most random conformations of AS are expected to have very large dipole moments and, thus, it was of interest to analyze the effect of an added AC field.

3.3.1 Nanopore analysis and voltage studies of Alpha-Synuclein

AS was studied previously by standard nanopore analysis (Madampage et al., 2012). The protein was analyzed in an aqueous solution of 10 mM HEPES buffer pH 7.8, which included 1 mM EDTA on the cis side to chelate metals that might be present in the solution (Krasniqi and Lee, 2012). Earlier, it was shown that the protein has a major translocation peak at -85 pA and a small bumping peak at -26 pA (Madampage et al., 2012). A voltage study was conducted at 60, 80, 100, 120 and 140 mV DC to show the effect of the DC field in the events profiles of AS. The results are shown in Figure 3.17 with the calculated times in Table 3.3.

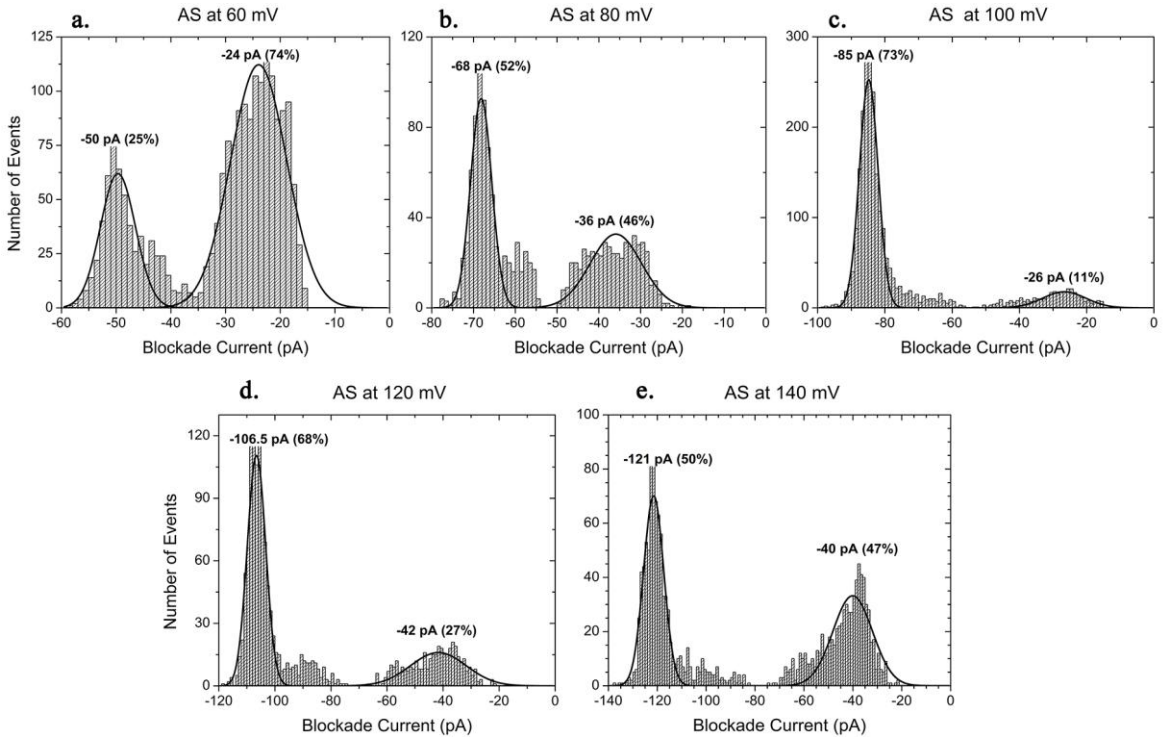

Figure 3.17 Blockade current histograms for AS at **a.** 60 mV, **b.** 80 mV, **c.** 100 mV, **d.** 120 mV and **e.** 140 mV

When the DC voltage was increased from 60 mV to 80 mV, both the percentage and the duration of translocation events increased (Figure 3.17 a and b). At 60 mV DC, the event frequency was very low. Two broad peaks were observed: a major bumping peak of 74% at -24 pA and a small translocation peak of 25% at 50 pA. At 80 mV, the translocation peak was narrower and increased significantly to 52%. The maximum translocation events occurred at 100 mV (Figure 3.17 c).

As the DC voltage increased to 120 mV, the population of the translocation events decreased slightly to 68% while the time also decreased (see Table 3.3). At 140 mV, the ionic current constantly dropped due to the blockage of the pore with AS, and the frequency of events was very fast (see Figure 3.18 a). At this high voltage, the translocation peak decreases further to 50% with a blockade time at 0.70 ms. Additionally, a small but wide bumping peak occurred at -40 pA (47%). Thus, the effect of voltage on the time of the translocation events is complicated and anomalous for the lowest and the highest DC voltages.

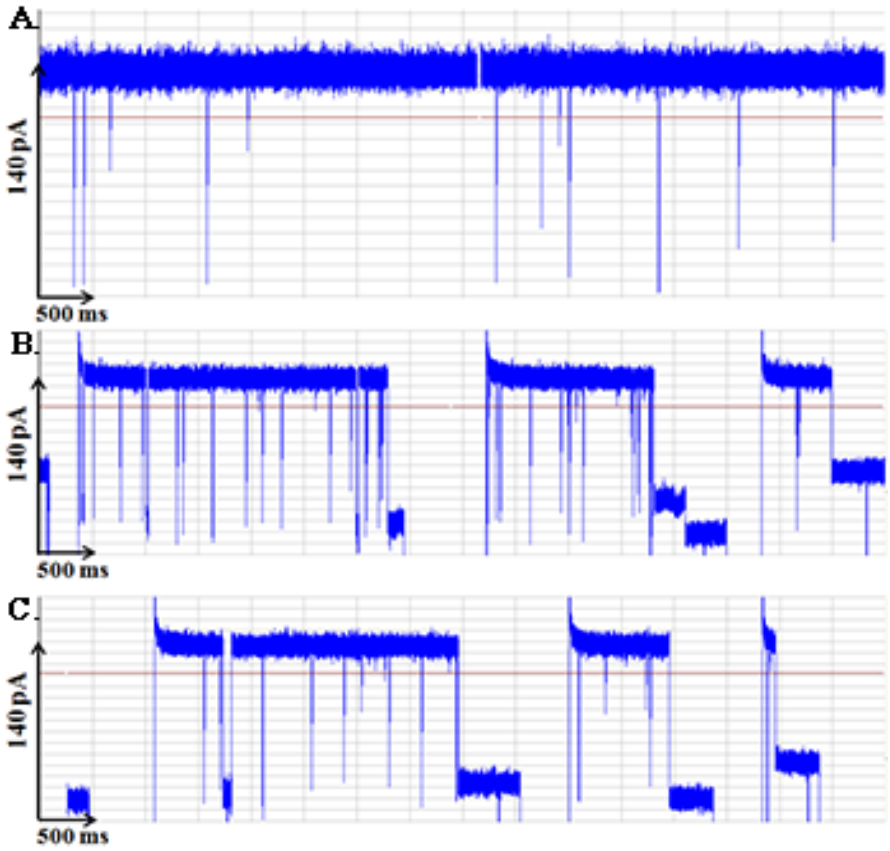

Figure 3.18 Screen shots of traces for AS at a DC voltage at 140 mV. **a.** no AC voltage; **b.** AC voltage with a 100 MHz frequency, **c.** AC voltage with a 1 GHz frequency.

Table 3.3 T values of AS at 60, 80, 100, 120 and 140 mV DC voltage. (The error estimated for T is ±10%)

	Time of Events (ms) of AS	
DC Voltage (mV)	Translocations	Bumping
60	0.41	0.07
80	0.82	0.08
100	0.52	0.05
120	0.47	0.11
140	0.70	0.14

3.3.2 Behaviour of Alpha-Synuclein in an AC field

As seen from Figure 3.17 c and 3.19 a, in the absence of an AC field with a 100 mV DC the blockade current histogram resembled the results from a previous study (Madampage et al., 2012). However, as the AC frequency is increased so did the population of the bumping events (see Figure 3.19). When an AC field of 200 mV at 100 MHz was applied, the number of translocation events dropped to 35% while the number of bumping events proportionally increased. As the AC frequency increased to 1 GHz, about 73% of the events are related to bumping.

AS was also analyzed at 60 and 140 mV DC, but for simplicity, the events blockade current for bumping (Bump), intercalation (Inter) and translocation (Trans) peaks are summarized in Table 3.4 below.

At 60 mV DC without an AC voltage, the blockade histograms for AS showed two Gaussian peaks: a small peak at -50 pA that was due to translocation and a large peak at -24 pA that was due to bumping events (Figure 3.18 a). With the application of an AC field, at a 10 MHz frequency, the ratio of translocation events dropped from 25% to 12%. Additionally, at 10 MHz, a third small peak appeared which was assumed to be intercalation events. With an increase of the AC frequency to 50 MHz, a minor increase in the number of translocation events to 15% was observed, which further increased to 17% at 100 MHz. However, when the AC frequency was increased to 1 GHz, the bumping population also increased, whereas the translocation peak decreased and remained at 13%.

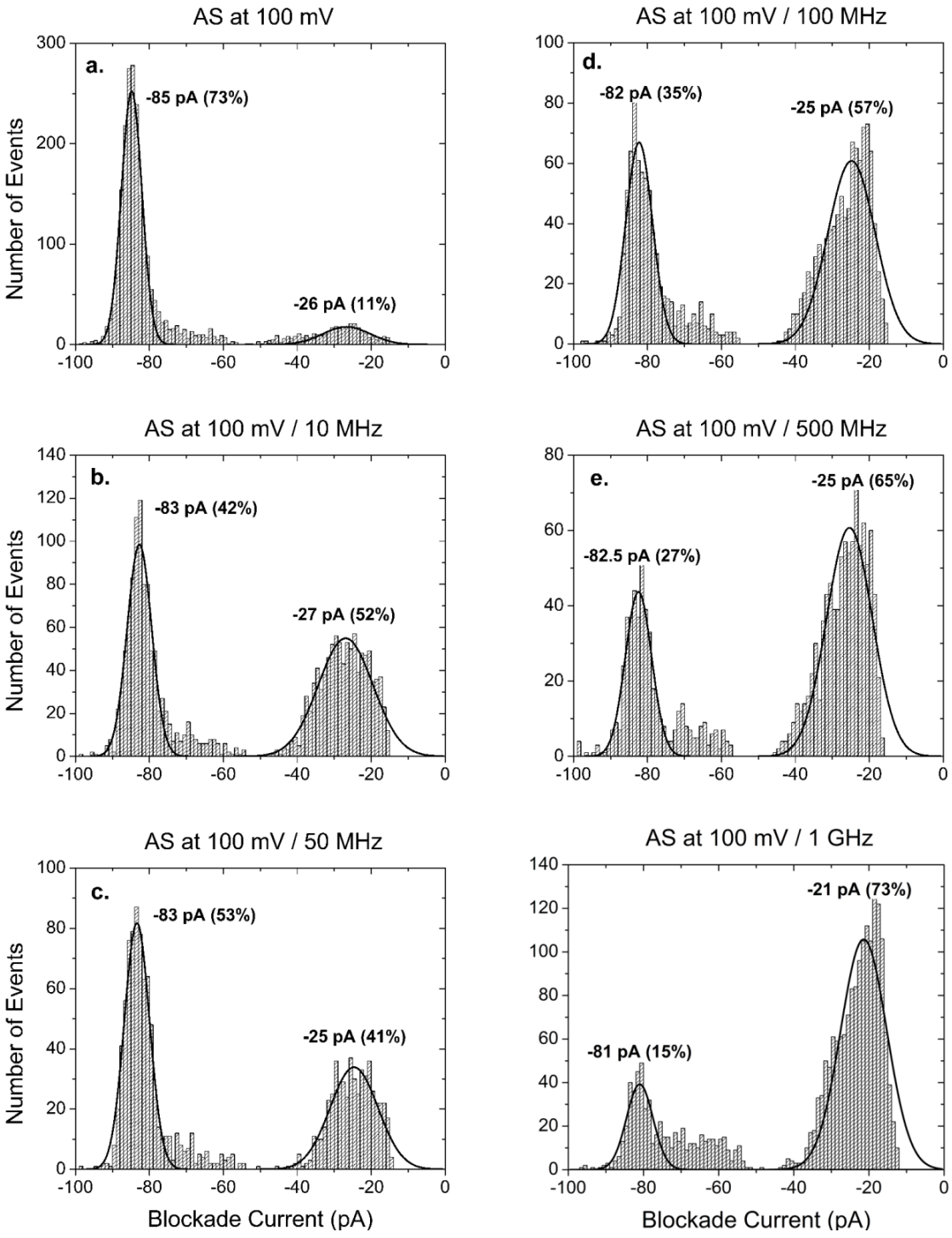

Figure 3.19 Blockade current histograms for AS at 100 mV DC. **a.** No AC, **b.** 10 MHz, **c.** 50 MHz, **d.** 100 MHz, **e.** 500 MHz and **f.** 1 GHz.

At the highest DC voltage of 140 mV, the behaviour of AS was complicated mostly due to the many drops in the ionic current, as seen in Figure 3.18. At the first application of an AC

field there is an increase in the percentage of bumping events from 51 to 75%. The blockade histograms of AS at 140 mV showed an initial decrease of the proportion of translocation events from 10 to 100 MHz followed by a steady increase back to 77% until 1 GHz, as seen in Table 3.4. The fluctuation of the proportion of the translocation events at 140 mV DC suggests that many factors are involved.

Table 3.4 Summary of the percentages of translocation, intercalation and bumping events for AS with 60, 100 and 140 mV DC amplitudes and 10 MHz to 1 GHz AC frequencies. (The error estimated for the percentages of events is ±10 %)

AC Freq. (MHz)	60 mV			100 mV			140 mV		
	Trans Event (%)	Inter Event (%)	Bump Event (%)	Trans Event (%)	Inter Event (%)	Bump Event (%)	Trans Event (%)	Inter Event (%)	Bump Event (%)
No AC	25	-	74	73	-	11	51	-	48
10	12	12	74	42	-	52	75	-	24
50	15	11	72	53	-	41	57	-	12
100	17	6	75	35	-	57	28	-	71
500	13	9	76	27	-	65	59	-	40
1000	13	6	79	15	-	73	77	-	22

3.3.3 Domains of Alpha-Synuclein in an AC field

The three domains of AS were studied under the same conditions as previously published (Tavassoly et al., 2014a). The blockade current histogram of the N-terminus, as seen in Figure 3.20 a, has a single Gaussian peak at -30 pA due to bumping events. The N-terminus is positively charged (+4) and as a consequence, it will be very difficult to orientate towards the pore and translocate through. Conversely, the C-terminus has a -12 charge and as a result, it will translocate easily through the pore as seen in Figure 3.21 a. The blockade current histogram has a large and wide translocation peak at -69 pA and a fairly small bumping peak at -30 pA. The ΔNAC with no AC field has two peaks, a large peak at -86 pA due to translocation and a smaller one at -27 pA due to bumping (see Figure 2.22 a). The domains were then tested in the AC voltage with an initial DC voltage of 100 mV.

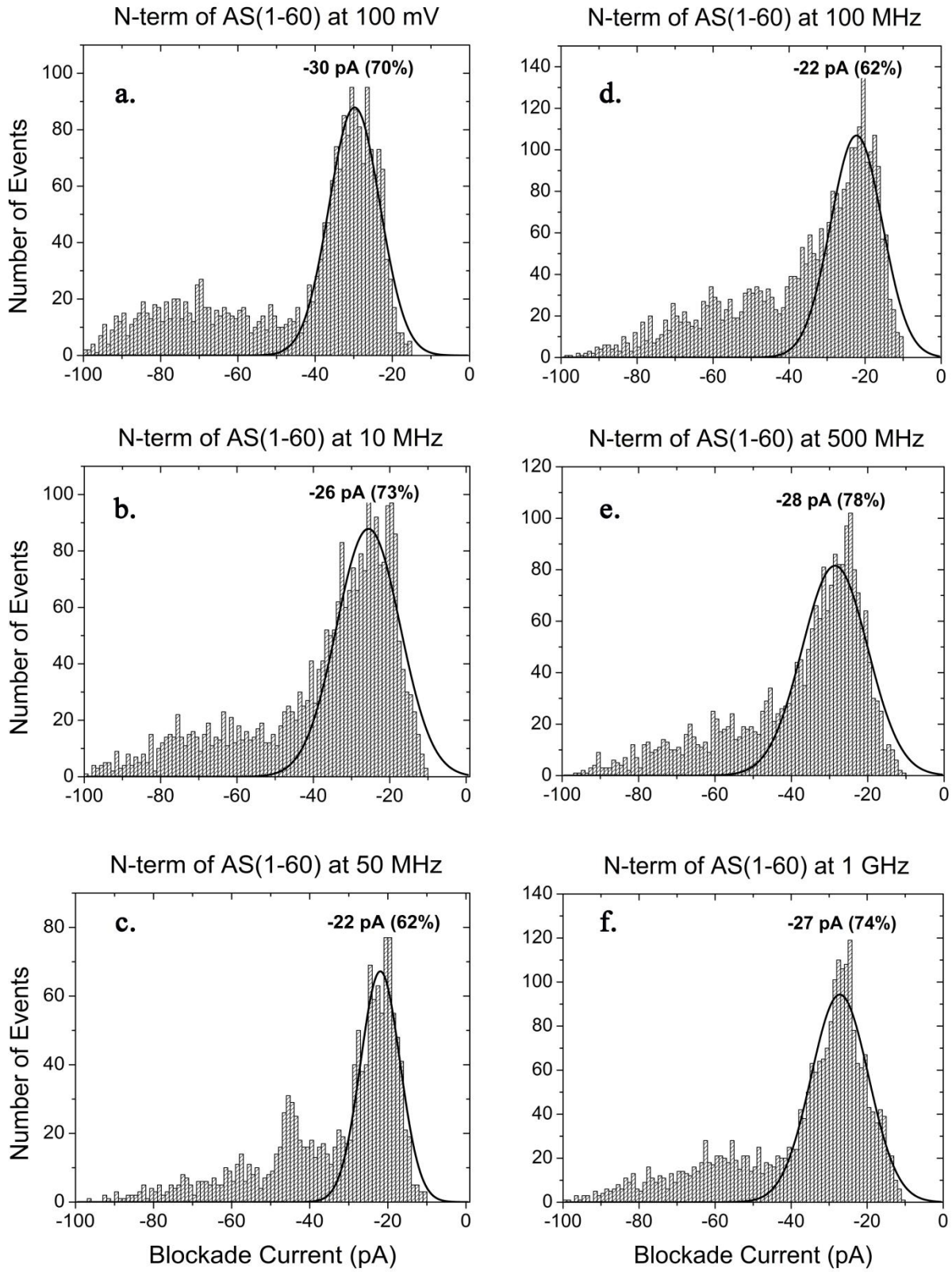

Figure 3.20 Blockade current histograms for the N-terminus of AS (1-60) at 100 mV DC. **a.** No AC, **b.** 10 MHz, **c.** 50 MHz, **d.** 100 MHz, **e.** 500 MHz and **f.** 1 GHz.

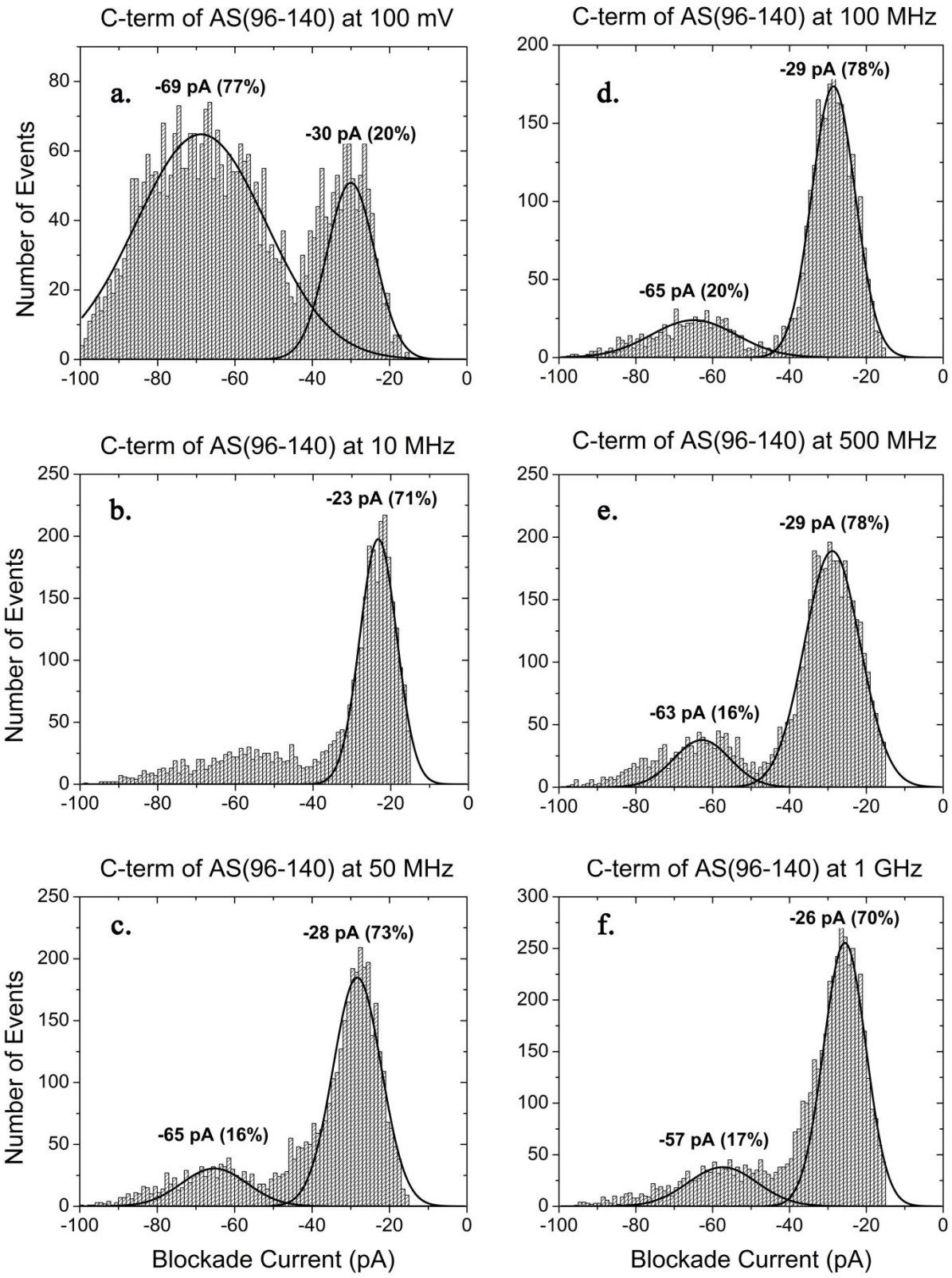

Figure 3.21 Blockade current histograms for the C-terminus of AS (96-140) at 100 mV DC. **a.** No AC, **b.** 10 MHz, **c.** 50 MHz, **d.** 100 MHz, **e.** 500 MHz and **f.** 1 GHz.

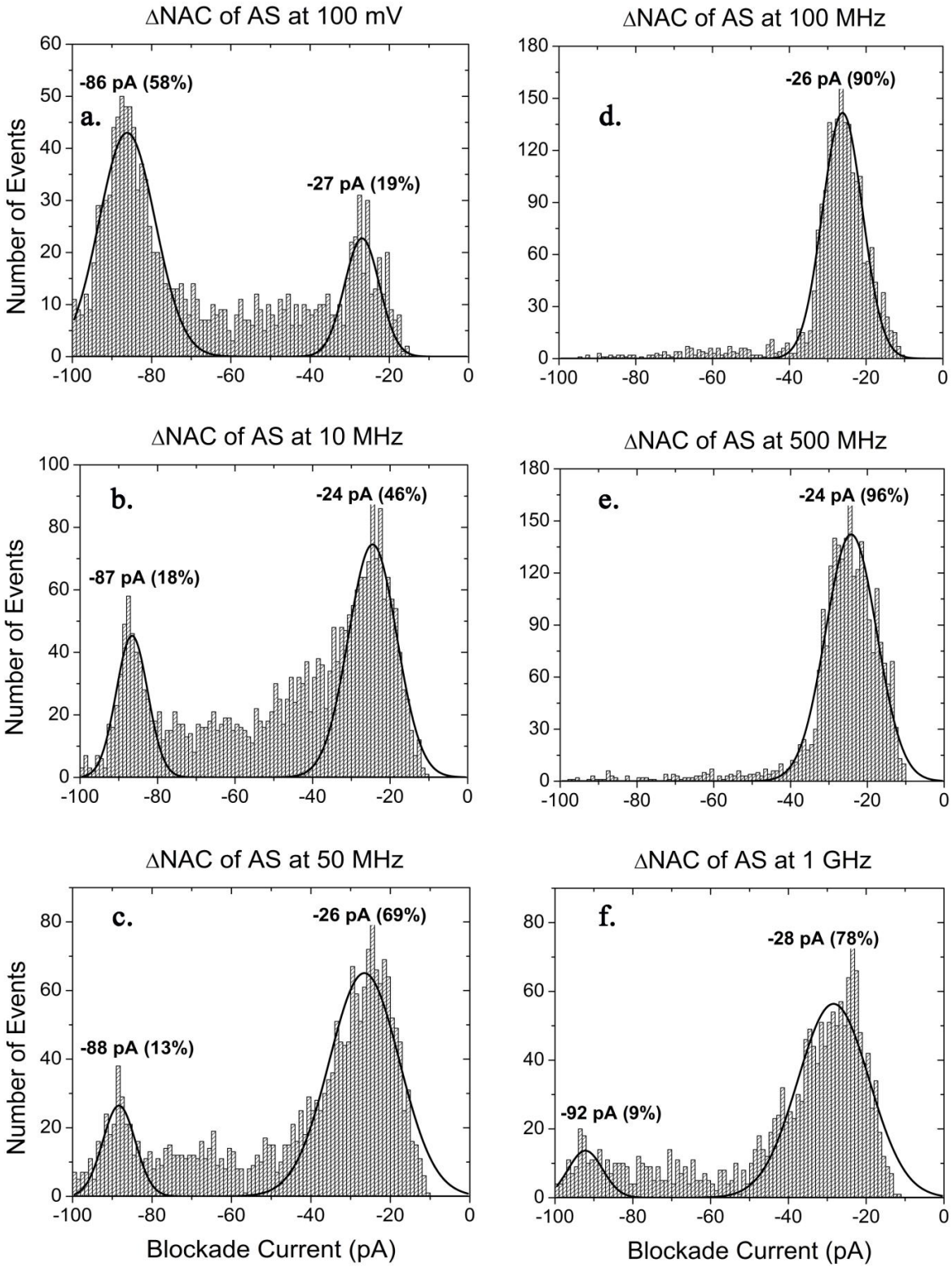

Figure 3.22 Blockade current histograms for ΔNAC at 100 mV DC. **a.** No AC, **b.** 10 MHz, **c.** 50 MHz, **d.** 100 MHz, **e.** 500 MHz and **f.** 1 GHz.

For the N-terminus, there are few consequences after application of an AC field. As shown in Figure 3.20 b, the bumping peak shifted to -26 pA after a frequency of 10 MHz was applied, as was previously observed with other peptides. However, the application of higher frequencies has little effect mostly due to the positive charge which prevent the N-terminus from entering the pore initially.

For the C-terminus domain, with the application of an AC field at a frequency of 10 MHz, the large translocation peak disappeared, as illustrated in Figure 3.21 b. There is a small disperse translocation peak at 50 MHz, which changed little as the AC frequency was increased. We assume that because of the large negative charge, the C-terminus is oscillating fast and thus is prevented from translocating.

With the application of the AC field, ΔNAC behaved as expected for a peptide with a negative C-terminus and/or with a large dipole moment. The proportion of bumping events increased with the increase of the AC frequency. The values of T are summarized in Table 3.5. The time of translocation events for the ΔNAC decreased significantly after the application of an AC frequency of 10 MHz from 1.23 ms to 0.64 ms. The translocation time decreases further at 50 MHz to 0.36 ms. At 100 and 500 MHz very few translocation events were observed, but a small peak at -92 pA appeared at 1 GHz with blockade time significantly smaller at 0.11 ms.

Table 3.5 Time of ΔNAC at 100 mV DC with AC frequencies from 10 MHz to 1 GHz. (The error estimated for T is ±10 %)

		Time of Events (ms)	
Domain	Frequency (MHz)	Translocations	Bumping
ΔNAC	**No AC**	1.23	0.05
	10	0.64	0.06
	50	0.36	0.04
	100	-	0.06
	500	-	0.08
	1000	0.11	0.05

3.4 Analysis of Alpha-Synuclein and Drug complexes in the AC field

Nanopore analysis with an AC field may be useful for probing the conformational states of AS which are induced by drugs (Kakish et al., 2015b; Shim et al., 2009; Tavassoly et al., 2014b). Seven drugs were chosen to be tested in an AC setup as shown in Figure 3.24. These drugs were chosen based on their neuroprotective or neurotoxic role. This separation based on their role in preventing further neuronal degeneration or causing Parkinson-like symptoms, is due to the new conformation AS adopts when the drug is bound to it. Previous results showed that drugs like S-1-aminoindane, 3-methoxytyramine, caffeine and (-)-nicotine bind to both the N- and C-termini and form a loop conformation (Kakish et al., 2015b; Tavassoly et al., 2014a). This loop conformation blocks the NAC region from future aggregation, which later will prevent the formation of the LBs (Kakish et al., 2015a). (+)-Amphetamine binds very tightly to the N-terminus forming a knot conformation, which leaves the NAC region ready for fibrillization (Kakish et al., 2015a). Other drugs like metformin and cocaine were chosen to be studied in an AC field based on previous binding sites. Cocaine binds to the NAC region of AS and metformin binds to the C-terminus. A control was conducted with the A10 peptide, one of the α-helical peptides mentioned previously, with S-1-aminoindan to show that the drug does not interact with either the pore or the membrane of the nanopore analysis setup.

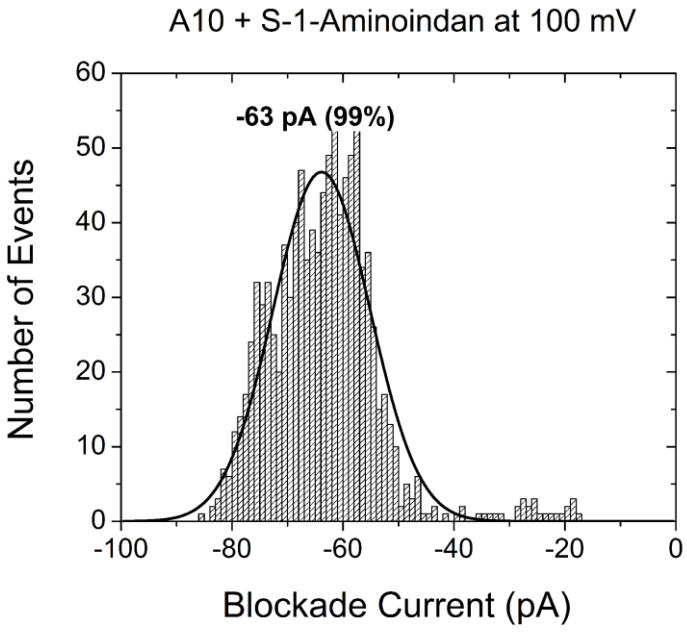

Figure 3.23 Blockade current histogram of A10 with S-1-Aminoindan at 100 mV DC.

Their behaviour in an AC field would benefit biochemists and drug designers as both these drugs have been shown to alter the induction of PD. Long term users of cocaine develop Parkinson-like symptoms, whereas diabetes patients who take metformin have shown decreased signs of PD or neuronal degeneration, which leads one to believe that this drug could be neuroprotective (Kakish et al., 2015a). All the drugs have similar binding constants, therefore differences in conformation and possible stripping is probably due to either the charge or the position where they bind in the protein.

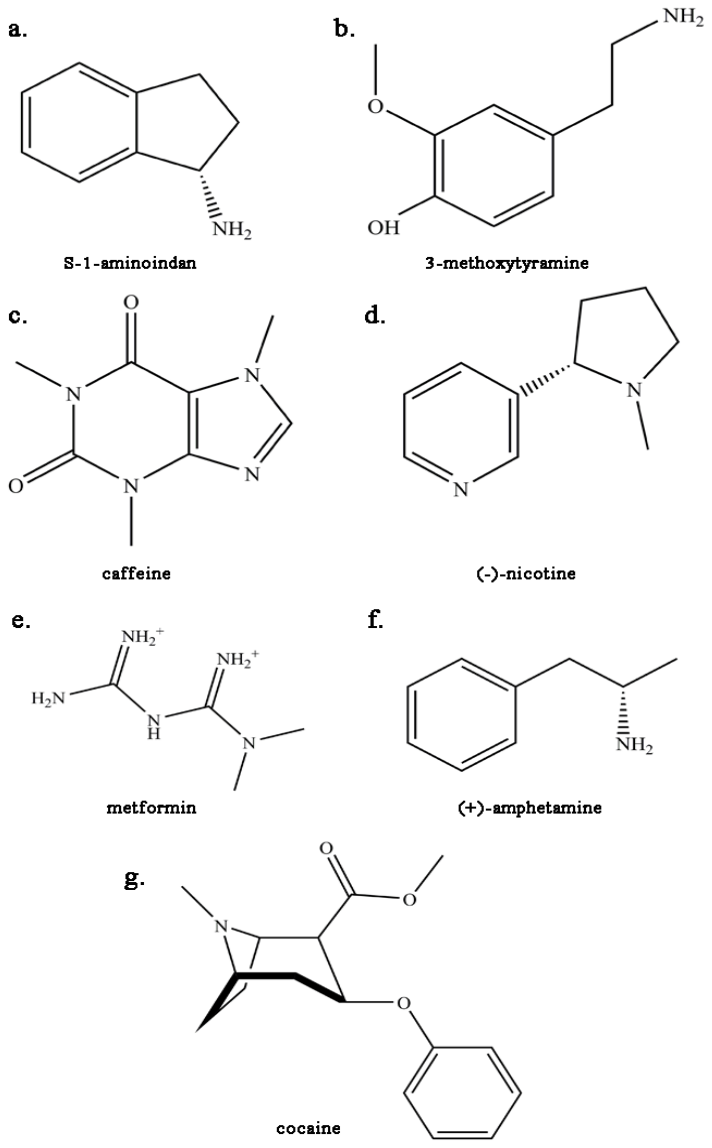

Figure 3.24 Structure of **a.** S-1-aminoindane, **b.** 3-methoxytyramine, **c.** metformin, **d.** caffeine, **e.** (-)-nicotine, **f.** (+)-amphetamine and **g.** cocaine. The nomenclature concerning stereoisomers conforms to the published literature, i.e. S, (-) and (+).

3.4.1 S-1-Aminoindan

The AS-drug complex with S-1-aminoindan was analyzed and the blockade current histograms are shown in Figure 3.25.

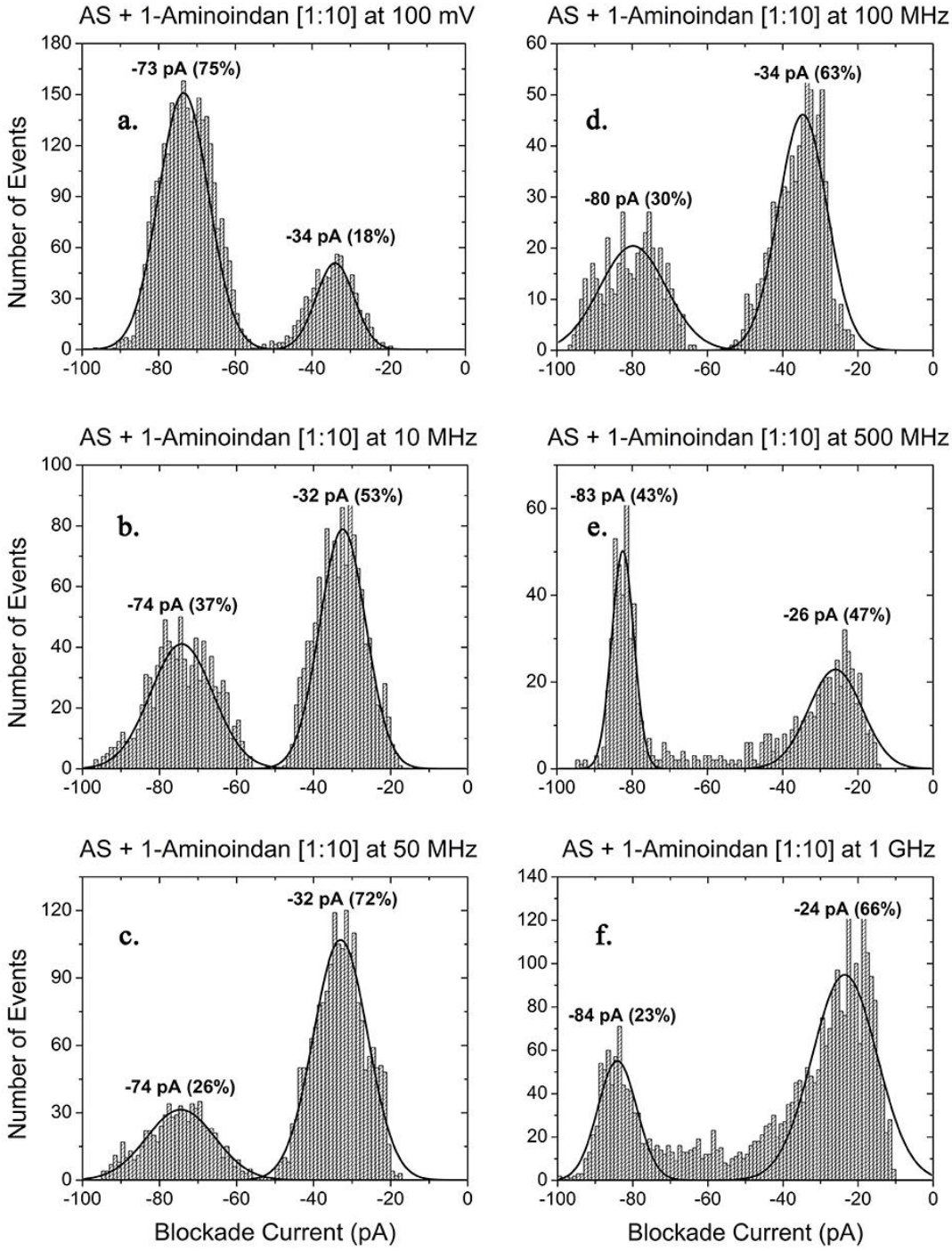

Figure 3.25 Blockade current histograms for AS with S-1-Aminoindan [1:10] at 100 mV DC. **a.** No AC, **b.** 10 MHz, **c.** 50 MHz, **d.** 100 MHz, **e.** 500 MHz and **f.** 1 GHz.

The blockade histograms for S-1-aminoindan in the absence of an AC field demonstrate that the majority of events are related to translocation, as observed previously (Kakish et al., 2015b). With the application of an AC voltage at a frequency of 10 MHz, the translocation peak remained broad but decreased to 40%. The translocation peak stayed at the same blockade current between this frequency and 50 MHz. Interestingly, the time of the translocation events increased significantly from 0.24 ms with no AC to 0.63 ms at 10 MHz, as seen in Table 3.7. Conversely, the proportion of bumping events increased significantly from 18% with no AC to 58% at 10 MHz and to 72% at 50 MHz (see Figure 3.25 b and c). At 100 MHz, the blockade current resembled the blockade current histogram of AS at 100 MHz (see Figure 3.19 d). The translocation peak increased to 30%, but remained broad, while the time of the translocation events also increased to 1.17 ms. However, at 500 MHz and 1 GHz, the translocation peak shifted to -84 pA, which was similar to AS at these frequencies (see Figure 3.19 e and f). At 500 MHz, the time of translocation events decreased to 0.51 ms and to 0.33 ms at 1 GHz. The increase of the blockade current of the translocation events to -84 pA suggests that the drug might be stripped off the protein due to the high AC frequencies, a model for which will be presented in the Discussion.

Table 3.6 Time of S-1-aminoindan events at 100 mV DC with AC frequencies from 10 MHz to 1 GHz. (The error estimated for T is ±10 %)

		Time of Events (ms)	
Drug	Frequency (MHz)	Translocations	Bumping
S-1-Aminoindan	**No AC**	0.24	0.07
	10	0.62	0.16
	50	0.69	0.14
	100	1.17	0.13
	500	0.51	0.07
	1000	0.33	0.07

3.4.2 3-Methoxytyramine

For 3-methoxytyramine (3-MT), in the absence of an AC field, the blockade current histogram shows a single Gaussian peak at -37 pA (see Figure 3.25 a). In the presence of an

AC field, the proportion of translocation events increased with an increase of the AC frequency. This is the first time that such an effect of an AC field was observed.

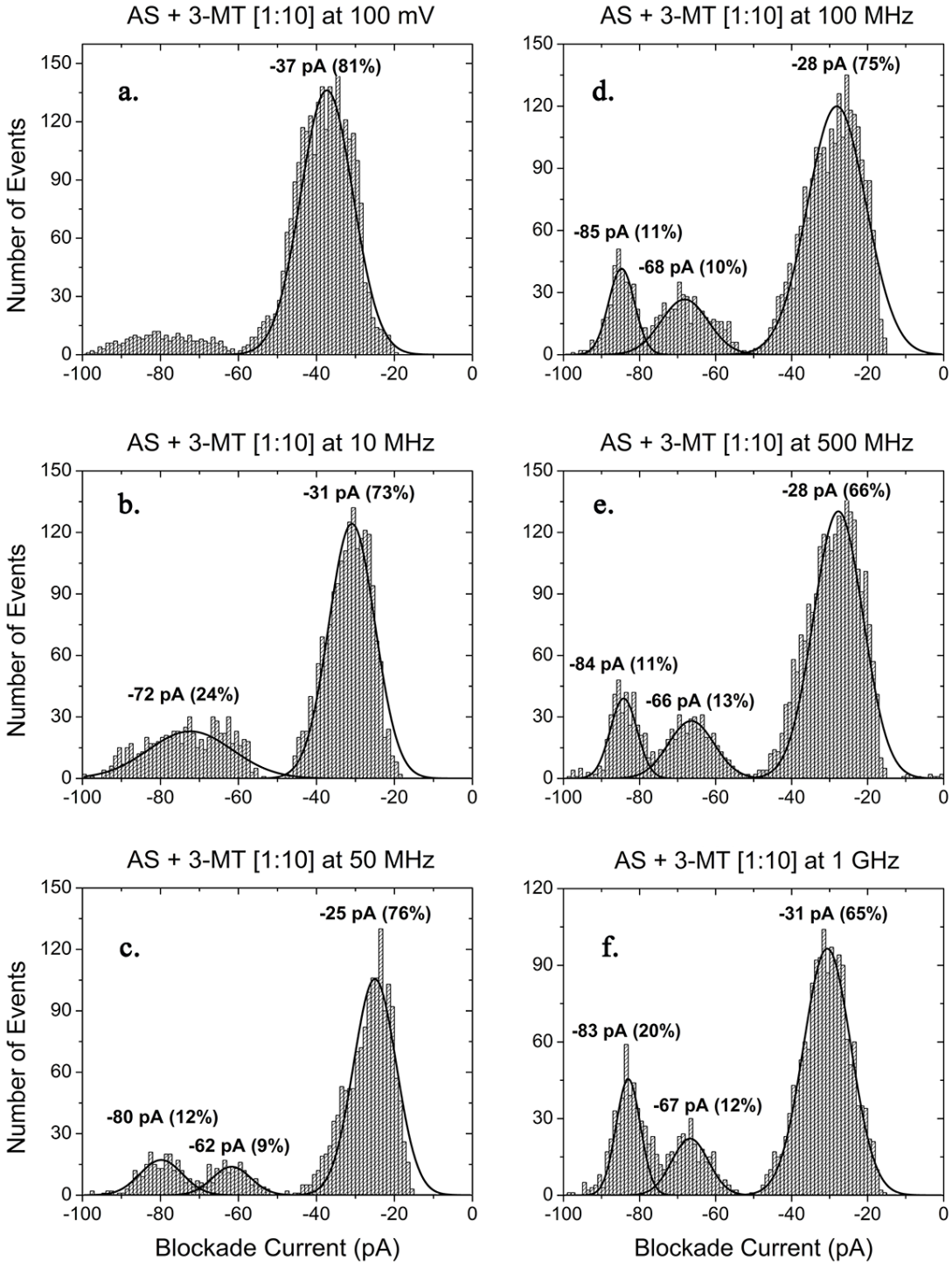

Figure 3.26 Blockade current histograms for AS with 3-Methoxytyramine [1:10] at 100 mV DC. **a.** No AC, **b.** 10 MHz, **c.** 50 MHz, **d.** 100 MHz, **e.** 500 MHz and **f.** 1 GHz.

With an AC field at a frequency of 10 MHz, a second very broad peak appeared at -72 pA due to translocation. In agreement with this assumption was the 0.45 ms duration of these events. At 50 MHz, a third peak emerges at -62 pA, which is thought to be due to intercalation events and the once broad translocation peak consolidates at -80 pA. The T values of the peaks at -62 pA and -80 pA are respectively 0.17 and 0.55 ms, which is in agreement with intercalation and translocation events, respectively. With a further increase of the AC frequency, the proportion of translocation events also increased from 12% at 50 MHz to 20% at 1 GHz. The blockade current of these events increased to -85 pA at 100 MHz and remained att his value between 500 MHz and 1 GHz, with a minor change of 1 pA. These values are similar to the blockade histograms of AS alone, especially at 1 GHz as seen in Figure 3.19 f. As seen in the case of S-1-aminoindan, the time of translocation events increased significantly at 100 MHz. This is a second example of possible drug stripping, i.e. the AC field causes the drug-protein complex to dissociate.

Table 3.7 Time of 3-methoxytyramine events at 100 mV DC with AC frequencies from 10 MHz to 1 GHz. (The error estimated for T is ±10 %)

		Time of Events (ms)		
Drug	Frequency (MHz)	Translocations	Intercalation	Bumping
3-Methoxytyramine	**No AC**	-	-	0.07
	10	0.45	-	0.13
	50	0.55	0.17	0.10
	100	1.12	0.20	0.09
	500	0.75	0.17	0.10
	1000	0.49	0.17	0.11

3.4.3 Caffeine

Caffeine has been thoroughly studied previously because of its neuroprotective role in PD so consequently it was studied in an AC field (Tavassoly et al., 2014a). Figure 3.27 shows the blockade current histograms of AS in the presence of 10 μM caffeine. As previously shown, caffeine causes a shift in the AS translocation peak from -86 pA to a lower current at -78 pA,

but with only a small change in the ratio of events (see Figure 3.27 a). The T value of the translocation events is 0.54 ms.

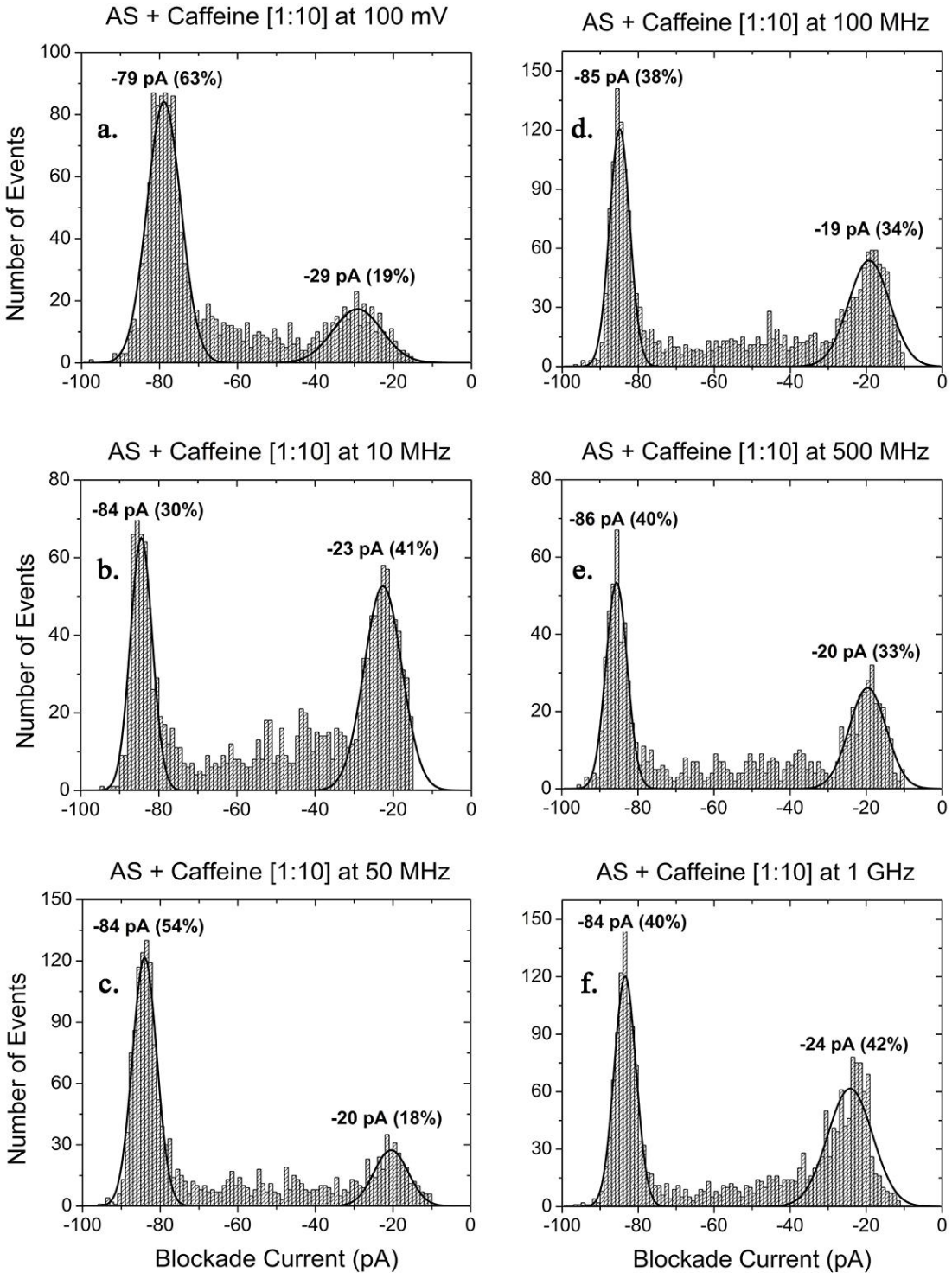

Figure 3.27 Blockade current histograms for AS with Caffeine [1:10] at 100 mV DC. **a.** No AC, **b.** 10 MHz, **c.** 50 MHz, **d.** 100 MHz, **e.** 500 MHz and **f.** 1 GHz.

With the application of an AC field of 10 MHz, the translocation peak shifted back to -84 pA, similar to the blockade histogram of AS, but the bumping peak was slightly broader (see Figure 3.19 b). Also at 10 MHz the percentage of bumping events increased significantly to 41% (see Figure 3.27 b). At 50 MHz, the bumping peak decreased in population to 18% but increased at 100 MHz to 34% (see Figure 3.27 c and d). The time of translocation events, as seen in Table 3.8, decreased from 0.39 ms at 10 MHz to 0.23 ms at 100 MHz. From 100 MHz to 1 GHz there are few distinct changes. It appears that the blockade current histograms of caffeine, after the application of an AC frequency, resembled those of AS. The only exception was that the proportion of bumping events was smaller. Caffeine is another drug that forms a complex with AS which dissociates in an AC field.

Table 3.8 Time of caffeine events at 100 mV DC with AC frequencies from 10 MHz to 1 GHz. (The error estimated for T is ±10 %)

		Time of Events (ms)	
Drug	Frequency (MHz)	Translocations	Bumping
Caffeine	**No AC**	0.56	0.10
	10	0.39	0.06
	50	0.26	0.03
	100	0.23	0.03
	500	0.30	0.03
	1000	0.48	0.08

3.4.4 (-)-Nicotine

It was previously shown that the (-)-nicotine isomer caused a large shift in the translocation peak of AS to a lower current of -66 pA with a smaller bumping peak with a population of 6% (Tavassoly et al., 2014a). However, with the application of an AC field, the ratio of bumping increased significantly to 42% at 10 MHz (see Figure 3.28 b). Similarly to caffeine, the blockade current translocation peak increases to -80 pA at 10 MHz. With the increase of the AC frequency to 100 MHz, the blockade current of the translocation peak increased to -84 pA and remained roughly constant between 10 MHz and 1 GHz, as seen in the

case of AS (see Figure 3.28 d-f and Figure 3.19). In addition, an increase in the proportion of bumping events was observed with the increase of the AC frequency. The blockade time of the translocation events appeared to decrease as the AC frequency was increased, as seen in Table 3.9. Interestingly, the translocation time increased significantly at 100 MHz, as was observed in the case of S-1-aminoindan and 3-methoxytyramine. The nicotine complex represents another example of possible drug stripping by the application of an AC field.

Table 3.9 Time of (-)-nicotine events at 100 mV DC with AC frequencies from 10 MHz to 1 GHz. (The error estimated for T is ±10 %)

		Time of Events (ms)	
Drug	Frequency (MHz)	Translocations	Bumping
(-)-Nicotine	**No AC**	0.48	0.06
	10	0.42	0.07
	50	0.50	0.11
	100	0.60	0.14
	500	0.49	0.10
	1000	0.42	0.08

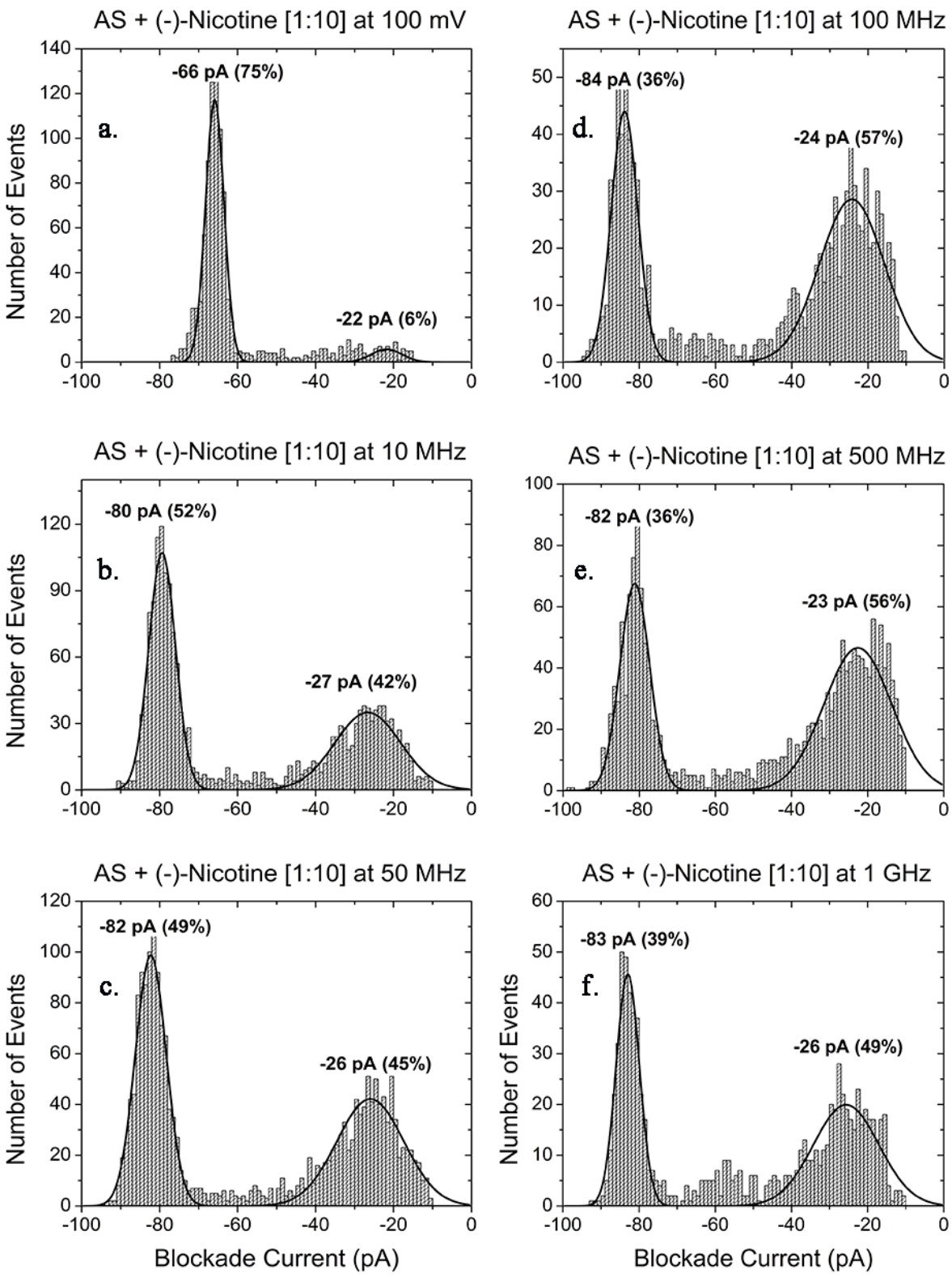

Figure 3.28 Blockade current histograms for AS with (-)-Nicotine [1:10] at 100 mV DC. **a.** No AC, **b.** 10 MHz, **c.** 50 MHz, **d.** 100 MHz, **e.** 500 MHz and **f.** 1 GHz.

3.4.5 Metformin

Metformin, a drug used to treat type 2 diabetes patients, was studied in an AC field as illustrated in Figure 3.29.

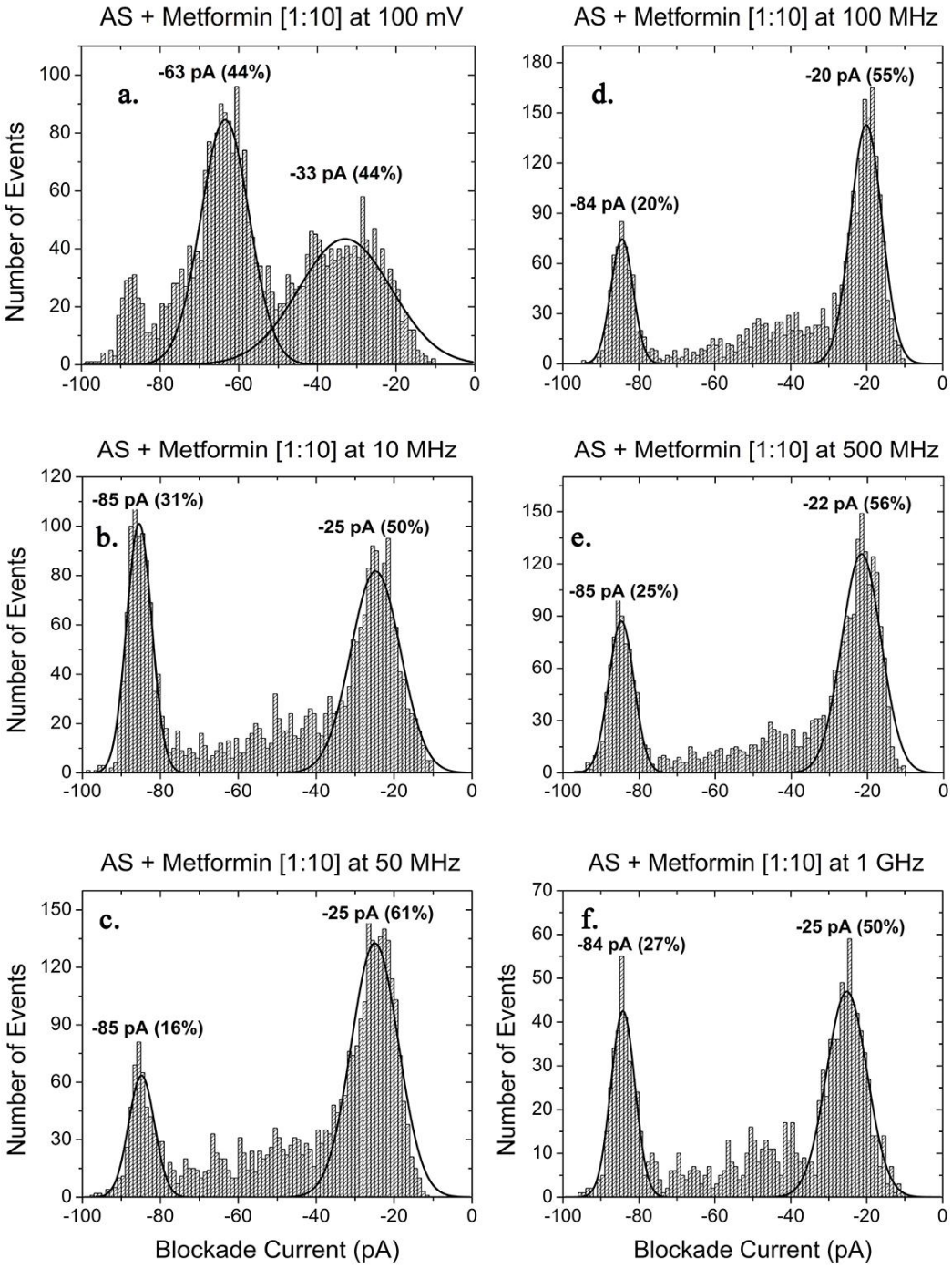

Figure 3.29 Blockade current histograms for AS with Metformin [1:10] at 100 mV DC. **a.** No AC, **b.** 10 MHz, **c.** 50 MHz, **d.** 100 MHz, **e.** 500 MHz and **f.** 1 GHz.

10 μM metformin caused a shift in the AS translocation peak to -63 pA, which is indicative of good binding to the protein (Kakish et al., 2015a). Two observations can be made after the application of an AC field. The application of a 10 MHz AC frequency caused the translocation peak to shift back to the original blockade of the AS control, at -85 pA, and remain approximately at the same blockade intensity at higher frequencies (see Figure 3.29 b and Figure 3.19). The second observation for this drug was that the bumping events intensity remained roughly constant at all AC frequencies, with percentages between 50% and 60%, which was similar to AS alone. In particular, for high frequencies such as 100 and 500 MHz, the blockade current histograms of metformin and AS were similar. As seen in Table 3.10, the time of the translocation events increased significantly after the application of an AC field, from 0.13 ms to 0.51 ms at 50 MHz. Surprisingly, in the case of metformin, the time decreases to 0.36 ms at 100 MHz, to further increase to 0.49 ms at 1 GHz. Based on the shift of the current of the translocation peak to -85 pA, similar to the peak of AS alone, it seems reasonable to assume that the drug might be stripped from the protein as an AC field is applied.

Table 3.10 Time of metformin events at 100 mV DC with AC frequencies from 10 MHz to 1 GHz. (The error estimated for T is ±10 %)

		Time of Events (ms)	
Drug	Frequency (MHz)	Translocations	Bumping
Metformin	**No AC**	0.20	0.07
	10	0.40	0.06
	50	0.51	0.06
	100	0.36	0.06
	500	0.44	0.05
	1000	0.49	0.06

3.4.6 (+)-Amphetamine

It was previously shown that (+)-amphetamine isomer binds to AS and increased the ratio of bumping events (Kakish et al., 2015a).

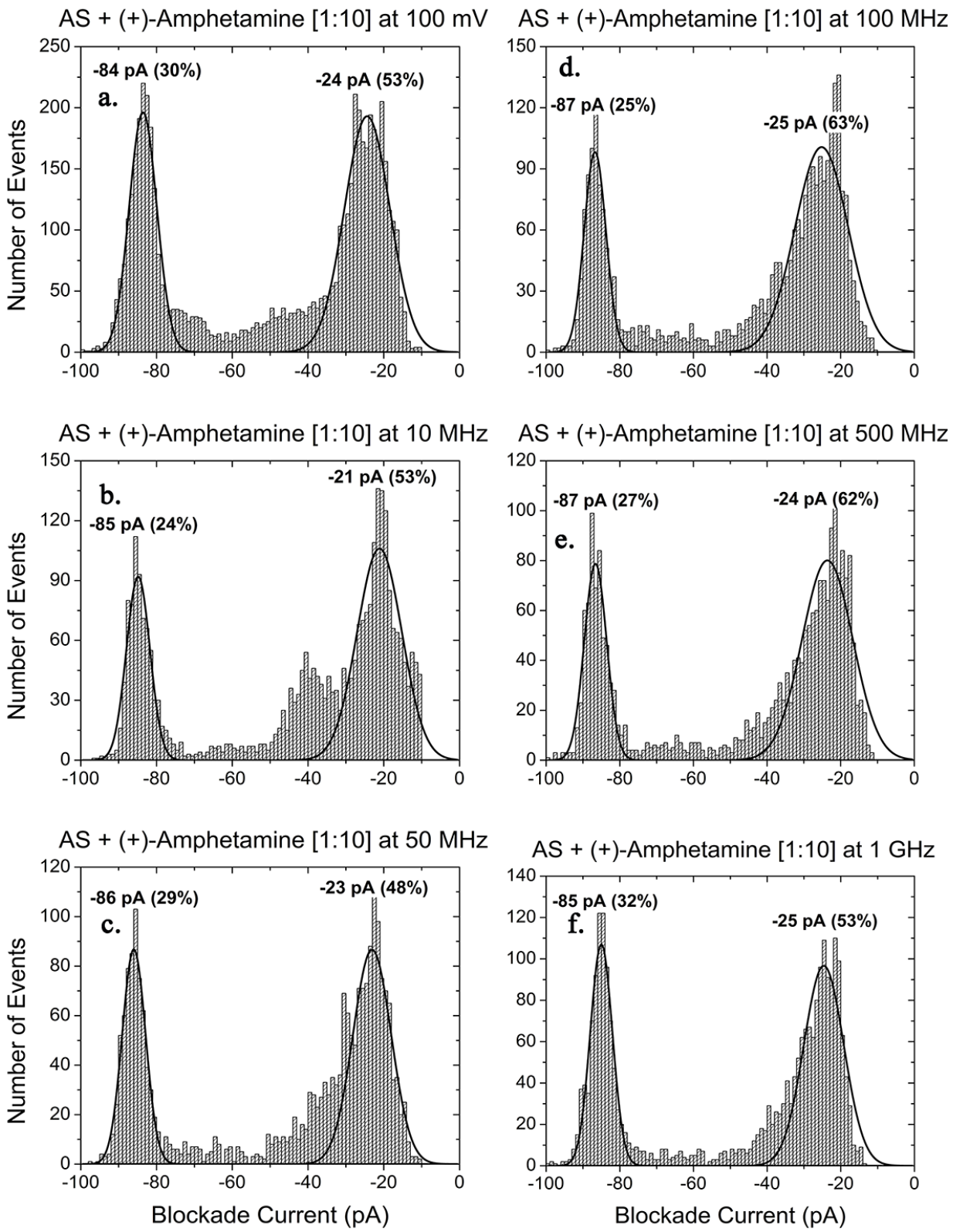

Figure 3.30 Blockade current histograms for AS with (+)-Amphetamine [1:10] at 100 mV DC. **a.** No AC, **b.** 10 MHz, **c.** 50 MHz, **d.** 100 MHz, **e.** 500 MHz and **f.** 1 GHz.

The translocation peak didn't shift from the original AS blockade current but decreased in proportion (see Figure 3.30 a). With the application of an AC voltage at a frequency of 10 MHz, the translocation population decreased by 6%, whereas the proportion of bumping events didn't change (see Figure 3.30 b). There are only small changes at higher frequencies (see Figure 3.30 c-f). Compared to just AS (see Figure 3.19), the blockade histograms of amphetamine at such high frequencies were very different, especially at 1 GHz. At this frequency, the ratio of the translocation events for amphetamine is twice the ratio of translocation events of AS alone.

The lack of change in the blockade current of the translocation events, as well as the constant ratio of these events during all the AC frequencies, suggests that the drug might not be stripped off the protein due to an AC field. However, the drug-protein complex is assumed to oscillate in the AC field as a single entity.

Table 3.11 Time of (+)-amphetamine events at 100 mV DC with AC frequencies from 10 MHz to 1 GHz. (The error estimated for T is ±10 %)

		Time of Events (ms)	
Drug	Frequency (MHz)	Translocations	Bumping
(+)-Amphetamine	**No AC**	0.46	0.02
	10	0.25	0.08
	50	0.39	0.06
	100	0.37	0.07
	500	0.38	0.06
	1000	0.24	0.05

3.4.7 Cocaine

The final drug to be studied in an AC field was cocaine as shown in Figure 3.31. As seen previously, without the presence of an AC field, cocaine exhibited a small translocation peak at -84 pA and a large bumping peak at -28 pA (Kakish et al., 2015a).

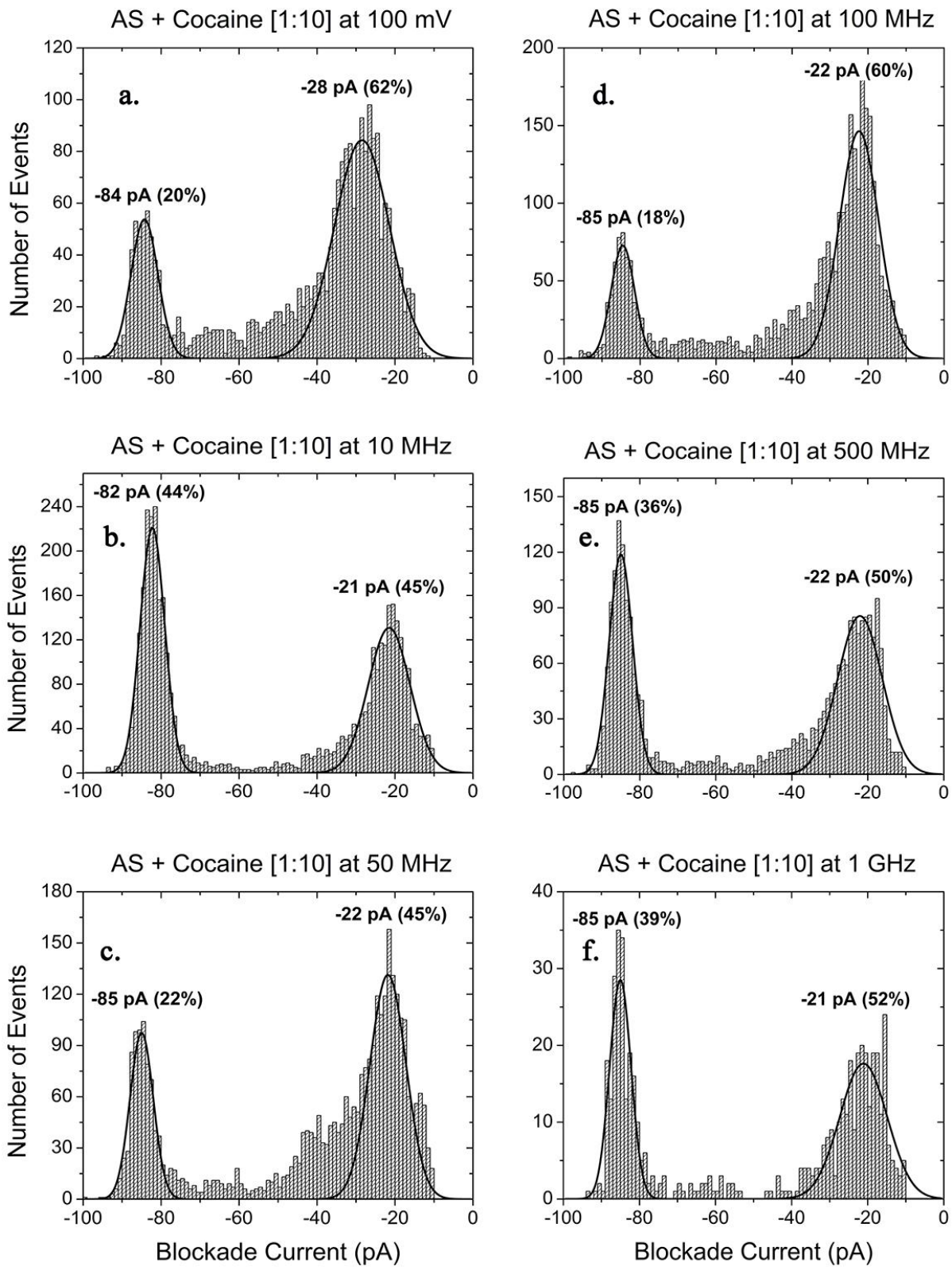

Figure 3.31 Blockade current histograms for AS with Cocaine [1:10] at 100 mV DC. **a.** No AC, **b.** 10 MHz, **c.** 50 MHz, **d.** 100 MHz, **e.** 500 MHz and **f.** 1 GHz.

After applying an AC voltage with a 10 MHz frequency, the proportion of translocation events increased significantly to 44% (see Figure 3.31 b). At 50 MHz the translocation peak decreased back to 22% and further dropped to 18% at 100 MHz (Figure 3.31 c-d). However, the blockade time of translocation increased to 0.48 ms at 50 MHz but dropped at 100 MHz to 0.37 ms (see Table 3.11). Nevertheless, the ratio of translocation increased again at 500 MHz and further at 1 GHz (see Figure 3.31 e-f), while the time decreased to 0.30 ms at 500 MHz and again at 1 GHz.

Similar to amphetamine, cocaine's blockade current histograms are very different from the histograms of AS alone but it is difficult to conclude that stripping is occurring.

Table 3.12 Time of cocaine events at 100 mV DC with AC frequencies from 10 MHz to 1 GHz. (The error estimated for T is ±10 %)

		Time of Events (ms)	
Drug	Frequency (MHz)	Translocations	Bumping
Cocaine	**No AC**	0.40	0.03
	10	0.44	0.09
	50	0.48	0.07
	100	0.37	0.07
	500	0.30	0.06
	1000	0.43	0.06

4. DISCUSSION

4.1 Introducing an AC field in standard nanopore analysis

The work of this thesis builds upon the initial observation of Radu Stefureac who showed that superimposing an AC field modulated the translocation of peptides (Stefureac et al., 2012). It was concluded that an oscillating electric field could interact with a peptide or protein to alter the interaction with the pore compared to a DC field. Others have also used AC fields in nanopore analysis to study the flow of ions through the pore. For example, in 2010, the AC field was used to observe the translocation of a DNA hairpin loop with a polydeoxyadenosine into the α-HML pore (Lathrop et al., 2010). The idea of this experiment was to trap the DNA hairpin inside the pore using an initial DC voltage; once the DNA hairpin was blocked inside the pore vestibule the DC voltage was turned off and an AC voltage with amplitudes in the range of 20 to 250 mV and frequencies from 60 to 200 kHz was applied to let it diffuse from the pore. Additionally, two protein pores, α-HML and Alamethicin (ALA), were studied in the AC field to understand how their ionic flow was altered by frequencies between 1 MHz and 1 GHz (Sujatha et al., 2010). It was shown that the ionic flow can be altered by applying the different AC voltages and frequencies. As well, it was shown that electric field stress could alter the conformation of Aβ peptides and lead to loss of secondary structure in the α-helical region of the β-chain of insulin (Budi et al., 2005; Toschi et al., 2009).

However, the primary conclusion of Stefureac et al. was that the AC field interacted with the dipole of the peptide and that peptides could be discriminated based on differences in dipole moment. The results in this thesis strongly support this hypothesis. First, the superposition of an AC field improved our understanding of the effect of the dipole moment on the translocation of some analytes. Peptides with larger dipole moments are thought to oscillate faster, causing more bumping into the pore, as in the case of RI-A10. This technique may also find applications where increased discrimination is required between a mixture of related molecules. Finally, the superposition of an AC field will facilitate the understanding of the many conformational states of intrinsically disordered proteins such as AS and it may be useful for probing the additional conformational states of AS which are induced by drugs.

4.2 Behaviour of alpha-helical peptides in an AC field

Originally, it was suggested that small peptides, which have small dipole moments, would rotate quickly in a DC voltage. This rotation will lead to restriction of translocation events for these peptides when it comes to orienting correctly into the vestibule and translocating through the α-HML pore. Conversely, for long peptides with large dipole moments, the rotation would be restricted and thus, it would be easier for the peptides to translocate (Stefureac et al., 2006). The superposition of an AC field on a constant DC voltage during nanopore analysis caused large changes to the event profiles. These changes include: (a) An increase in the proportion of bumping events for peptides with large dipole moments; (b) The appearance of intercalation events and (c) Changes to the time of translocation events. The effect is mostly due to the interaction between the AC field and the dipole of the molecule and thus, molecules with different dipole moments can be individually manipulated by appropriate adjustments to the DC voltage and AC frequency. In other words, the molecules can be made to dance to an electronic tune.

4.2.1 Differentiating peptides based on their dipole moment

Initially, A10, A14 and A18 were studied at DC voltages of 60, 100 and 140 mV with and without an AC field, as seen summarized in Table 3.2. At a DC voltage of 100 mV, the AC field has only a small effect on A10 peptide whereas a DC voltage of 60 mV, previously reported, caused a large increase in the proportion of the bumping peak (Stefureac et al., 2012). The histograms of A14, at all the three DC voltages, were very similar to A10.

As previously noticed, there are three consequences to the application of an AC field for A10. First the translocation peak shifts to a lower current. A possible explanation for this observation was that the AC field allows the K^+ and Cl^- ions to move around the peptide more easily. Second, the increase of the AC frequency decreased the proportion of translocation events. Such an effect was modest compared to that previously reported for 60 mV DC. It seems likely that as the DC voltage increases, the AC field has a larger effect on the oscillation of the peptide as it approaches the entrance to the pore. Thus, it is assumed that the peptide will bump into the pore more and therefore will have fewer translocation events. Lastly, at an AC frequency of 50 MHz, a third peak appears due to intercalation events. It seems possible that as the molecule enters the vestibule of the pore, the AC field causes it to rotate so that it is

perpendicular to the lumen of the pore and cannot make any further progress (see Figure 1.3). When the AC field reverses, it will rotate in the opposite direction and then be ejected from the pore. Conversely, the interrelation of the AC frequency with the DC voltage was difficult to explain. At high DC voltages, for A10 and A14, the blockade histograms did not change with the increase of the AC frequency; this led us to believe that the peptide itself doesn't undergo significant conformational changes with the increase of the AC frequency at 140 mV DC.

For RI-A10 it is hypothesized that the larger dipole moment of this peptide (see Table 3.1), is the main reason why RI-A10 is bumping into the pore at a greater rate than A10, even though they have the same length. Additionally, for RI-A10, the helix dipole is in the same direction as the charge dipole with the addition of one more negative charge is at the C-terminus. The C-terminus, which is the side the peptide will enter the pore first, will have three negative charges, and the Fmoc group is now to the rear of the peptide (Krasniqi et al., 2012). Compared to A10, these two differences allow easy access to the vestibule of the pore but not the lumen, therefore, RI-A10 is prevented from translocating.

We assume that, based on the behaviour of the four peptides in an AC field, as the dipole moment increases so does the ratio of bumping events. Additionally, the increase of the AC frequency will lead to a decrease of the translocation events, as well as an increase in the proportion of the bumping and intercalation events.

4.2.1.1 Behaviour of a large alpha-helical peptide in an AC field

For A18 at 100 mV DC with the application of an AC frequency, as seen in Figure 3.8, the proportion of translocation events was reduced while the bumping peak increased. These changes are thought to be due to fast oscillation of the strand in the presence of an AC field. The appearance of a shoulder, at about -65 pA, on the translocation events at 50 MHz was very interesting. These events are thought to be due to the translocation of A18 as would be observed in the absence of an AC field. Interestingly, for the first time, it was observed that the current blockade of translocation events increased with the increase of the AC frequency. Initially, the translocation peak at -66 pA with no AC field, increased to -68 pA at 10 MHz and to -73 pA from 50 MHz to 1 GHz.

As mentioned, the very sharp peak at -73 pA is probably due to a bent conformation, as shown in Figure 4.1. It is assumed that the peptide enters the pore lumen, the AC field bends

the α-helix so that part of the peptide remains in the pore vestibule, because of the length of the peptide. At some point, the peptide will re-orient and continue to translocate but the blockade current will be slightly larger and the overall time for the event will be increased considerably, as seen in Figure 4.1 b. This putative bent conformation did not occur at 60 mV or at 140 mV, based on the open pore current of the α-HML. It didn't occur as well for A10 or A14 because these peptides are shorter and have a smaller dipole moment. This could be the reason why the AC field is insufficient to cause conformational changes.

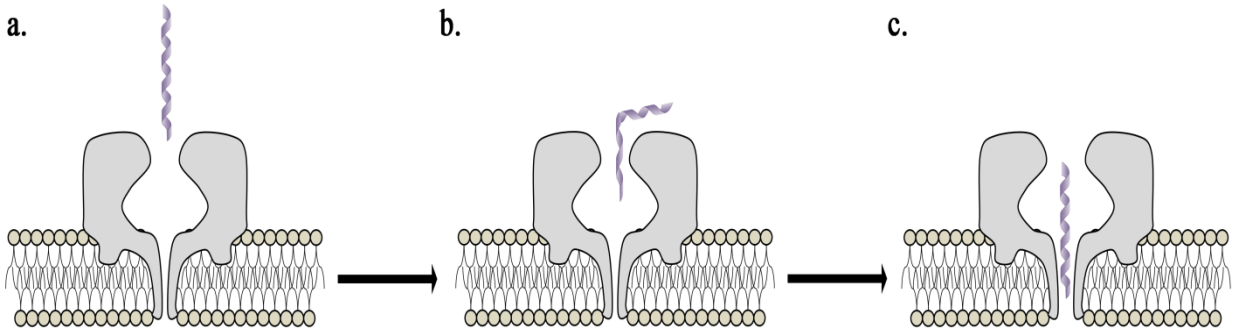

Figure 4.1 a. Normal approach of the peptide as trying to enter the pore vestibule. **b.** Peptide bends due to the force from the AC field. **c.** The peptide reforms an alpha-helix and continue translocating.

4.2.2 Discrimination of molecular mixtures with the aid of an AC field

This technique may also be applied to the discrimination of molecular mixtures. In this case, A10 and RI-A10 have very similar properties even to the extent that the antibodies raised against RI-A10 will bind to A10 and their individual blockade current profiles overlap (see Figure 3.2 a and Figure 3.3 a) (Krasniqi et al., 2012; Stefureac et al., 2012).

An equimolar mixture of the two peptides was analyzed with and without an AC field. Without the application of an AC field, the blockade histogram gave rise to a broad translocation peak at -59 pA and a minor bumping peak (see Figure 3.5 a). Comparing the experimental histogram with the calculated one (see Figure 3.5 d), it is clear that the bumping peak is much smaller in the calculated histogram. The reason for the high ratio of bumping events in the experimental histogram may be due to interference between the two peptides as they approach the pore. The addition of an AC field at either 10 MHz or 100 MHz increases the proportion of bumping events for the experimental histograms as expected since the

translocation of RI-A10 is prevented. Additionally, there is a good fit with the calculated blockade histograms for both frequencies. To conclude, the addition of an AC field allows the analysis of A10 even in the presence of a related peptide.

4.3 Behaviour of d18 and oligo-dT20 in an AC field

Surprisingly, it was observed that at the same concentration of 1 μM, the two different ssDNAs have very different event frequencies (see Figure 3.12). The similar time of the translocation events for both strands at 100 mV DC without the application of an AC field is an indication that both strands interact similarly with the pore. d18 has a similar behaviour to the previously studied peptides, e.g. A10 and A14, in that the percentage of translocation decreases with the increase of the AC frequency. Conversely, the dT20 behaviour is more complex. It was previously shown that oligo-dT forms an ideal chain due to the weak assembly of thymine bases, compared to the stable secondary structure of oligo-dA or oligo-dC (Egli and Saenger, 2013). Since there is little secondary structure, it is easy for the dT20 to orient in the pore in the DC field and translocate compared to d18. A possible explanation for the two translocation and bumping peaks observed in Figure 3.14, is that this strand is threading through the pore in two directions, either from the 5' end and/or the 3' end (see Figure 4.2). It was previously observed that ssDNA could enter the α-HML pore from its 3’ and 5’ end, although the ratio of the events from the entrance of ssDNA from its 5' end is lower than the ratio of the events from the entrance from the 3' end (Chen and Li, 2007).

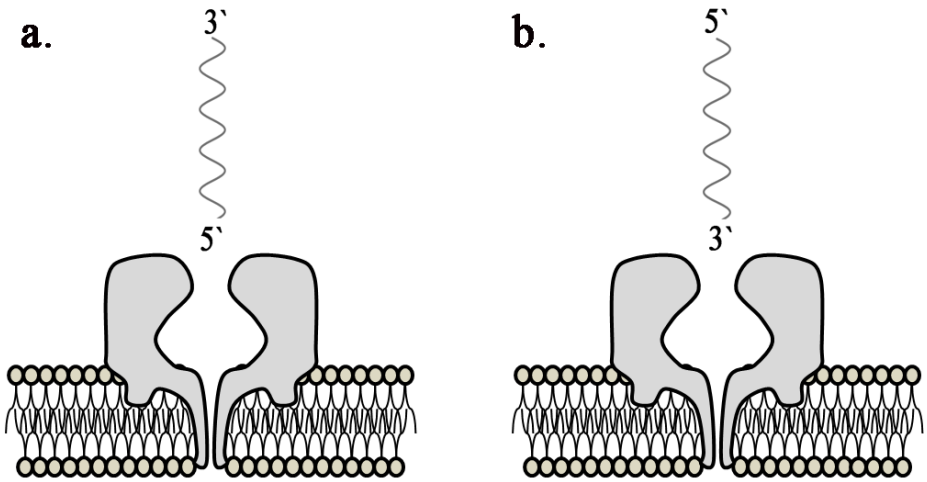

Figure 4.2 Oligo-dT entering the α-HML pore from its **a.** 5' end and **b.** 3' end.

4.4 Alpha-Synuclein and fragments

4.4.1 Voltage studies and Nanopore analysis

It was previously reported that an increase of the DC voltage led to a decrease of the duration of the translocation events (Madampage et al., 2012). This observation was confirmed in this thesis when the DC voltage was increased from 80 mV to 120 mV. The time of translocation events dropped from 0.82 ms at 80 mV to 0.52 ms at 100 mV. As well, at 120 mV the duration of these events decreased to 0.47 ms. Thus, when increasing the electrophoretic voltage, the dipole moment will aid AS to orient into the pore vestibule and make translocating easier. Interestingly the same relationship between time and voltage was not observed in the case of 60 and 140 mV. At 60 mV there are very few translocation events due to the small electrophoretic voltage. Similarly, at 140 mV there are also very few translocation events due to the blockage of the pore, as seen from the several droppings in the ionic current in Figure 3.17. This may explain why the translocation times at these voltages are anomalous.

4.4.2 Behaviour of Alpha-Synuclein and its domains in an AC field

AS was studied at DC voltages between 60, 100 and 140 mV. With the application of an AC field, AS behaves differently for each DC amplitude.

At 60 mV DC, the proportion of translocation events decreased after the application of an AC frequency at 10 MHz. The ratio of the translocation peak remains fairly constant at around 15%. It appears that at 60 mV DC, in the presence of an AC field, AS oscillates fast preventing the protein from entering the pore. At 100 mV DC in the absence of an AC field, the majority of the events were translocation events (Madampage et al., 2012). With the application of an AC field at a frequency of 10 MHz, the ratio of bumping events increased to 52%. As previously noted, the bumping peak increased with a further increase of the AC frequency, until 1 GHz, where the ratio of bumping peak is 73%. Conversely, at 140 mV DC with the application of an AC field, the bumping peak decreased to 24% at 10 MHz and further to 12% at 50 MHz. However, a frequency of 100 MHz causes AS to oscillate faster and it bumps more into the pore vestibule; this frequency seems to prevent the protein from entering the pore. With a further increase of the AC frequency, the bumping peak decreased once more.

The AS domains (N-terminus, C-terminus, and ΔNAC) were also studied in an AC field, as their behaviour in a DC field is well known (Tavassoly et al., 2014a). After the application of an AC field, the blockade histograms for the N-terminus and C-terminus were very similar. After a 10 MHz AC frequency was applied, the N-terminal's bumping peak increased to 73% and remained constant through all the other AC frequencies. The C-terminus at 10 MHz lost the broad translocation peak and the bumping peak increased to 64% and remained constant throughout. Having a large negative charge, the C-terminus presumably oscillates fast in an AC field, and is thus prevented from entering the pore. For the ΔNAC, the proportion of translocation events decreased with the increase of the AC frequency until 100 MHz, where the peptide was prevented completely from translocating. The same event profile was observed at 500 MHz, but a small peak at -92 pA appeared at 1 GHz. The ΔNAC behaved as expected for a peptide with a negative C-terminus and a large dipole moment.

4.5 Protein-drug complexes

4.5.1 Drugs studied in an AC field

Table 4.1 shows the binding constants and probable binding site for seven drugs which induce conformational changes of AS (Kakish et al., 2015a; Kakish et al., 2015b; Tavassoly et al., 2014a). These drugs were shown not to interact with the α-HML pore.

Table 4.1 ITC results of the seven drugs that bind AS (Kakish et al., 2015a; Kakish et al., 2015b; Tavassoly et al., 2014a).

Compound	Ka (M^{-1})	Binding site
S-1-Aminoindan	$3 * 10^5$	N- and C-term
3-Methoxytyramine	$3.2 * 10^6$	N- and C-term
Caffeine	$7 * 10^5$	N- and C-term
(-)-Nicotine	$1 * 10^6$	N- and C-term
Metformin	$9 * 10^6$	2 binding sites C-term
(+)-Amphetamine	$6.8 * 10^5$	N-terminus
Cocaine	$7.8 * 10^5$	NAC-region

4.5.1.1 Drugs that are possibly stripped from AS by an AC field

From the results it appears that S-1-aminoindan, 3-methoxytyramine, caffeine, (-)-nicotine and metformin at high AC frequencies, were assumed to strip from the binding site of the protein (see Figure 4.3). ITC and nanopore analysis results suggests that these drugs bind to both the N- and C-termini of AS, except for metformin, which appears to bind to two sites in the C-terminus.

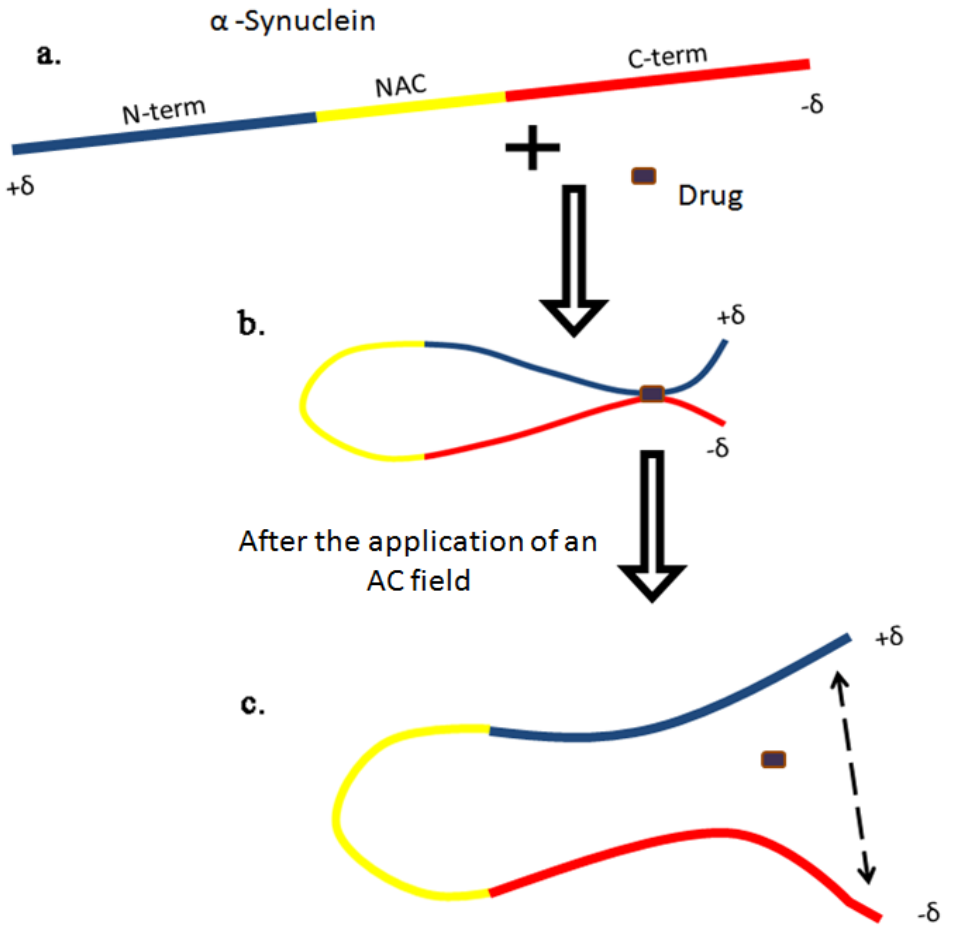

Figure 4.3 Model of drug striping from AS in the presence of an AC field. **a.** The drug binds the N- and the C-terminus forming **b.** a loop conformation. **c.** The N- and the C-termini move in the opposite direction, thus stripping the drug from the protein.

A loop conformation blocks the aggregation of the ΔNAC, which is linked directly to AS fibrillization. In the presence of an AC field, the complex is expected to oscillate. In this loop conformation, the two charged ends are very close, and therefore, an AC frequency will force them to move in opposite directions. Thus, it is assumed that an AC field with an initial

frequency of 10 MHz (e.g. caffeine and (-)-nicotine); or higher frequencies such as 500 MHz or 1 GHz (e.g. S-1-aminoindan and 3-methoxytyramine), will disassociate the drug from its binding site. Conversely, for metformin, it is assumed that, because the drug binds to the C-terminus, which is highly negatively charged and the drug is a dication, the application of an AC it is hypothesized to lead to stripping.

Additionally, based on their weak binding constant, there is AS-free in the solution (free AS: 30-10% based on the Ka: 10^5-10^6 M^{-1}). It is thought that with the application of an AC field the pore selectivity will change, giving priority to the free form of AS rather the AS-drug complex. This is observed very clearly in the case of (-)-nicotine knowing that its binding constants is in 10^5 range. Additionally, caffeine behaves in a very similar manner to (-)-nicotine, even though its binding constant is slightly higher, in the 10^6 range. As mentioned above, we don't see the passage of free AS for neither 3-methoxytyramine and S-1-aminoindan until higher AC frequencies are applied. It must be assumed that there is a relationship between the AC frequency and the binding constant that will allow the pore to be more selective towards the free AS in the solution or to cause a stripping of the drug.

4.5.1.2 Drugs that oscillate with the AS complex in an AC field

The other drugs, (+)-amphetamine and cocaine form a compact conformation with AS. These drugs are neurotoxic based on their ability to induce PD-like symptoms. Amphetamine binds to AS at the N-terminus based on previous nanopore analysis and ITC results (Kakish et al., 2015a). This conformation does not involve the C-terminus and in an AC field, there may be little effect on the drug binding. It is assumed that the AS-amphetamine complex oscillates in the presence of an AC field as an entity, based on the blockade current histograms, which show no significant changes throughout all the AC frequencies (see Figure 3.29). Additionally, cocaine was studied with AS WT and its domains in nanopore analysis and ITC (Kakish et al., 2015a). It is thought to bind to the NAC region of AS and it is assumed that this complex oscillates in an AC field as an entity as well, without any sign of drug stripping.

Based on the pore selectivity hypothesis, cocaine and metformin have weak binding constants as well, but there seem to be no sign of the passage of AS-alone. It appears that the complex is translocating through the pore as an entity.

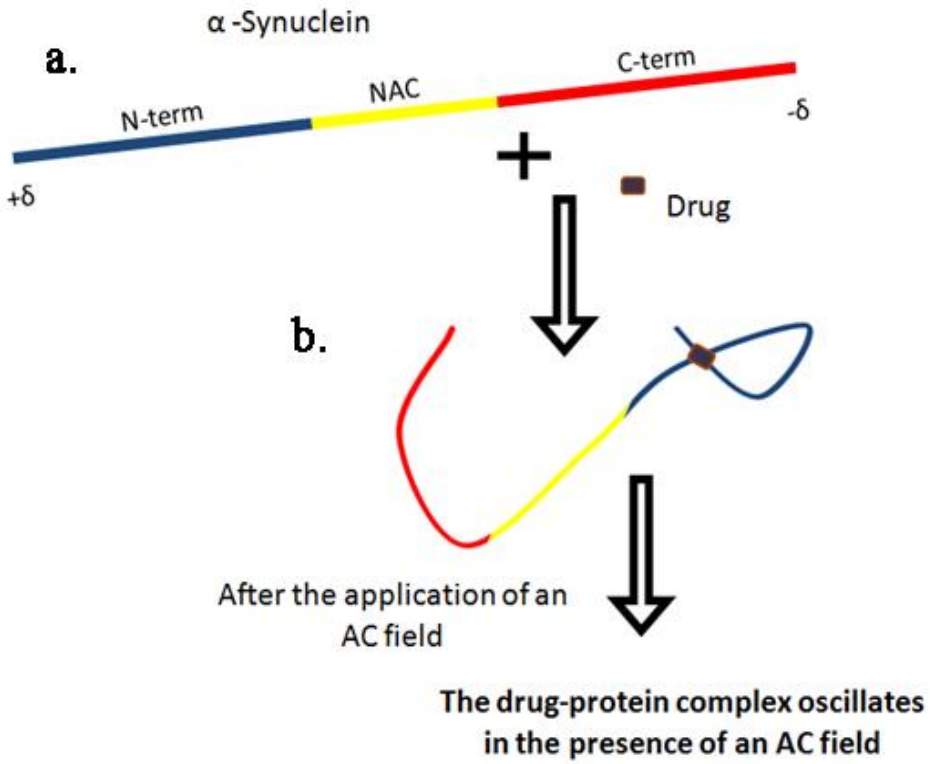

Figure 4.4 The AS-amphetamine complex and its behaviour in the presence of an AC field. **a.** Initially the drug binds the N-terminus and **b.** forms a knot conformation. **c.** which then oscillates in the AC field.

4.6 Future directions

Nanopore analysis with an AC field may be useful for probing the conformational states of AS induced by other drugs and metal ions (Kakish et al., 2015a; Kakish et al., 2015b; Shim et al., 2009; Tavassoly et al., 2014a; Tavassoly et al., 2014b).

Recently, it was demonstrated that solid-state pores on a silicon nitride membrane can be used to detect AS and the several intermediate states of partially unfolded oligomers, due to AS aggregation (Hu et al., 2016). One innovation for this new solid-state pore technique was coating of the membrane by Polysorbate 20 (Tween 20), which gave a smooth membrane surface and allows AS to translocate easily. Major problems observed with the solid-state pores such as dropping of the ionic current due to clogging, and the constant fluctuation of current traces were solved with the application of the Tween 20 layer. This technique was successful because it was able to identify four types of AS oligomers. We assume that an AC voltage

could be superimposed on this new solid-state pore and thus help in probing further conformational states of different analytes, such as AS multimers and/or AS-drug complexes.

Additionally, fluorescent labeling methods could be used in nanopore analysis to further observe the stripping of the drug from AS. A similar technique has been used before, especially for labeling DNA strands to observe their translocation in solid–state pores (Chen et al., 2004; McNally et al., 2010; Soni et al., 2010). With the aid of fluorescent labeling it was possible to view in real-time the passage of the strand through the pore. This technique could help witness the actual moment of the drug being stripped from AS due to the AC field. For instance, metformin, buformin or phenformin are some of the drugs previously studied in nanopore analysis (Kakish et al., 2015a; Schweiger et al., 2012). These drugs would be good candidates to be studied in the AC field, as their DC behaviour is well known. We suppose that using fluorescent labeling it will be possible to monitor the activity of the pore in real-time. However, this technique is difficult to achieve and requires very expensive equipment.

Finally, it would of a great interest to observe the behaviour of protein-protein complexes in an AC field. Proteins with different charges, which form a complex, are expected to behave differently in an AC field. It was shown that polar amino acids and accumulation of positive or negative charges over the protein-protein border causes a destabilizing effect in the electrostatic characteristics of certain protein-protein complexes (Sheinerman et al., 2000). We assume that, under an AC field, it could possible to observe dissociation in the case of protein-protein complexes, as their fast oscillation in the AC filed will pull them apart.

5. REFERENCES

Acha, V., Andrews, T., Huang, Q., Sardar, D., and Hornsby, P. (2010). Tissue-Based Biosensors. In Recognition Receptors in Biosensors, M. Zourob, ed. (Springer New York), pp. 365-381.

Akca, S., Foroughi, A., Frochtzwajg, D., and Postma, H.W.C. (2011). Competing Interactions in DNA Assembly on Graphene. PLOS ONE *6*, e18442.

Aksimentiev, A., and Schulten, K. (2005). Imaging α-Hemolysin with Molecular Dynamics: Ionic Conductance, Osmotic Permeability, and the Electrostatic Potential Map. Biophys. J. *88*, 3745-3761.

Albery, W.J., Haggett, B.G.D., and Svanberg, L.R. (1985). The development of sensors for hydroponics. Biosensors *1*, 369-397.

Amblard, M., Fehrentz, J.-A., Martinez, J., and Subra, G. (2006). Methods and protocols of modern solid phase peptide synthesis. Mol. Biotechnol. *33*, 239-254.

Appel-Cresswell, S., Vilarino-Guell, C., Encarnacion, M., Sherman, H., Yu, I., Shah, B., Weir, D., Thompson, C., Szu-Tu, C., Trinh, J., *et al.* (2013). Alpha-synuclein p.H50Q, a novel pathogenic mutation for Parkinson's disease. Mov. Disord. *28*, 811-813.

Asandei, A., Apetrei, A., and Luchian, T. (2011). Uni-molecular detection and quantification of selected β-lactam antibiotics with a hybrid α-hemolysin protein pore. J. Mol. Recogn. *24*, 199-207.

Ascherio, A., Zhang, S.M., Hernán, M.A., Kawachi, I., Colditz, G.A., Speizer, F.E., and Willett, W.C. (2001). Prospective study of caffeine consumption and risk of Parkinson's disease in men and women. Ann. Neurol. *50*, 56-63.

Astrakas, L.G., Gousias, C., and Tzaphlidou, M. (2012). Structural destabilization of chignolin under the influence of oscillating electric fields. J. Appl. Phys. *111*, 074702.

Ayub, M., Ivanov, A., Hong, J., Kuhn, P., Instuli, E., Edel, J.B., and Albrecht, T. (2010). Precise electrochemical fabrication of sub-20 nm solid-state nanopores for single-molecule biosensing. J. Phys. Condens. Matter *22*, 454128.

Baaken, G., Ankri, N., Schuler, A.-K., Rühe, J., and Behrends, J.C. (2011). Nanopore-Based Single-Molecule Mass Spectrometry on a Lipid Membrane Microarray. ACS Nano *5*, 8080-8088.

Baba, M., Nakajo, S., Tu, P.H., Tomita, T., Nakaya, K., Lee, V.M., Trojanowski, J.Q., and Iwatsubo, T. (1998). Aggregation of alpha-synuclein in Lewy bodies of sporadic Parkinson's disease and dementia with Lewy bodies. Am. J. Pathol. *152*, 879-884.

Baltic, S., Perovic, M., Mladenovic, A., Raicevic, N., Ruzdijic, S., Rakic, L., and Kanazir, S. (2004). α-Synuclein is expressed in different tissues during human fetal development. J. Mol. Neurosci. *22*, 199-203.

Baran, C., Smith, G.S.T., Bamm, V.V., Harauz, G., and Lee, J.S. (2010). Divalent cations induce a compaction of intrinsically disordered myelin basic protein. Biochem. Biophys. Res. Comm. *391*, 224-229.

Bayley, H. (1995). Pore-Forming Proteins with Built-in Triggers and Switches. Bioorg. Chem. *23*, 340-354.

Bayley, H. (1997). Building doors into cells. Sci. Am. *277*, 62-67.

Bayley, H. (1999). Designed membrane channels and pores. Curr. Opin. Biotechnol. *10*, 94-103.

Bayley, H., and Cremer, P.S. (2001). Stochastic sensors inspired by biology. Nature *413*, 226-230.

Bayley, H., Cronin, B., Heron, A., Holden, M.A., Hwang, W.L., Syeda, R., Thompson, J., and Wallace, M. (2008). Droplet interface bilayers. Mol. BioSyst. *4*, 1191-1208.

Bayley, H., and Jayasinghe, L. (2004). Functional engineered channels and pores (Review). Mol. Membr. Biol. *21*, 209-220.

Bayley, H., and Martin, C.R. (2000). Resistive-pulse sensing from microbes to molecules. Chem. Rev. *100*, 2575-2594.

Bekris, L.M., Mata, I.F., and Zabetian, C.P. (2010). The Genetics of Parkinson Disease. J. Geriatr. Psychiatry Neurol. *23*, 228-242.

Belkin, S., Smulski, D.R., Dadon, S., Vollmer, A.C., Van Dyk, T.K., and Larossa, R.A. (1997). A panel of stress-responsive luminous bacteria for the detection of selected classes of toxicants. Water Res. *31*, 3009-3016.

Berry, C., La Vecchia, C., and Nicotera, P. (2010). Paraquat and Parkinson's disease. Cell Death Differ *17*, 1115-1125.

Bhakdi, S., and Tranum-Jensen, J. (1991). Alpha-toxin of Staphylococcus aureus. Microbiol. Rev. *55*, 733-751.

Braha, O., Walker, B., Cheley, S., Kasianowicz, J.J., Song, L., Gouaux, J.E., and Bayley, H. (1997). Designed protein pores as components for biosensors. Chem. Biol. *4*, 497-505.

Branton, D., Deamer, D.W., Marziali, A., Bayley, H., Benner, S.A., Butler, T., Di Ventra, M., Garaj, S., Hibbs, A., Huang, X., *et al.* (2008). The potential and challenges of nanopore sequencing. Nat. Biotech. *26*, 1146-1153.

Breese, G.R., Knapp, D.J., Criswell, H.E., Moy, S.S., Papadeas, S.T., and Blake, B.L. (2005). The neonate-6-hydroxydopamine-lesioned rat: a model for clinical neuroscience and neurobiological principles. Brain Res. *48*, 57-73.

Breydo, L., Wu, J.W., and Uversky, V.N. (2012). α-Synuclein misfolding and Parkinson's disease. Biochim. Biophys. Acta *1822*, 261-285.

Budi, A., Legge, F.S., Treutlein, H., and Yarovsky, I. (2005). Electric Field Effects on Insulin Chain-B Conformation. J. Phys. Chem. B *109*, 22641-22648.

Butler, T.Z., Pavlenok, M., Derrington, I.M., Niederweis, M., and Gundlach, J.H. (2008). Single-molecule DNA detection with an engineered MspA protein nanopore. Proc. Natl. Acad. Sci. USA *105*, 20647-20652.

Canepari, M., Bove, M., Maeda, E., Cappello, M., and Kawana, A. (1997). Experimental analysis of neuronal dynamics in cultured cortical networks and transitions between different patterns of activity. Biol. Cybern. *77*, 153-162.

Caras, S., and Janata, J. (1980). Field effect transistor sensitive to penicillin. Anal, Chem. *52*, 1935-1937.

Chan, W.C., and White, P.D. (2000). Fmoc solid phase peptide synthesis (Oxford University Press).

Chandra, S., Gallardo, G., Fernández-Chacón, R., Schlüter, O.M., and Südhof, T.C. (2005). α-Synuclein Cooperates with CSPα in Preventing Neurodegeneration. Cell *123*, 383-396.

Chen, P., Gu, J., Brandin, E., Kim, Y.-R., Wang, Q., and Branton, D. (2004). Probing Single DNA Molecule Transport Using Fabricated Nanopores. Nano Lett. *4*, 2293-2298.

Chen, P., and Li, C.M. (2007). Nanopore Unstacking of Single-Stranded DNA Helices. Small *3*, 1204-1208.

Cheng, J., Sheldon, E.L., Wu, L., Uribe, A., Gerrue, L.O., Carrino, J., Heller, M.J., and O'Connell, J.P. (1998). Preparation and hybridization analysis of DNA/RNA from E. coli on microfabricated bioelectronic chips. Nat. Biotech. *16*, 541-546.

Chiti, F., and Dobson, C.M. (2006). Protein Misfolding, Functional Amyloid, and Human Disease. Annu. Rev. Biochem. *75*, 333-366.

Christensen, C., Baran, C., Krasniqi, B., Stefureac, R.I., Nokhrin, S., and Lee, J.S. (2011). Effect of charge, topology and orientation of the electric field on the interaction of peptides with the α-hemolysin pore. J. Pept. Sci. *17*, 726-734.

Church, G., Deamer, D.W., Branton, D., Baldarelli, R., and Kasianowicz, J. (1998). Characterization of individual polymer molecules based on monomer-interface interactions. (Google Patents).

Clark, L.C., and Lyons, C. (1962). Electrode systems for continuous monitoring in cardiovascular surgery. Ann. NY Acad. Sci. *102*, 29-45.

Clark, L.C.J. (1956). Monitor and control of blood and tussue oxigen tensions. ASAIO J. *2*, 41-48.

Clayton, D.F., and George, J.M. (1998). The synucleins: a family of proteins involved in synaptic function, plasticity, neurodegeneration and disease. Trends Neurosci. *21*, 249-254.

Collins, S., and Janata, J. (1982). A critical evaluation of the mechanism of potential response of antigen polymer membranes to the corresponding antiserum. Anal. Chim. Acta *136*, 93-99.

Connolly, P., Clark, P., Curtis, A.S.G., Dow, J.A.T., and Wilkinson, C.D.W. (1990). An Extracellular microelectrode Array for monitoring electrogenic cells in culture. Biosens. Bioelectron. *5*, 223-234.

Conway, K.A., Lee, S.-J., Rochet, J.-C., Ding, T.T., Williamson, R.E., and Lansbury, P.T. (2000). Acceleration of oligomerization, not fibrillization, is a shared property of both α-synuclein mutations linked to early-onset Parkinson's disease: Implications for pathogenesis and therapy. Proc. Natl. Acad. Sci. *97*, 571-576.

Cookson, M.R. (2009). alpha-Synuclein and neuronal cell death. In Mol. Neurodegener., p. 9.

Cools, R. (2006). Dopaminergic modulation of cognitive function-implications for l-DOPA treatment in Parkinson's disease. Neurosci. Biobehav. Rev. *30*, 1-23.

Cooper, J.C., and Hall, E.A.H. (1988). The nature of biosensor technology. J. Biomed. Eng. *10*, 210-219.

Cornell, B., Braach-Maksvytis, V., King, L., Osman, P., Raguse, B., Wieczorek, L., and Pace, R. (1997). A biosensor that uses ion-channel switches. Nature (London), 580-582.

Cotzias , G.C., Papavasiliou , P.S., and Gellene , R. (1969). Modification of Parkinsonism — Chronic Treatment with L-Dopa. N. Engl. J. Med. *280*, 337-345.

Coulter, W.H. (1956). High speed automatic blood cell counter and cell size analyzer. In Proc. Natl. Electron. Conf., pp. 1034-1040.

Creighton, T.E. (1993). Proteins: Structures and Molecular Properties (W. H. Freeman).

Curtin, K., Fleckenstein, A.E., Robison, R.J., Crookston, M.J., Smith, K.R., and Hanson, G.R. (2015). Methamphetamine/amphetamine abuse and risk of Parkinson's disease in Utah: A population-based assessment. Drug Alcohol Depend. *146*, 30-38.

Degiacomi, M.T., Iacovache, I., Pernot, L., Chami, M., Kudryashev, M., Stahlberg, H., van der Goot, F.G., and Dal Peraro, M. (2013). Molecular assembly of the aerolysin pore reveals a swirling membrane-insertion mechanism. Nat. Chem. Biol. *9*, 623-629.

DeGuzman, V.S., Lee, C.C., Deamer, D.W., and Vercoutere, W.A. (2006). Sequence-dependent gating of an ion channel by DNA hairpin molecules. Nucleic Acids Res. *34*, 6425-6437.

Dekker, C. (2007). Solid-state nanopores. Nat. Nano. *2*, 209-215.

Dhopesh, V.P., Yagnik, P.M., and Weddington, W.W. (1997). Can Cocaine Abuse Cause Parkinsonism? Am. J. Addict. *6*, 177-179.

Di Monte, D.A., Lavasani, M., and Manning-Bog, A.B. (2002). Environmental Factors in Parkinson's Disease. NeuroToxicology *23*, 487-502.

Dorward, E.J., and Barisas, B.G. (1984). Acute toxicity screening of water pollutants using a bacterial electrode. Environ. Sci. Technol. *18*, 967-972.

Dunn, C.J., and Peters, D.H. (1995). Metformin. Drugs *49*, 721-749.

Dunn, K.W., Mayor, S., Myers, J.N., and Maxfield, F.R. (1994). Applications of ratio fluorescence microscopy in the study of cell physiology. FASEB J. *8*, 573-582.

Edman, C.F., Raymond, D.E., Wu, D.J., Tu, E., Sosnowski, R.G., Butler, W.F., Nerenberg, M., and Heller, M.J. (1997). Electric Field Directed Nucleic Acid Hybridization on Microchips. Nucleic Acids Res. *25*, 4907-4914.

Egli, M., and Saenger, W. (2013). Principles of nucleic acid structure (Springer Science & Business Media).

El-Mir, M.-Y., Detaille, D., R-Villanueva, G., Delgado-Esteban, M., Guigas, B., Attia, S., Fontaine, E., Almeida, A., and Leverve, X. (2008). Neuroprotective Role of Antidiabetic Drug Metformin Against Apoptotic Cell Death in Primary Cortical Neurons. J. Mol. Neurosci. *34*, 77-87.

Emmanouilidou, E., Stefanis, L., and Vekrellis, K. (2010). Cell-produced α-synuclein oligomers are targeted to, and impair, the 26S proteasome. Neurobiol. Aging *31*, 953-968.

Emregül, E. (2005). Development of a new biosensor for superoxide radicals. Anal. Bioanal. Chem. *383*, 947-954.

Engelender, S., Kaminsky, Z., Guo, X., Sharp, A.H., Amaravi, R.K., Kleiderlein, J.J., Margolis, R.L., Troncoso, J.C., Lanahan, A.A., Worley, P.F., *et al.* (1999). Synphilin-1 associates with [alpha]-synuclein and promotes the formation of cytosolic inclusions. Nat. Genet. *22*, 110-114.

Eric, B., Harold, K., Vincent, T.-C., and Michel, G. (2012). Precise control of the size and noise of solid-state nanopores using high electric fields. Nanotechnology *23*, 405301.

Eroglu, A., Russo, M.J., Bieganski, R., Fowler, A., Cheley, S., Bayley, H., and Toner, M. (2000). Intracellular trehalose improves the survival of cryopreserved mammalian cells. Nat. Biotech. *18*, 163-167.

Ervin, E.N., Kawano, R., White, R.J., and White, H.S. (2008). Simultaneous Alternating and Direct Current Readout of Protein Ion Channel Blocking Events Using Glass Nanopore Membranes. Anal. Chem. *80*, 2069-2076.

Exner, N., Lutz, A.K., Haass, C., and Winklhofer, K.F. (2012). Mitochondrial dysfunction in Parkinson's disease: molecular mechanisms and pathophysiological consequences. EMBO J. *31*, 3038-3062.

Faller, M., Niederweis, M., and Schulz, G.E. (2004). The Structure of a Mycobacterial Outer-Membrane Channel. Science *303*, 1189-1192.

Farrer, M., Gwinn-Hardy, K., Muenter, M., DeVrieze, F.W., Crook, R., Perez-Tur, J., Lincoln, S., Maraganore, D., Adler, C., Newman, S., *et al.* (1999). A Chromosome 4P Haplotype Segregating with Parkinson's Disease and Postural Tremor. Hum. Mol. Genet. *8*, 81-85.

Farrer, M.J. (2006). Genetics of Parkinson disease: paradigm shifts and future prospects. Nat. Rev. Genet. *7*, 306-318.

Feany, M.B. (2004). New genetic insights into Parkinson's disease. N. Engl. J. Med. *351*, 1937-1940.

Fertig, N., Klau, M., George, M., Blick, R.H., and Behrends, J.C. (2002). Activity of single ion channel proteins detected with a planar microstructure. Appl. Phys. Lett. *81*, 4865-4867.

Forman, M.S., Lee, V.M.Y., and Trojanowski, J.Q. (2005). Nosology of Parkinson's Disease: Looking for the Way Out of a Quackmire. Neuron *47*, 479-482.

Franco, R., Li, S., Rodriguez-Rocha, H., Burns, M., and Panayiotidis, M.I. (2010). Molecular mechanisms of pesticide-induced neurotoxicity: Relevance to Parkinson's disease. Chem. Biol. Interact. *188*, 289-300.

Funakoshi, K., Suzuki, H., and Takeuchi, S. (2006). Lipid bilayer formation by contacting monolayers in a microfluidic device for membrane protein analysis. Anal. Chem. *78*, 8169-8174.

Galdiero, S., and Gouaux, E. (2004). High resolution crystallographic studies of α-hemolysin–phospholipid complexes define heptamer–lipid head group interactions: Implication for understanding protein–lipid interactions. Protein Sci. *13*, 1503-1511.

Gallagher, D.A., and Schrag, A. (2008). Impact of newer pharmacological treatments on quality of life in patients with Parkinson's disease. CNS drugs *22*, 563-586.

Galvin, J.E., Uryu, K., Lee, V.M.-Y., and Trojanowski, J.Q. (1999). Axon pathology in Parkinson's disease and Lewy body dementia hippocampus contains α-, β-, and γ-synuclein. Proc. Natl. Acad. Sci. USA *96*, 13450-13455.

Gasser, T., Müller-Myhsok, B., Wszolek, Z.K., Oehlmann, R., Calne, D.B., Bonifati, V., Bereznai, B., Fabrizio, E., Vieregge, P., and Horstmann, R.D. (1998). A susceptibility locus for Parkinson's disease maps to chromosome 2p13. Nature Genet. *18*, 262-265.

Gawin, F.H., and Ellinwood, E.H. (1988). Cocaine and Other Stimulants. N. Engl. J. Med. *318*, 1173-1182.

George, J.M. (2002). The synucleins. Genome Biol. *3*, reviews3002.3001-reviews3002.3006.

Giasson, B.I., Virginia, M.-Y.L., and Trojanowski, J.Q. (2004). Parkinson's disease, dementia with Lewy bodies, multiple system atrophy and the spectrum of diseases with a-synuclein inclusions. The neuropathology of dementia, 353.

Goedert, M. (2001). Alpha-synuclein and neurodegenerative diseases. Nat. Rev. Neurosci. *2*, 492-501.

Goodrich, C.P., Kirmizialtin, S., Huyghues-Despointes, B.M., Zhu, A., Scholtz, J.M., Makarov, D.E., and Movileanu, L. (2007). Single-Molecule Electrophoresis of β-Hairpin Peptides by Electrical Recordings and Langevin Dynamics Simulations. J. Phys. Chem. B *111*, 3332-3335.

Gouaux, E. (1998). α-Hemolysin fromStaphylococcus aureus:An Archetype of β-Barrel, Channel-Forming Toxins. J. Struct. Biol. *121*, 110-122.

Gouaux, E., and MacKinnon, R. (2005). Principles of Selective Ion Transport in Channels and Pumps. Science *310*, 1461-1465.

Graybiel, A.M., Moratalla, R., and Robertson, H.A. (1990). Amphetamine and cocaine induce drug-specific activation of the c-fos gene in striosome-matrix compartments and limbic subdivisions of the striatum. Proc. Natl. Acad. Sci. USA *87*, 6912-6916.

Group, D.P.P.R. (2002). Reduction in the Incidence of Type 2 Diabetes with Lifestyle Intervention or Metformin. N. Engl. J. Med. *346*, 393-403.

Gu, L.-Q., and Bayley, H. (2000). Interaction of the Noncovalent Molecular Adapter, β-Cyclodextrin, with the Staphylococcal α-Hemolysin Pore. Biophys. J. *79*, 1967-1975.

Gu, L.-Q., Braha, O., Conlan, S., Cheley, S., and Bayley, H. (1999). Stochastic sensing of organic analytes by a pore-forming protein containing a molecular adapter. Nature *398*, 686-690.

Gu, L.-Q., Cheley, S., and Bayley, H. (2001). Prolonged Residence Time of a Noncovalent Molecular Adapter, β-Cyclodextrin, within the Lumen of Mutant α-Hemolysin Pores. J. Gen. Physiol. *118*, 481-494.

Gu, L.-Q., and Shim, J.W. (2010). Single molecule sensing by nanopores and nanopore devices. Analyst *135*, 441-451.

Guan, X., de Zoysa, R., Jayawardhana, D., and Zhao, Q. (2011). Stochastic Detection of Terrorist Agents and Biomolecules in a Biological Channel. In Nanopores, S.M. Iqbal, and R. Bashir, eds. (Springer US), pp. 313-334.

Guan, X., Gu, L.-Q., Cheley, S., Braha, O., and Bayley, H. (2005). Stochastic Sensing of TNT with a Genetically Engineered Pore. ChemBioChem *6*, 1875-1881.

Haes, A.J., and Van Duyne, R.P. (2002). A Nanoscale Optical Biosensor: Sensitivity and Selectivity of an Approach Based on the Localized Surface Plasmon Resonance Spectroscopy of Triangular Silver Nanoparticles. ACS *124*, 10596-10604.

Hall, E.A.H. (1986). The developing biosensor arena. Enzyme Microb. Tech. *8*, 651-658.

Hall, E.A.H. (1988). Recent progress in biosensor development. Int. J. Biochem. *20*, 357-362.

Hille, B. (2001). Ion channels of excitable membranes, Vol 507 (Sinauer Sunderland, MA).

Holden, M.A., Needham, D., and Bayley, H. (2007). Functional Bionetworks from Nanoliter Water Droplets. J. Am. Chem. Soc. *129*, 8650-8655.

Horn, R., and Marty, A. (1988). Muscarinic activation of ionic currents measured by a new whole-cell recording method. J. Gen. Physiol. *92*, 145-159.

Howard, S.P., and Buckley, J.T. (1986). Molecular cloning and expression in Escherichia coli of the structural gene for the hemolytic toxin aerolysin from Aeromonas hydrophila. Mol. Gen. Genet. *204*, 289-295.

Howorka, S., Cheley, S., and Bayley, H. (2001). Sequence-specific detection of individual DNA strands using engineered nanopores. Nat. Biotech. *19*, 636-639.

Howorka, S., and Siwy, Z. (2009). Nanopore analytics: sensing of single molecules. Chem. Soc. Rev *38*, 2360-2384.

Hu, R., Diao, J., Li, J., Tang, Z., Li, X., Leitz, J., Long, J., Liu, J., Yu, D., and Zhao, Q. (2016). Intrinsic and membrane-facilitated α-synuclein oligomerization revealed by label-free detection through solid-state nanopores. Sci. Rep. *6*, 20776.

Huang, T., Nallathamby, P.D., Gillet, D., and Xu, X.-H.N. (2007). Design and Synthesis of Single-Nanoparticle Optical Biosensors for Imaging and Characterization of Single Receptor Molecules on Single Living Cells. Anal. Chem. *79*, 7708-7718.

Huang, T., Nallathamby, P.D., and Xu, X.-H.N. (2008). Photostable Single-Molecule Nanoparticle Optical Biosensors for Real-Time Sensing of Single Cytokine Molecules and Their Binding Reactions. J. Am. Chem. Soc. *130*, 17095-17105.

Huang, W., Chen, Y., Shohami, E., and Weinstock, M. (1999). Neuroprotective effect of rasagiline, a selective monoamine oxidase-B inhibitor, against closed head injury in the mouse. Eur. J. Pharmacol. *366*, 127-135.

Jankovic, J. (2008). Parkinson's disease: clinical features and diagnosis. J. Neurol. Neurosurg. Psychiatry *79*, 368-376.

Janshoff, A., and Steinem, C. (2006). Transport across artificial membranes-an analytical perspective. Anal. Bioanal. Chem. *385*, 433-451.

Jetha, N., Wiggin, M., and Marziali, A. (2009). Forming an α-Hemolysin Nanopore for Single-Molecule Analysis. In Micro and Nano Technologies in Bioanalysis, R.S. Foote, and J.W. Lee, eds. (Humana Press), pp. 113-127.

Kahle, P. (2008). α-Synucleinopathy models and human neuropathology: similarities and differences. Acta neuropathol. *115*, 87-95.

Kakish, J., Lee, D., and Lee, J.S. (2015a). Drugs That Bind to α-Synuclein: Neuroprotective or Neurotoxic? ACS Chem. Neurosci. *6*, 1930-1940.

Kakish, J., Tavassoly, O., and Lee, J.S. (2015b). Rasagiline, a Suicide Inhibitor of Monoamine Oxidases, Binds Reversibly to α-Synuclein. ACS Chem. Neuroscience *6*, 347-355.

Karoum, F., Chrapusta, S.J., and Egan, M.F. (1994). 3-Methoxytyramine Is the Major Metabolite of Released Dopamine in the Rat Frontal Cortex: Reassessment of the Effects of Antipsychotics on the Dynamics of Dopamine Release and Metabolism in the Frontal Cortex, Nucleus Accumbens, and Striatum by a Simple Two Pool Model. J. Neurochem. *63*, 972-979.

Kasianowicz, J.J., and Bezrukov, S.M. (1995). Protonation dynamics of the alpha-toxin ion channel from spectral analysis of pH-dependent current fluctuations. Biophys. J. *69*, 94-105.

Kasianowicz, J.J., Brandin, E., Branton, D., and Deamer, D.W. (1996). Characterization of individual polynucleotide molecules using a membrane channel. Proc. Natl. Acad. Sci. USA *93*, 13770-13773.

Kelton, M.C., Kahn, H.J., Conrath, C.L., and Newhouse, P.A. (2000). The effects of nicotine on Parkinson's disease. Brain Cogn. *43*, 274-282.

Keyser, U.F. (2011). Controlling molecular transport through nanopores. J. R. Soc. Interface *8*, 1369-1378.

Kim, M.J., Wanunu, M., Bell, D.C., and Meller, A. (2006). Rapid fabrication of uniformly sized nanopores and nanopore arrays for parallel DNA analysis. Adv. Mater. *18*, 3149.

Kitada, T., Asakawa, S., Hattori, N., Matsumine, H., Yamamura, Y., Minoshima, S., Yokochi, M., Mizuno, Y., and Shimizu, N. (1998). Mutations in the parkin gene cause autosomal recessive juvenile parkinsonism. Nature *392*, 605-608.

Klein, C., and Ziegler, A. (2011). From GWAS to clinical utility in Parkinson's disease. Lancet *377*, 613-614.

Koschwanez, H.E., and Reichert, W.M. (2007). In vitro, in vivo and post explantation testing of glucose-detecting biosensors: Current methods and recommendations. Biomaterials *28*, 3687-3703.

Kowolenko, M., Keese, C.R., Lawrence, D.A., and Giaever, I. (1990). Measurement of macrophage adherence and spreading with weak electric fields. J. Immunol. Methods *127*, 71-77.

Krasniqi, B., and Lee, J.S. (2012). The importance of adding EDTA for the nanopore analysis of proteins. Metallomics *4*, 539-544.

Krasniqi, B., Scruten, E., Piller, J., Lee, J., and Napper, S. (2012). Stability, toxicity and biological activity of retro, inversed and retro-inversed glucagon isomers. J. Pept. Sci. *18*, 519-526.

Krüger, R., Kuhn, W., Müller, T., Woitalla, D., Graeber, M., Kösel, S., Przuntek, H., Epplen, J.T., Schols, L., and Riess, O. (1998). Ala30Pro mutation in the gene encoding α-synuclein in Parkinson's disease. Nat. Genet. *18*, 106-108.

Kupfer, L., Hinrichs, W., and Groschup, M.H. (2009). Prion Protein Misfolding. Curr. Mol. Med. *9*, 826-835.

Lamichhane, U., Islam, T., Prasad, S., Weingart, H., Mahendran, K., and Winterhalter, M. (2013). Peptide translocation through the mesoscopic channel: binding kinetics at the single molecule level. Eur. Biophys. J. *42*, 363-369.

Larkin, J., Carson, S., Stoloff, D.H., and Wanunu, M. (2013). Nanopore-Based Analysis of Chemically Modified DNA and Nucleic Acid Drug Targets. Isr. J. Chem. *53*, 431-441.

Lathrop, D.K., Ervin, E.N., Barrall, G.A., Keehan, M.G., Kawano, R., Krupka, M.A., White, H.S., and Hibbs, A.H. (2010). Monitoring the Escape of DNA from a Nanopore Using an Alternating Current Signal. J. Am. Chem. Soc. *132*, 1878-1885.

Lee, K.J., Nallathamby, P.D., Browning, L.M., Desai, T., Cherukuri, P.K., and Xu, X.-H.N. (2012). Single nanoparticle spectroscopy for real-time in vivo quantitative analysis of transport and toxicity of single nanoparticles in single embryos. Analyst *137*, 2973-2986.

Lennernäs, H., Palm, K., Fagerholm, U., and Artursson, P. (1996). Comparison between active and passive drug transport in human intestinal epithelial (caco-2) cells in vitro and human jejunum in vivo. Int. J. Pharm. *127*, 103-107.

Lesage, S., Anheim, M., Letournel, F., Bousset, L., Honoré, A., Rozas, N., Pieri, L., Madiona, K., Dürr, A., Melki, R., *et al.* (2013). G51D α-synuclein mutation causes a novel Parkinsonian–pyramidal syndrome. Ann. Neurol. *73*, 459-471.

Li, J., Stein, D., McMullan, C., Branton, D., Aziz, M.J., and Golovchenko, J.A. (2001). Ion-beam sculpting at nanometre length scales. Nature *412*, 166-169.

Liu, B., Gao, H.-M., and Hong, J.-S. (2003). Parkinson's disease and exposure to infectious agents and pesticides and the occurrence of brain injuries: role of neuroinflammation. Environ. Health Perspect. *111*, 1065-1073.

Lloyd, S.A., Faherty, C.J., and Smeyne, R.J. (2006). Adult and in utero exposure to cocaine alters sensitivity to the parkinsonian toxin 1-methyl-4-phenyl-1,2,3,6-tetrahydropyridine. Neuroscience *137*, 905-913.

Lowe, C.R., Small, D.A.P., and Atkinson, A. (1981). Some preparative and analytical applications of triazine dyes. Int. J. Biochem. *13*, 33-40.

Lücking, C., and Brice, A. (2000). Cell. Mol. Life Sci. Cellular and Molecular Life Sciences CMLS *57*, 1894-1908.

Ma, L., and Cockroft, S.L. (2010). Biological Nanopores for Single-Molecule Biophysics. ChemBioChem *11*, 25-34.

Madampage, C.A., Andrievskaia, O., and Lee, J.S. (2010). Nanopore detection of antibody prion interactions. Anal. Biochem. *396*, 36-41.

Madampage, C.A., Tavassoly, O., Christensen, C., Kumari, M., and Lee, J.S. (2012). Nanopore analysis: An emerging technique for studying the folding and misfolding of proteins. Prion *6*, 116-123.

Manrao, E.A., Derrington, I.M., Pavlenok, M., Niederweis, M., and Gundlach, J.H. (2011). Nucleotide Discrimination with DNA Immobilized in the MspA Nanopore. PLOS ONE *6*, 25723.

Maroteaux, L., Campanelli, J., and Scheller, R. (1988). Synuclein: a neuron-specific protein localized to the nucleus and presynaptic nerve terminal. J. Neurosci. *8*, 2804-2815.

McKeith, I.G., Galasko, D., Kosaka, K., Perry, E., Dickson, D., Hansen, L.a., Salmon, D., Lowe, J., Mirra, S., and Byrne, E. (1996). Consensus guidelines for the clinical and pathologic diagnosis of dementia with Lewy bodies (DLB) Report of the consortium on DLB international workshop. Neurology *47*, 1113-1124.

McNally, B., Singer, A., Yu, Z., Sun, Y., Weng, Z., and Meller, A. (2010). Optical Recognition of Converted DNA Nucleotides for Single-Molecule DNA Sequencing Using Nanopore Arrays. Nano Lett. *10*, 2237-2244.

Meng, H., Detillieux, D., Baran, C., Krasniqi, B., Christensen, C., Madampage, C., Stefureac, R.I., and Lee, J.S. (2010). Nanopore analysis of tethered peptides. J. Pept. Sci. *16*, 701-708.

Mereuta, L., Schiopu, I., Asandei, A., Park, Y., Hahm, K.-S., and Luchian, T. (2012). Protein Nanopore-Based, Single-Molecule Exploration of Copper Binding to an Antimicrobial-Derived, Histidine-Containing Chimera Peptide. Langmuir *28*, 17079-17091.

Meusel, M., and Vering, T. (1998). Concerted action 'biosensor stability' in the EC-programme on industrial and materials technologies (BRITE-EURAM). Biosens. Bioelectron. *13*, ix-xi.

Minami, H., Sugawara, M., Odashima, K., Umezawa, Y., Uto, M., Michaelis, E.K., and Kuwana, T. (1991). Ion channel sensors for glutamic acid. Anal. Chem. *63*, 2787-2795.

Mohammad, Prakash, S., Matouschek, A., and Movileanu, L. (2008). Controlling a Single Protein in a Nanopore through Electrostatic Traps. J. Am. Chem. Soc. *130*, 4081-4088.

Mohammad, M., and Movileanu, L. (2008). Excursion of a single polypeptide into a protein pore: simple physics, but complicated biology. Eur. Biophys. J. *37*, 913-925.

Mohammad, M.M., Iyer, R., Howard, K.R., McPike, M.P., Borer, P.N., and Movileanu, L. (2012). Engineering a Rigid Protein Tunnel for Biomolecular Detection. J. Am. Chem. Soc. *134*, 9521-9531.

Moniatte, M., van der Goot, F.G., Buckley, J.T., Pattus, F., and van Dorsselaer, A. (1996). Characterisation of the heptameric pore-forming complex of the Aeromonas toxin aerolysin using MALDI-TOF mass spectrometry. FEBS Lett. *384*, 269-272.

Montgomery, E.B. (1995). Heavy metals and the etiology of Parkinson's disease and other movement disorders. Toxicology *97*, 3-9.

Montoya, M., and Gouaux, E. (2003). β-Barrel membrane protein folding and structure viewed through the lens of α-hemolysin. Biochimica et Biophysica Acta (BBA) - Biomembranes *1609*, 19-27.

Moore, D.J., West, A.B., Dawson, V.L., and Dawson, T.M. (2005). MOLECULAR PATHOPHYSIOLOGY OF PARKINSON'S DISEASE. Annu. Rev. Neurosc. *28*, 57-87.

Morth, J.P., Pedersen, B.P., Buch-Pedersen, M.J., Andersen, J.P., Vilsen, B., Palmgren, M.G., and Nissen, P. (2011). A structural overview of the plasma membrane Na+,K+-ATPase and H+-ATPase ion pumps. Nat. Rev. Mol. Cell. Biol. *12*, 60-70.

Movileanu, L., Howorka, S., Braha, O., and Bayley, H. (2000). Detecting protein analytes that modulate transmembrane movement of a polymer chain within a single protein pore. Nat. Biotech. *18*, 1091-1095.

Mulder, M. (1996). Basic principles of membrane technology (Springer Science & Business Media).

Munge, B., Liu, G., Collins, G., and Wang, J. (2005). Multiple Enzyme Layers on Carbon Nanotubes for Electrochemical Detection Down to 80 DNA Copies. Anal. Chem. *77*, 4662-4666.

Murphy, D.D., Rueter, S.M., Trojanowski, J.Q., and Lee, V.M.-Y. (2000). Synucleins Are Developmentally Expressed, and α-Synuclein Regulates the Size of the Presynaptic Vesicular Pool in Primary Hippocampal Neurons. J. Neurosci. *20*, 3214-3220.

Murray, R.W. (2008). Nanoelectrochemistry: metal nanoparticles, nanoelectrodes, and nanopores. Chem. Rev. *108*, 2688-2720.

Myers, J.A., and Earnest, M.P. (1984). Generalized seizures and cocaine abuse. Neurol. *34*, 675-675.

Nalls M. A., Plagnol V., Hernandez D. G., Sharma M., Sheerin U. M., Saad M., Simon-Sanchez J., Schulte C., Lesage S., and Sveinbjornsdottir S., e.a. (2011). Imputation of sequence variants for identification of genetic risks for Parkinson's disease: a meta-analysis of genome-wide association studies. Lancet *377*, 641-649.

Nankai, S., Kawaguri, M., Ohtani, M., and Iijima, T. (1992). Biosensor and a process for preparation thereof. (Google Patents).

Nelson, D.L., Lehninger, A.L., and Cox, M.M. (2008). Lehninger principles of biochemistry (Macmillan).

Nimjee, S.M., Rusconi, C.P., and Sullenger, B.A. (2005). Aptamers: An Emerging Class of Therapeutics. Annu. Rev. Med. *56*, 555-583.

Nishizawa, M., Menon, V.P., and Martin, C.R. (1995). Metal Nanotubule Membranes with Electrochemically Switchable Ion-Transport Selectivity. Science *268*, 700-702.

Notingher, I. (2007). Raman spectroscopy cell-based biosensors. Sensors *7*, 1343-1358.

Ohtake, H., Limprasert, P., Fan, Y., Onodera, O., Kakita, A., Takahashi, H., Bonner, L.T., Tsuang, D.W., Murray, I.V.J., Lee, V.M.-Y., *et al.* (2004). β-Synuclein gene alterations in dementia with Lewy bodies. Neurology *63*, 805-811.

Oukhaled, A., Cressiot, B., Bacri, L., Pastoriza-Gallego, M., Betton, J.-M., Bourhis, E., Jede, R., Gierak, J., Auvray, L., and Pelta, J. (2011). Dynamics of Completely Unfolded and Native Proteins through Solid-State Nanopores as a Function of Electric Driving Force. ACS Nano. *5*, 3628-3638.

Owicki, J.C., and Wallace Parce, J. (1992). Biosensors based on the energy metabolism of living cells: The physical chemistry and cell biology of extracellular acidification. Biosens. Bioelectron. *7*, 255-272.

Palchetti, I., and Mascini, M. (2010). Biosensor Technology: A Brief History. In Sensors and Microsystems: AISEM 2009 Proceedings, P. Malcovati, A. Baschirotto, A. d'Amico, and C. Natale, eds. (Dordrecht: Springer Netherlands), pp. 15-23.

Panchal, R.G., Cusack, E., Cheley, S., and Bayley, H. (1996). Tumor protease-activated, pore-forming toxins from a combinatorial library. Nat. Biotech. *14*, 852-856.

Pancrazio, J. (2001). Biosensors and Bioelectronics: Preface. Biosens. Bioelectron. *16*, 427-428.

Pancrazio, J.J., Whelan, J.P., Borkholder, D.A., Ma, W., and Stenger, D.A. (1999). Development and Application of Cell-Based Biosensors. Ann. Biomed. Eng. *27*, 697-711.

Park, J.-Y., and Lansbury, P.T. (2003). β-Synuclein Inhibits Formation of α-Synuclein Protofibrils: A Possible Therapeutic Strategy against Parkinson's Disease†. Biochemistry *42*, 3696-3700.

Parker, M.W., Buckley, J.T., Postma, J.P.M., Tucker, A.D., Leonard, K., Pattus, F., and Tsernoglou, D. (1994). Structure of the Aeromonas toxin proaerolysin in its water-soluble and membrane-channel states. Nature *367*, 292-295.

Patil, S.P., Jain, P.D., Ghumatkar, P.J., Tambe, R., and Sathaye, S. (2014). Neuroprotective effect of metformin in MPTP-induced Parkinson's disease in mice. Neuroscience *277*, 747-754.

Patterson, N., Adams, D.P., Hodges, V.C., Vasile, M.J., Michael, J.R., and Kotula, P.G. (2008). Controlled fabrication of nanopores using a direct focused ion beam approach with back face particle detection. Nanotechnology *19*, 235304.

Perutz, M.F., Pope, B.J., Owen, D., Wanker, E.E., and Scherzinger, E. (2002). Aggregation of proteins with expanded glutamine and alanine repeats of the glutamine-rich and asparagine-rich domains of Sup35 and of the amyloid β-peptide of amyloid plaques. Proc. Natl. Acad. Sci. USA *99*, 5596-5600.

Polymeropoulos, M.H., Lavedan, C., Leroy, E., Ide, S.E., Dehejia, A., Dutra, A., Pike, B., Root, H., Rubenstein, J., Boyer, R., *et al.* (1997). Mutation in the α-Synuclein Gene Identified in Families with Parkinson's Disease. Science *276*, 2045-2047.

Postma, H.W.C. (2010). Rapid Sequencing of Individual DNA Molecules in Graphene Nanogaps. Nano Lett. *10*, 420-425.

Potyrailo, R.A., Conrad, R.C., Ellington, A.D., and Hieftje, G.M. (1998). Adapting Selected Nucleic Acid Ligands (Aptamers) to Biosensors. Anal. Chem. *70*, 3419-3425.

Prusiner, S.B. (1998). Prions. Proc. Natl. Acad. Sci. USA *95*, 13363-13383.

Prusiner, S.B., Woerman, A.L., Mordes, D.A., Watts, J.C., Rampersaud, R., Berry, D.B., Patel, S., Oehler, A., Lowe, J.K., Kravitz, S.N., *et al.* (2015). Evidence for α-synuclein prions causing multiple system atrophy in humans with parkinsonism. Proc. Natl. Acad. Sci. *112*, E5308-E5317.

Quik, M. (2004). Smoking, nicotine and Parkinson's disease. Trends Neurosci. *27*, 561-568.

Recchia, A., Debetto, P., Negro, A., Guidolin, D., Skaper, S.D., and Giusti, P. (2004). α-Synuclein and Parkinson's disease. FASEB J. *18*, 617-626.

Reininger-Mack, A., Thielecke, H., and Robitzki, A.A. (2002). 3D-biohybrid systems: applications in drug screening. Trends Biotechnol. *20*, 56-61.

Ross, G., Abbott, R.D., Petrovitch, H., and et al. (2000). ASsociation of coffee and caffeine intake with the risk of parkinson disease. J. Am. Med. Assoc. *283*, 2674-2679.

Rotem, D., Jayasinghe, L., Salichou, M., and Bayley, H. (2012). Protein Detection by Nanopores Equipped with Aptamers. J. Am. Chem. Soc. *134*, 2781-2787.

Sassolas, A., Prieto-Sim¨®n, B., and Marty, J.-L. (2012). Biosensors for Pesticide Detection: New Trends. Am. J. Anal. Chem. *Vol.03No.03*, 23.

Savitt, J.M., Dawson, V.L., and Dawson, T.M. (2006). Diagnosis and treatment of Parkinson disease: molecules to medicine. J. Clin. Invest. *116*, 1744-1754.

Scatton, B., Javoy-Agid, F., Rouquier, L., Dubois, B., and Agid, Y. (1983). Reduction of cortical dopamine, noradrenaline, serotonin and their metabolites in Parkinson's disease. Brain Res. *275*, 321-328.

Schneider, G.F., and Dekker, C. (2012). DNA sequencing with nanopores. Nat. Biotechnol. *30*, 326-328.

Schneider, G.F., Kowalczyk, S.W., Calado, V.E., Pandraud, G., Zandbergen, H.W., Vandersypen, L.M.K., and Dekker, C. (2010). DNA Translocation through Graphene Nanopores. Nano Lett. *10*, 3163-3167.

Schweiger, S., Schneider, R., and Glossmann, H. (2012). Treatment of Alzheimer's Disease. (Google Patents).

Sheinerman, F.B., Norel, R., and Honig, B. (2000). Electrostatic aspects of protein–protein interactions. Curr. Opin. Struct. Biol. *10*, 153-159.

Shim, J.W., Tan, Q., and Gu, L.-Q. (2009). Single-molecule detection of folding and unfolding of the G-quadruplex aptamer in a nanopore nanocavity. Nuc. acids res. *37*, 972-982.

Sibbald, A., Whalley, P.D., and Covington, A.K. (1984). A miniature flow-through cell with a four-function chemfet integrated circuit for simultaneous measurements of potassium, hydrogen, calcium and sodium ions. Anal. Chim. Acta *159*, 47-62.

Sigalov, G., Comer, J., Timp, G., and Aksimentiev, A. (2008). Detection of DNA Sequences Using an Alternating Electric Field in a Nanopore Capacitor. Nano Lett. *8*, 56-63.

Simon, S.M., and Blobel, G. (1992). Signal peptides open protein-conducting channels in E. coli. Cell *69*, 677-684.

Singh, P.R., Bárcena-Uribarri, I., Modi, N., Kleinekathöfer, U., Benz, R., Winterhalter, M., and Mahendran, K.R. (2012). Pulling Peptides across Nanochannels: Resolving Peptide Binding and Translocation through the Hetero-oligomeric Channel from Nocardia farcinica. ACS Nano *6*, 10699-10707.

Singleton, A.B., Farrer, M., Johnson, J., Singleton, A., Hague, S., Kachergus, J., Hulihan, M., Peuralinna, T., Dutra, A., Nussbaum, R., *et al.* (2003). α-Synuclein Locus Triplication Causes Parkinson's Disease. Science *302*, 841.

Skeen, R.S., Kisaalita, W.S., Van Wie, B.J., Fung, S.J., and Barnes, C.D. (1990). Evaluation of neuron-based sensing with the neurotransmitter serotonin. Biosens. Bioelectron. *5*, 491-510.

Song, L., Hobaugh, M.R., Shustak, C., Cheley, S., Bayley, H., and Gouaux, J.E. (1996). Structure of Staphylococcal α-Hemolysin, a Heptameric Transmembrane Pore. Science *274*, 1859-1865.

Soni, G.V., Singer, A., Yu, Z., Sun, Y., McNally, B., and Meller, A. (2010). Synchronous optical and electrical detection of biomolecules traversing through solid-state nanopores. Rev. Sci. Instrum. *81*, 014301.

Soskine, M., Biesemans, A., De Maeyer, M., and Maglia, G. (2013). Tuning the Size and Properties of ClyA Nanopores Assisted by Directed Evolution. J. Am. Chem. Soc. *135*, 13456-13463.

Soskine, M., Biesemans, A., Moeyaert, B., Cheley, S., Bayley, H., and Maglia, G. (2012). An Engineered ClyA Nanopore Detects Folded Target Proteins by Selective External Association and Pore Entry. Nano Lett. *12*, 4895-4900.

Spillantini, M.G., Schmidt, M.L., Lee, V.M., Trojanowski, J.Q., Jakes, R., and Goedert, M. (1997). Alpha-synuclein in Lewy bodies. Nature *388*, 839-840.

Stefan, W.K., Alexander, Y.G., Yitzhak, R., and Cees, D. (2011). Modeling the conductance and DNA blockade of solid-state nanopores. Nanotechnology *22*, 315101.

Stefanis, L. (2012). α-Synuclein in Parkinson's Disease. Cold Spring Harbor Perspectives in Medicine *2*.

Stefureac, R., Long, Y.-t., Kraatz, H.-B., Howard, P., and Lee, J.S. (2006). Transport of α-Helical Peptides through α-Hemolysin and Aerolysin Pores†. Biochemistry *45*, 9172-9179.

Stefureac, R., Waldner, L., Howard, P., and Lee, J.S. (2008). Nanopore Analysis of a Small 86-Residue Protein. Small *4*, 59-63.

Stefureac, R.I., Kachayev, A., and Lee, J.S. (2012). Modulation of the translocation of peptides through nanopores by the application of an AC electric field. Chem. Comm. *48*, 1928-1930.

Stefureac, R.I., and Lee, J.S. (2008). Nanopore Analysis of the Folding of Zinc Fingers. Small *4*, 1646-1650.

Stefureac, R.I., Madampage, C.A., Andrievskaia, O., and Lee, J.S. (2010). Nanopore analysis of the interaction of metal ions with prion proteins and peptides. This paper is one of a selection of papers published in this special issue entitled “Canadian Society of Biochemistry, Molecular &

Cellular Biology 52nd Annual Meeting — Protein Folding: Principles and Diseases" and has undergone the Journal's usual peer review process. Biochem. Cell Biol. *88*, 347-358.

Storm, A.J., Chen, J.H., Ling, X.S., Zandbergen, H.W., and Dekker, C. (2003). Fabrication of solid-state nanopores with single-nanometre precision. Nat. Mater. *2*, 537-540.

Sujatha, R., Robert, H.B., and Daniel, W.v.d.W. (2010). Radio frequency rectification on membrane bound pores. Nanotechnology *21*, 075201.

Surguchov, A., McMahan, B., Masliah, E., and Surgucheva, I. (2001). Synucleins in ocular tissues. J. Neurosci. Res. *65*, 68-77.

Sutherland, T.C., Long, Y.-T., Stefureac, R.-I., Bediako-Amoa, I., Kraatz, H.-B., and Lee, J.S. (2004). Structure of Peptides Investigated by Nanopore Analysis. Nano Lett. *4*, 1273-1277.

Tanaka, Y., Hirano, N., Kaneko, J., Kamio, Y., Yao, M., and Tanaka, I. (2011). 2-Methyl-2,4-pentanediol induces spontaneous assembly of staphylococcal α-hemolysin into heptameric pore structure. Protein Science *20*, 448-456.

Tavassoly, O., Kakish, J., Nokhrin, S., Dmitriev, O., and Lee, J.S. (2014a). The use of nanopore analysis for discovering drugs which bind to α-synuclein for treatment of Parkinson's disease. Eur. J. Med. Chem. *88*, 42-54.

Tavassoly, O., and Lee, J.S. (2012). Methamphetamine binds to α-synuclein and causes a conformational change which can be detected by nanopore analysis. FEBS Lett. *586*, 3222-3228.

Tavassoly, O., Nokhrin, S., Dmitriev, O.Y., and Lee, J.S. (2014b). Cu(II) and dopamine bind to α-synuclein and cause large conformational changes. FEBS J. *281*, 2738-2753.

Terry, L.A., White, S.F., and Tigwell, L.J. (2005). The Application of Biosensors to Fresh Produce and the Wider Food Industry. J. Agric. Food Chem. *53*, 1309-1316.

Toschi, F., Lugli, F., Biscarini, F., and Zerbetto, F. (2009). Effects of Electric Field Stress on a β-Amyloid Peptide. J. Phys. Chem. B *113*, 369-376.

Tsofina, L., Liberman, E., and Babakov, A. (1966). Production of bimolecular protein-lipid membranes in aqueous solution. Nature.

Turner, A.P.F., Karube, I., and Wilson, G.S. (1987). Biosensors : fundamentals and applications (Oxford [etc.]: Oxford University Press).

Uéda, K., Fukushima, H., Masliah, E., Xia, Y., Iwai, A., Yoshimoto, M., Otero, D.A., Kondo, J., Ihara, Y., and Saitoh, T. (1993). Molecular cloning of cDNA encoding an unrecognized component of amyloid in Alzheimer disease. Proc. Natl. Acad. Sci. USA *90*, 11282-11286.

Ulmer, T.S., Bax, A., Cole, N.B., and Nussbaum, R.L. (2005). Structure and Dynamics of Micelle-bound Human α-Synuclein. J. Biol. Chem. *280*, 9595-9603.

Valente, E.M., Bentivoglio, A.R., Dixon, P.H., Ferraris, A., Ialongo, T., Frontali, M., Albanese, A., and Wood, N.W. (2001). Localization of a Novel Locus for Autosomal Recessive Early-Onset Parkinsonism, PARK6, on Human Chromosome 1p35-p36. Am. J. Hum. Genet. *68*, 895-900.

Van der Schoot, B.H., and Bergveld, P. (1988). ISFET based enzyme sensors. Biosensors *3*, 161-186.

Venkatesan, B.M., and Bashir, R. (2011). Nanopore sensors for nucleic acid analysis. Nat. Nano. *6*, 615-624.

Villafane, G., Cesaro, P., Rialland, A., Baloul, S., Azimi, S., Bourdet, C., Le Houezec, J., Macquin-Mavier, I., and Maison, P. (2007). Chronic high dose transdermal nicotine in Parkinson's disease: an open trial. Eur. J. Neurol. *14*, 1313-1316.

Walker, B., Kasianowicz, J., Krishnasastry, M., and Bayley, H. (1994). A pore-forming protein with a metal-actuated switch. Protein Eng. *7*, 655-662.

Walker, B., Krishnasastry, M., Zorn, L., and Bayley, H. (1992). Assembly of the oligomeric membrane pore formed by Staphylococcal alpha-hemolysin examined by truncation mutagenesis. J. Biol. Chem. *267*, 21782-21786.

Wang, H.-Y., Ying, Y.-L., Li, Y., Kraatz, H.-B., and Long, Y.-T. (2011). Nanopore Analysis of β-Amyloid Peptide Aggregation Transition Induced by Small Molecules. Anal. Chem. *83*, 1746-1752.

Wang, X., Li, Y., He, X., Chen, S., and Zhang, J.Z.H. (2014). Effect of Strong Electric Field on the Conformational Integrity of Insulin. J. Phys. Chem. A *118*, 8942-8952.

Wanunu, M., Soni, G., and Meller, A. (2009). Single-Molecule Studies of Nucleic Acid Interactions Using Nanopores. In Handbook of Single-Molecule Biophysics, P. Hinterdorfer, and A. Oijen, eds. (Springer US), pp. 265-291.

White, R.J., Ervin, E.N., Yang, T., Chen, X., Daniel, S., Cremer, P.S., and White, H.S. (2007). Single Ion-Channel Recordings Using Glass Nanopore Membranes. J. Am. Chem. Soc. *129*, 11766-11775.

Wilmsen, H.U., Pattus, F., and Buckley, J.T. (1990). Aerolysin, a hemolysin fromAeromonas hydrophila, forms voltage-gated channels in planar lipid bilayers. J. Membr. Biol. *115*, 71-81.

Wood, P.L., and Altar, C.A. (1988). Dopamine release in vivo from nigrostriatal, mesolimbic, and mesocortical neurons: utility of 3-methoxytyramine measurements. Pharmacol. Rev. *40*, 163-187.

Wu, D., Bi, S., Zhang, L., and Yang, J. (2014). Single-Molecule Study of Proteins by Biological Nanopore Sensors. Sensors *14*, 18211.

Xu, H., Nallathamby, P.D., and Xu, X.-H.N. (2009). Real-Time Imaging and Tuning Subcellular Structures and Membrane Transport Kinetics of Single Live Cells at Nanosecond Regime. J. Phys. Chem. B *113*, 14393-14404.

Yamamoto, N., Nagasawa, Y., Sawai, M., Sudo, T., and Tsubomura, H. (1978). Potentiometric investigations of antigen-antibody and enzyme-enzyme inhibitor reactions using chemically modified metal electrodes. J. Immunol. Methods *22*, 309-317.

Zarranz, J.J., Alegre, J., Gómez-Esteban, J.C., Lezcano, E., Ros, R., Ampuero, I., Vidal, L., Hoenicka, J., Rodriguez, O., Atarés, B., *et al.* (2004). The new mutation, E46K, of α-synuclein causes parkinson and Lewy body dementia. Ann. Neurol. *55*, 164-173.

Zengin, A., Tamer, U., and Caykara, T. (2013). A SERS-Based Sandwich Assay for Ultrasensitive and Selective Detection of Alzheimer's Tau Protein. Biomacromolecules *14*, 3001-3009.

Zhang, B., Galusha, J., Shiozawa, P.G., Wang, G., Bergren, A.J., Jones, R.M., White, R.J., Ervin, E.N., Cauley, C.C., and White, H.S. (2007). Bench-Top Method for Fabricating Glass-Sealed Nanodisk Electrodes, Glass Nanopore Electrodes, and Glass Nanopore Membranes of Controlled Size. Anal. Chem. *79*, 4778-4787.

Zhao, Q., Jayawardhana, D.A., Wang, D., and Guan, X. (2009). Study of Peptide Transport through Engineered Protein Channels. J. Phys. Chem. B *113*, 3572-3578.

Ziegler, C. (2000). Cell-based biosensors. Fresenius J. Anal. Chem. *366*, 552-559.

Zilkova, M., Koson, P., and Zilka, N. (2006). The hunt for dying neurons: insight into the neuronal loss in Alzheimer's disease. Bratisl Lek Listy *107*, 366-373.